University of Naples Federico II
Polytechnic and Basic Sciences School

Department of Chemical Sciences

Ph.D. in Chemical Sciences

Structural and functional properties of complexes involving G-quadruplex-based DNA aptamers

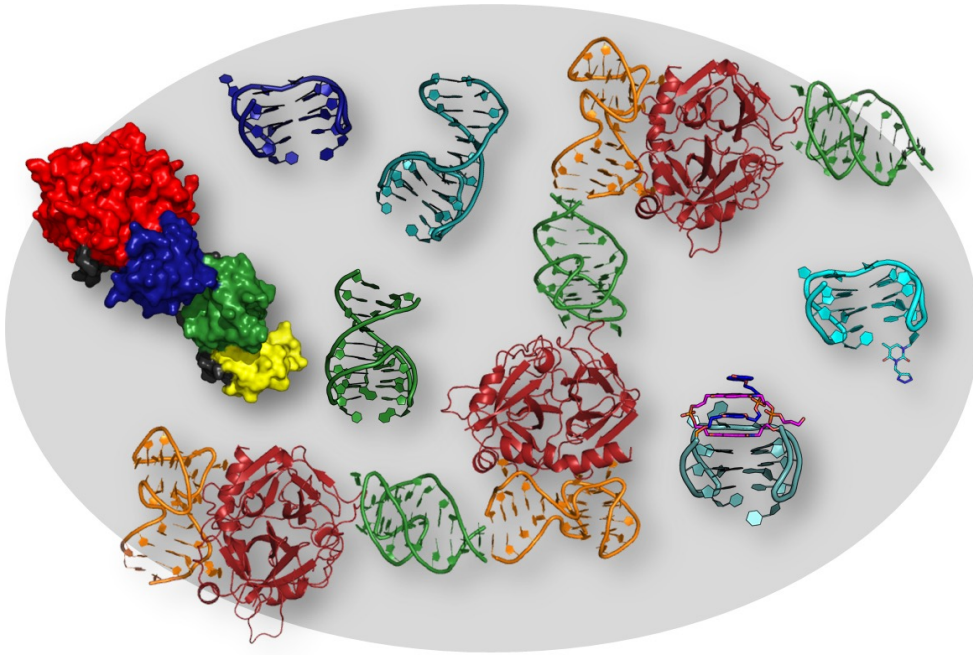

Romualdo Troisi

Advisor:
Prof. Filomena Sica

Examiner:
Prof. Domenica Musumeci

XXXIII Cycle 2018 – 2021
Coordinator: Prof. Angela Lombardi

UNIVERSITY OF NAPLES FEDERICO II

Polytechnic and Basic Sciences School

Ph.D. School in Chemical Sciences

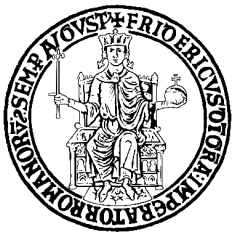

STRUCTURAL AND FUNCTIONAL PROPERTIES OF COMPLEXES INVOLVING G-QUADRUPLEX-BASED DNA APTAMERS

Romualdo Troisi

Advisor:

Prof. Filomena Sica

Examiner:

Prof. Domenica Musumeci

XXXIII Cycle 2018 - 2021

Coordinator: Prof. Angela Lombardi

SUMMARY **1**

SECTION 1: *INTRODUCTION* **3**

1. INTRODUCTION **5**

1.1. Oligonucleotide aptamers **5**

1.1.1. G-quadruplex folding *6*

1.2. Anti-thrombin aptamers **9**

1.2.1. TBA and RE31 ..... *10*

1.2.2. NU172 ..... *13*

1.2.3. HD22 ..... *15*

1.3. Simultaneous binding of two aptamers to thrombin exosites **17**

1.4. Thrombin binding aptamer modifications **20**

1.4.1. TBA variants with N3-modified Thy3 and Thy12 ..... *20*

1.4.2. Cyclic and pseudo-cyclic TBA analogues *22*

1.4.3. NU172 variants incorporating hexitol nucleotides *23*

1.5. Inhibition of the prothrombin activation by aptamers **25**

1.6. Aim of the project **29**

SECTION 2: *RESULTS AND DISCUSSION* **33**

2. RESULTS AND DISCUSSION **35**

2.1. Simultaneous binding of two aptamers to thrombin exosites **35**

2.1.1. NU172-thrombin-HD22_27mer crystal structure *36*

2.1.2. Aptamer-guided cooperation between the two exosites revealed by molecular dynamics simulations *43*

2.1.3. Anticoagulant activity of NU172 in the ternary complex *60*

2.2. Modified thrombin binding aptamers **61**

2.2.1. Crystal structures of TBA-3L, -3G, and -3Leu in complex with thrombin *62*

2.2.2. Crystal structures of cycTBA II and TBA NN/DD in complex with thrombin 70

2.2.3. Spectroscopic and functional studies of NU172 incorporating hexitol nucleotides 78

2.3. Aptamer/prothrombin interaction 88

2.3.1. ITC analysis 88

2.3.2. Prothrombin as molecular chaperone of aptamers 94

2.3.3. Crystallization trials of the complexes between wild-type prothrombin and aptamers 97

2.3.4. Design of prethrombin-2 and prothrombin mutants 98

2.3.5. Recombinant production of prethrombin-2 and prothrombin mutants 102

2.3.6. Crystallization trials of the complexes between NU172 and prethrombin-2 or prothrombin mutants 108

2.4. Concluding remarks 109

SECTION 3: *EXPERIMENTAL SECTION* 115

3. EXPERIMENTAL SECTION 117

3.1. Materials 117

3.2. Methods 117

3.2.1. Crystallography 117

3.2.2. Molecular dynamics: models and protocols 120

3.2.3. Spectroscopic analysis 125

3.2.4. ITC studies 127

3.2.5. Recombinant production of prethrombin-2 and prothrombin mutants 127

REFERENCES 135

SUMMARY

Despite significant advances in the prevention and treatment of thrombosis, this disease is still one of the leading causes of death worldwide. The anticoagulant drugs often used to control blood coagulation in many cases show adverse effects. Oligonucleotide aptamers have shown to be alternative specific anticoagulants, which are characterized by nonimmunogenicity and nontoxicity. Interestingly, a subclass of these aptamers that adopts a G-quadruplex-based structure is able to effectively modulate the activity and the generation of the human α-thrombin (thrombin). In particular, anti-thrombin aptamers that recognize either thrombin exosite I (TBA, NU172) or exosite II (HD22) were selected. Despite their excellent anticoagulant properties, new studies expand day-to-day in order to in-depth elucidate their mechanism of action and overcome some long-standing limitations, as the short circulating half-life *in vivo*.

The research activity carried out in the frame of this PhD project has been focused on three intriguing aspects of the interaction between thrombin or its zymogen prothrombin and aptamers adopting a G-quadruplex or a mixed duplex/quadruplex structure.

First, using a repertoire of different experimental and computational techniques, the impact that the binding of HD22_27mer aptamer at the exosite II has on the binding of TBA or NU172 at exosite I, and *vice versa*, was investigated. In particular, the crystal structure of the ternary complex formed by the thrombin with NU172 and HD22_27mer, extensive molecular dynamics simulations of different thrombin/aptamer complexes, and anticoagulant activity experiments were performed. Collectively, the findings provide a clear and detailed picture of the cooperative action that TBA or NU172 and HD22_27mer exert on thrombin inhibition.

Secondly, structural studies on new analogues of thrombin binding aptamers were carried out. In particular, the crystal structures of the complexes between thrombin

and three TBA variants, in which Thy3 contains functional substituents at N3 of the pyrimidine heterocycle, were solved. The results suggest an explanation for their higher binding affinity toward thrombin with respect to that of TBA. Moreover, a preliminary analysis of the crystal structures of the complexes between thrombin and two TBA variants, carrying modifications at 5′ and 3′ ends, was presented. Conversely, the structural and biochemical properties of NU172 variants incorporating hexitol nucleotides were investigated in solution, indicating the modification at the Thy9 as the most promising.

Finally, a preliminary investigation of the interaction between prothrombin and some anti-thrombin aptamers recognizing exosite I was carried out. In particular, a thermodynamic analysis of the binding of TBA, RE31 and NU172 aptamers to thrombin and prothrombin was performed by means of ITC experiments. The results indicate the ability of the examined aptamers to recognize prothrombin pro-exosite I with an affinity similar to that shown for thrombin exosite I. Furthermore, the ability of prothrombin to act as molecular chaperone of aptamers was revealed by CD experiments. To increase the possibility to obtain crystallographic information on aptamer-prothrombin complexes, considering the high flexibility of the wild-type protein, the prethrombin-2 intermediate and two prothrombin mutants were recombinantly produced.

SECTION 1:
Introduction

1. INTRODUCTION

1.1. Oligonucleotide aptamers

In the past few decades, the remarkable progress in research pertaining to nucleic acids has unrevealed that these biomolecules are not exclusively genetic information carriers but are also involved in a series of other less known processes.[1]

At the beginning of the 1990s, it was observed that short DNA or RNA oligonucleotides, named aptamers, could specifically bind different non-nucleic acid targets adopting well-defined three-dimensional structures.[2] They are generated by an iterative selection process, SELEX (Systematic Evolution of Ligands by Exponential Enrichment), a technique that was invented in 1990 independently by two teams (Ellington/Szostak and Tuerk/Gold).[3,4] The process relies on multiple rounds of selection and replication until high specificity and low dissociation aptamers towards a target molecule are generated. These aptamers are isolated, cloned, sequenced, and validated to find the oligonucleotide with the highest binding affinity for the target. Since being implemented, the SELEX protocol has undergone many modifications and improvements including its combination with such techniques as surface plasmon resonance (SPR) or capillary electrophoresis (CE).[5]

Aptamers are comparable to monoclonal antibodies in terms of specificity and affinity to their target, with dissociation constants (K_d) in the picomolar (10^{-12} M) to nanomolar (10^{-9} M) range, showing peculiar properties making them attractive for *in vivo* applications.[6,7] The advantages of aptamers over other materials include their thermal and pH stability, ease of synthesis and inclusion of chemical modifications that allow controlled modulation of bioavailability and pharmacokinetics, the reversible unfolding, low batch-to-batch variation, short time of selection.[8,9] Another aptamer property is the ability to discriminate among related proteins that share common sets of structural domains, enantiomers, and

small alterations in macromolecular sequence.[10,11] Furthermore, aptamers can be relatively small and consequently can penetrate tissues faster and more efficiently than antibodies.[12,13] Rationally designed oligonucleotide antidotes can easily reverse the effects of aptamers.[14] Moreover, they are virtually non-immunogenic *in vivo* since they should not be recognized by the immune system.[13,15]

Currently, there are several aptamers in different stage of clinical trials.[9,16–18] Indeed, therapeutic applications are the most extensively investigated and resource-consuming branch of aptamer research.[19] The majority of therapeutic aptamers inhibit target molecules and some act as receptor agonists.[20] However, diagnostics seems to be the most dynamic field in aptamer research.[21,22] Numerous research groups are engaged in a fierce competition to develop more and more sensitive, time-efficient, and inexpensive methods to detect specific molecules or cells by aptamer.[23,24] Apart from quantitative evaluation, aptamers may also serve as probes to image tumour cells and might become very helpful in cancer diagnosis.[25,26] Finally, DNA and RNA aptamers are also attractive capture probes for the separation and purification of proteins, separation of small molecules and enantiomers.[27–29]

Aptamers can fold in unique and well-defined three-dimensional structures, such as hairpin, pseudoknot, and G-quadruplex,[20,30–33] assuming intricate and sometimes unpredictable conformations to adhere to the surface of their target.

1.1.1. G-quadruplex folding

G-quadruplexes are formed by guanine-rich sequences that can arrange in a quadruple helix structure (Figure 1.1A). The main component of G-quadruplexes is the G-tetrad (also known as G-quartet) (Figure 1.1B), a planar arrangement of four guanine bases associated through a cyclic array of Hoogsteen hydrogen bonds, in which each guanine base accepts and donates two hydrogen bonds.[34,35]

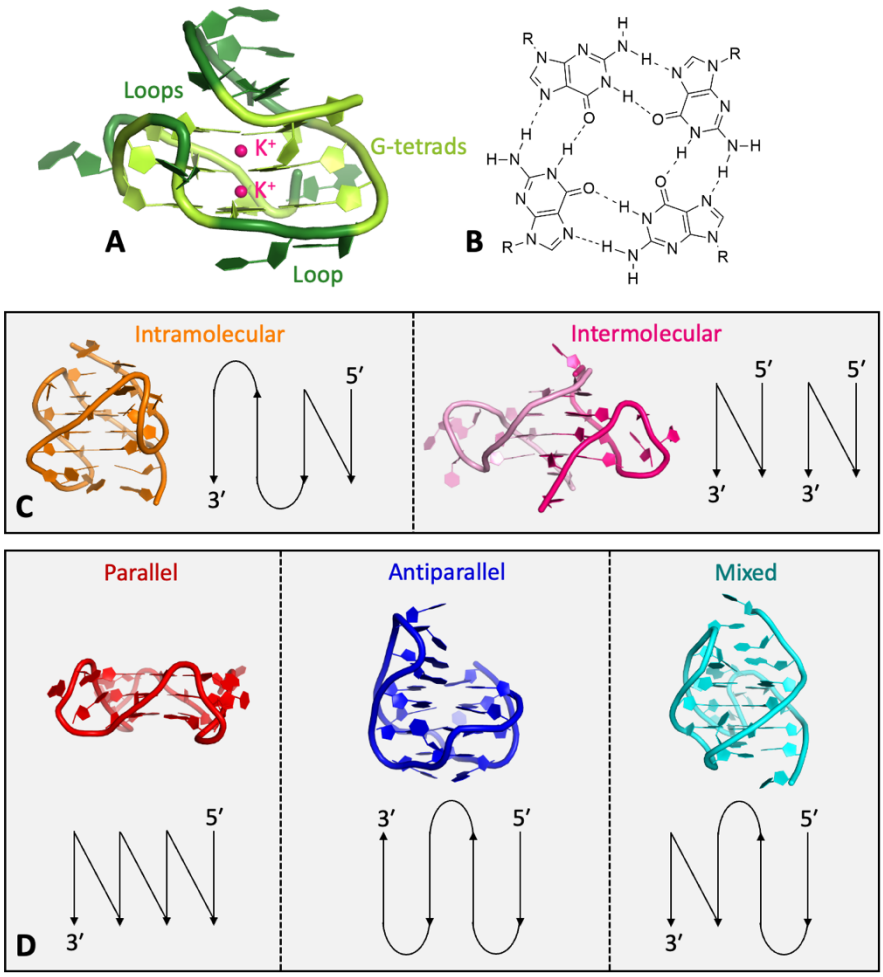

Figure 1.1. A) Cartoon representation of a G-quadruplex (PDB code: 3QXR)[36]. G-tetrads and loops are light and dark green, respectively. Potassium ions sandwiched between tetrads are pink. B) Top view of a G-tetrad. The Hoogsteen hydrogen bonds are shown in dashed lines. C) Cartoon and schematic representations of intramolecular (PDB code: 2HY9)[37] and intermolecular (PDB code: 3CE5)[38] G-quadruplexes. D) Cartoon and schematic representations of parallel (PDB code: 1KF1)[39], antiparallel (PDB code: 6JKN)[40], and mixed (PDB code: 2JPZ)[41] G-quadruplexes. The reported X-ray (3QXR, 3CE5, 1KF1, and 6JKN) or NMR (2HY9 and 2JPZ) structures are telomeric oligonucleotides and the promoter region of the c-kit gene, G-rich sequences able to adopt a G-quadruplex folding *in vivo*.

G-quadruplexes are topologically very polymorphic and can arise from the intramolecular or intermolecular folding of G-rich strands (Figure 1.1C).[37,38,42] Intramolecular folding requires the presence of four or more G-tracts in one strand, whereas intermolecular folding can arise from two or four strands.[34,42] Two main conformations are allowed to the glycosidic bond angles, χ (O4′ -C1′-N9-C4): *syn* and *anti*.[35] Depending on the orientation of the strands a G-quadruplex could assume a parallel, an antiparallel, or a mixed folding (Figure 1.1D).[39–41,43] Parallel G-quadruplexes have all guanine glycosidic angles in an *anti*-conformation.[34] Instead, antiparallel quadruplexes have both *anti* and *syn* guanine glycosidic torsion angles and their distribution along the strand depends on distinctive topological arrangements.[44] The residues connecting the G-tetrads define the connecting loops, that are regions of variable sequence and size (Figure 1.1A). All quadruplex structures have four grooves, defined as the cavities bounded by the phosphodiester backbones. Groove dimensions are variable and depend on the overall topology and the nature of the loops. They are populated by water molecules, that stabilizes the folded DNA structures.[34] Overall, the same stabilizing factors found in duplex DNA structures such as π-π base stacking, hydrogen bonding, hydration structure, and electrostatic interactions are associated with G-quadruplexes. On the contrary, the arrangement of the guanine O6 carbonyl groups central to the G-quartet, which creates negatively charged cavities located between the G-tetrads that needs to be stabilized by the coordination of cations (Figure 1.1A), is a peculiar structural feature of the G-quadruplex architecture.[45,46] The overall stability of the folded quadruplex dramatically depends on the selection of a suitable cation. Potassium ions are perfectly sandwiched between G-tetrads, almost equidistant from the eight oxygen atoms, whereas the smaller sodium ion explores a wider variety of coordination geometries.[47] The thermal stability of G-quadruplexes is dependent on features

such as the number of G-quartets present in the structure and the length and composition of the connection loops.[48]

1.2. Anti-thrombin aptamers

The coagulation is a complex process by which blood forms clots upon the damage of a blood vessel wall.[49] This process involves both a cellular component, the platelet, and a protein component, which includes several coagulation factors. Immediately upon the injury, platelets start to aggregate. Simultaneously, the coagulation factors, circulating in the plasma as inactive zymogens, trigger a complex succession of reactions that results in the final production of fibrin strands.[50]

Human α-thrombin (thrombin) is a trypsin-like serine protease that has the unique ability to convert soluble fibrinogen in insoluble fibrin clot. This enzyme is activated during the last steps of coagulation cascade and shows both pro-coagulant and anticoagulant properties.[51–53] The delicate equilibrium between these two functions is essential in the normal physiological state, preventing clot formation in undamaged vessels and triggering the coagulation cascade in the damaged ones. Indeed, thrombin generation is closely regulated to locally achieve rapid haemostasis after injury, without causing uncontrolled systemic thrombosis.[54] Thrombin exerts such different functions recognizing a large variety of substrates, inhibitors, and cofactors.[52] This ability is finely regulated by two distinct positively charged regions on the protein surface, known as exosites I and II, which provide specificity to the proteolytic activity of the protein (Figure 1.2).[55,56] In particular, exosite I is also known as the fibrinogen recognition site since it is the binding site of thrombin substrate, whereas exosite II is the binding site of heparin.[57] In particular, the latter, recognizing the exosite II, drives the formation of the complex between thrombin and antithrombin III, which is a physiological inhibitor of thrombin.[58,59]

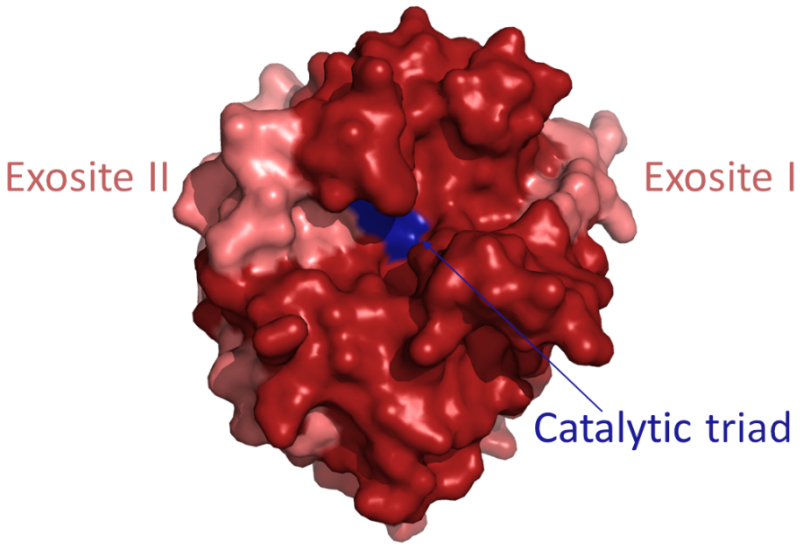

Figure 1.2. Surface representation of the crystal structure of the thrombin (PDB code: 1PPB)[60,61]. The exosites and the catalytic triad (His57, Asp102, and Ser195) are highlighted in different colours. Thrombin is composed by the heavy chain (259 residues) and the light chain (36 residues), covalently linked via a disulphide bond.

Given the ability to modulate the recognition with a large number of molecules, thrombin is usually considered a suitable target for anticoagulant and antithrombotic agents. Among them, anticoagulant aptamers constitute a special class of thrombin synthetic ligands specific to exosites.[62,63]

1.2.1. TBA and RE31

In 1992 a 15mer DNA oligonucleotide (5′-GGTTGGTGTGGTTGG-3′), which inhibits thrombin clotting activity at nanomolar concentration, was identified.[64] This oligonucleotide, named TBA (or HD1), is a strong anticoagulant *in vitro*, acting on the two procoagulant function of thrombin, since it inhibits thrombin-catalysed activation of fibrinogen and thrombin induced platelet aggregation.[65] TBA was considered as a promising anticoagulant drug and, with the name ARC183, reached Phase I clinical trials (Archemix Corp. and Nuvelo) as an

anticoagulant for potential use in acute cardiovascular settings, such as coronary artery bypass graft (CABG) surgery. The finding that the amount of drug needed to achieve the desired anticoagulation for use in CABG surgery corresponds to a suboptimal dosing profile blocked the TBA development.[62]

Structural studies revealed that TBA adopts a G-quadruplex architecture both in the free and liganded state.[66–68] According to the crystallographic structures of the TBA-thrombin complex (Figure 1.3), the aptamer folds as a chair-like G-quadruplex with a core formed by two stacked G-quartets which are covered on one side by the TGT loop (Thy7-Gua8-Thy9) protruding in the solvent and on the opposite side by the two TT loops (Thy3-Thy4 and Thy12-Thy13) acting as a pincer-like system that embraces the protruding region of thrombin exosite I.[66]

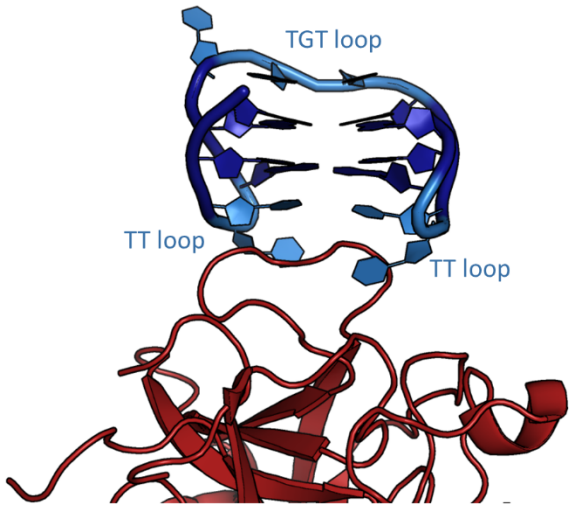

Figure 1.3. Cartoon representation of the crystal structure in which TBA is bound to thrombin exosite I (PDB code: 4DII)[66]. Thrombin is red and TBA is blue. The G-quadruplex loops are labelled.

Interestingly, structural and thermal properties of TBA depend on the nature of the bound cation, sodium or potassium.[66,67] In particular, the aptamer flexibility increases in the presence of sodium. Consequently, a better fit on the thrombin surface and an optimization of the intermolecular contacts were observed when

Na^+ is bound to TBA.[66] Moreover, it is noteworthy to recall that TBA, due to its approximate 2-fold rotational symmetry, can bind the protein in two orientations related by a *pseudo* 180° rotation around the G-quadruplex axis. The two binding modes are basically equivalent, and the only significant difference is confined to the orientation of the TGT loop that is far away from the binding contacts with thrombin. It can be supposed that both binding modes involving TT loops exist in solution and just one of them is selected in the crystallization process.[66] Modifications that lower the symmetry of the two TT loops differentiate the energetics of the two modes of binding, leading to a different population of the two species in solution.[69–71] In this context, exosite I can be described as formed by two sub-regions, referred to as A and B.[70] In the former, a hydrophobic crevice on the protein surface forms a well-shaped joint that interlocks a thymine of a TT loop. A thymine of the other TT loop interacts with the B-region, which is less extended than the A-region, through a π-π stacking with thrombin Tyr76.

The addition of a duplex motif to the G-quadruplex module of TBA produced a new generation of aptamers with more sophisticated structure.[67,72] The most promising TBA-derived duplex/quadruplex aptamer is RE31 (5′-GTGACGTAGGTTGGTGTGGTTGGGGCGTCAC-3′).[73,74] It binds exosite I of the thrombin with higher affinity (K_d = 7.2 nM) with respect to TBA.[75] The crystallographic structure of the RE31-thrombin complex shows that RE31 adopts a mixed duplex/quadruplex fold (Figure 1.4),[76] as it was suggested using a combination of spectrophotometric and calorimetric studies in solution.[67] The G-quadruplex domain adopts the antiparallel structure observed for TBA. However, in RE31 the TGT loop is involved in the transit from the duplex to the quadruplex region with the result that a continuous base stacking runs along the whole molecule (Figure 1.4). Consequently, the helical axes of the two regions maintain almost the same orientation, preventing the interaction of the duplex region with

the thrombin molecule. Briefly, the thrombin/RE31 interaction does not involve the duplex, but only the quadruplex domain, as observed for TBA.[76]

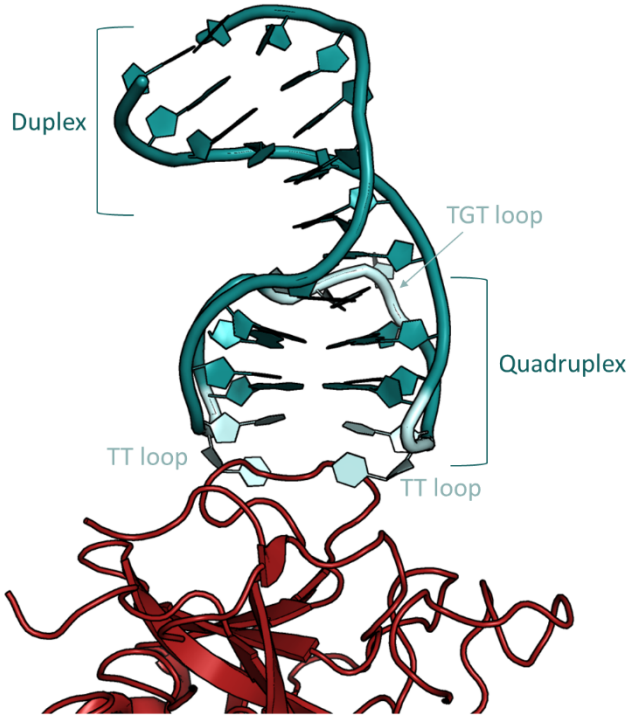

Figure 1.4. Cartoon representation of the crystal structure in which RE31 is bound to thrombin exosite I (PDB code: 5CMX)[76]. Thrombin is red and RE31 is dark cyan. The G-quadruplex loops are labelled.

1.2.2. NU172

A more advanced version of duplex/quadruplex aptamer against thrombin exosite I is NU172 (or ARC2172) (5′-CGCCTAGGTTGGGTAGGGTGGTGGCG-3′), which was discovered from a degenerate DNA library by SELEX and was subsequently truncated to 26 nucleotides without additional chemical modification.[2] NU172 possesses a pharmacokinetic profile similar to that of TBA with a significantly higher potency as an anticoagulant, having an IC_{50} value of 5–10 μg/ml in plasma.[27] Currently, NU172 is the only thrombin binding aptamer

evaluated in Phase II of clinical trials (ClinicalTrials.gov identifier NCT00808964) for anticoagulation in heart disease treatments by ARCA Biopharma, Inc.[77] Due to its high affinity (K_d = 0.1 nM) toward the target protein, which is about one order of magnitude greater than that of TBA,[78] NU172 represents a promising biorecognition element for the development of high-performance thrombin aptasensors.[79]

Structural studies revealed that NU172 adopts a mixed duplex/quadruplex architecture both in solution and in the solid state when it is bound to thrombin.[67,80] In particular, the crystal structure of the NU172-thrombin complex reveals that the aptamer spine is a continuous stacking of bases from the duplex to the quadruplex region (Figure 1.5).[80] The latter adopts an antiparallel conformation, where the strands forming the two G-tetrads are connected by three intervening lateral loops (Thy9-Thy10, Gua18-Thy19, and Gua13-Thy14-Ade15), all driving the interaction with thrombin. Notably, the transition between the two structural domains is sharp and formed by a reverse Hoogsteen base pair (Thy5/Ade15) and a base triad (Thy22/Ade6/Thy14), which involves two loop residues of the quadruplex domain (Thy14 and Ade15). The aptamer-protein interface involves not only the two-residue loops (TT ang GT), but also the GTA loop that in turn is directly involved in the stabilization of the duplex/quadruplex organization. Indeed, Gua13 forms a GG base pair with Gua18 of the GT loop (Figure 1.5), further locking the quadruplex structure and stiffening the assembly of the nucleotide bases around the guanidium group of Arg75 of thrombin exosite I. The compactness of the overall structure of NU172 can also explain the observed relative insensitivity of the complex versus the K^+/Na^+ exchange,[80] differently from what found in the case of the TBA-thrombin complex.[66]

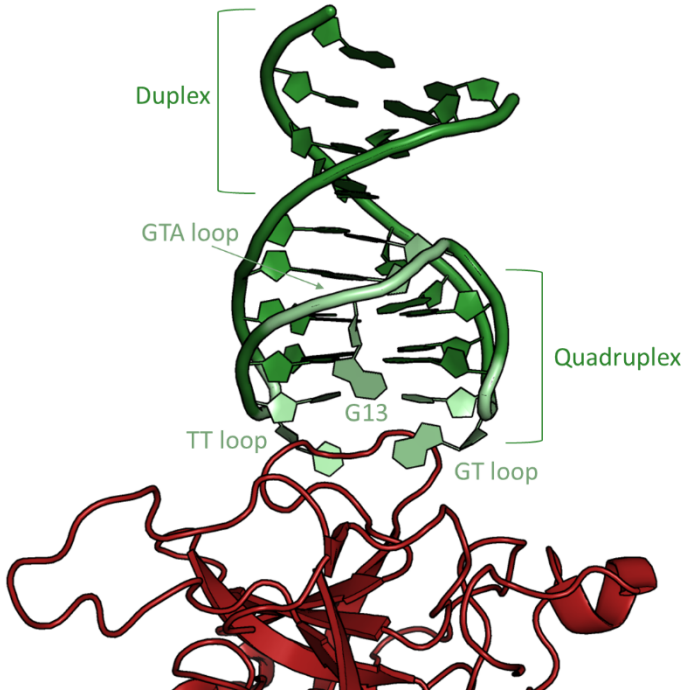

Figure 1.5. Cartoon representation of the crystal structure in which NU172 is bound to thrombin exosite I (PDB code: 6EVV)[80]. Thrombin is red and NU172 is green. The G-quadruplex loops are labelled. The Gua13 that forms a base pair with Gua18 of the GT loop is indicated.

1.2.3. HD22

One of the most interesting results of SELEX protocols directed towards thrombin was the identification of potent second-generation aptamers that adopt a mixed duplex/quadruplex conformation and bind thrombin exosite II.[81] In particular, this family of aptamers includes a HD22_29mer (5′-AGTCCGTGGTAGGGCAGGTTGGGGTGACT-3′), and the truncated HD22_27mer (5′-GTCCGTGGTAGGGCAGGTTGGGGTGAC-3′).[67] Both aptamers bind thrombin with high affinity (K_d = 0.5 and 0.7 nM for the 29mer and 27mer aptamers, respectively) but without exerting a potent anti-thrombotic activity.[81,82]

Crystallographic analysis of the HD22_27mer-thrombin complex shows that the aptamer adopts a kinked conformation in which the helical axis of the regular duplex segment and that of the *pseudo*-G-quadruplex motif are approximately at right angle (Figure 1.6).[83] The *pseudo*-G-quadruplex segment preserves the base stacking among the guanines of the core but lacks the stabilizing effects produced by cyclic Hoogsteen hydrogen bonds in one of the two tetrads. In particular, the Gua5 is displaced from the position required for the formation of a canonical G-tetrad.

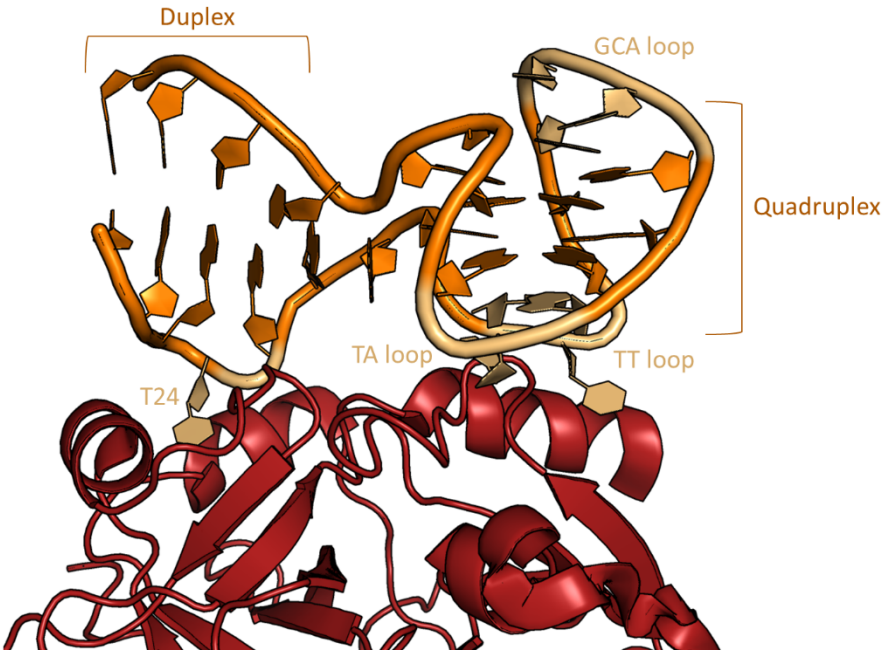

Figure 1.6. Cartoon representation of the crystal structure in which HD22_27mer is bound to thrombin exosite II (PDB code: 4I7Y)[83]. Thrombin is red and HD22_27mer is orange. The G-quadruplex loops are labelled. The Thy24 that bulging out from the duplex region fits into a pocket on the thrombin surface is indicated.

The resulting overall shape of the molecule allows both duplex and quadruplex domains to interact with the protein. Indeed, the exosite II recognition involves an extended region of the aptamer that includes the duplex segment (Gua23, Ade26

and Cyt27), a bulged-out residue Thy24 (Figure 1.6), the *pseudo*-G-quadruplex core (Gua20), and the quadruplex connecting loops (Thy9, Thy18 and Thy19).[83]

1.3. Simultaneous binding of two aptamers to thrombin exosites

The function of thrombin is regulated by long-range effects induced by the interaction with cofactors, substrates, or inhibitors.[52] Allosteric interactions were found between thrombin active cleft and the two exosites, or between the exosites themselves.[84–86] Several studies provided evidence of conformational variations of one exosite after a ligand binding at the other one.[87–92] Moreover, the influence of the binding state of an exosite on the binding affinity of a ligand to the other exosite was extensively examined and suggested a ligand dependent allosteric interaction between the two thrombin exosites (Table 1.1).

The data on the mutual effects of the binding of oligonucleotide aptamers at the two exosites of the thrombin clearly indicate an allosteric cooperation.[93,94] In particular, the presence of HD22 aptamers on exosite II increases the binding affinity of TBA towards the thrombin exosite I, and *vice versa* (Table 1.1). Detailed information on the simultaneous binding mode of these aptamers to thrombin were obtained through the analysis of the crystallographic structures of two ternary complexes (PDB code: 5EW1 and 5EW2) in which exosite II is bound to HD22_27mer and exosite I interacts with TBA-like aptamers lacking either the nucleobase of Thy3 (TBAΔT3) or the nucleobase of Thy12 (TBAΔT12) (Figure 1.7).[95]

Table 1.1. Ligand dependent allosteric interactions between the two thrombin exosites.

Exosite I ligands	Exosite II ligands	Effect on affinity towards:		References
		exosite I	exosite II	
Hirudin	sF2[a]	Reduced	Reduced	84,87
	Heparin		-	
Fibrin	γ′-peptide[b]	Reduced	-	90
	EV22[c]		-	
	Heparin		-	
TM456[d]	GPIbα[e]	Reduced	-	86
	γ′-peptide[b]		-	
	HD22_29mer		-	
PAR1 (49-62)[f]	(269-282, 3Yp)[g]	Increased	-	92
PAR3 (44-56)[f]		Increased		
TBA	γ′-peptide[b]	-	Reduced	90
Hirudin		-		
TBA	HD22_38mer	Increased	Increased	93,94
	HD22_29mer		Increased	

[a] Synthetic peptide corresponding to residues 63–116 of prothrombin fragment 2; [b] Analogue of the carboxy terminus of the γ′-chain of fibrinogen; [c] HD22 aptamer variant; [d] Thrombomodulin-derived peptide; [e] Peptide analogue of glycoprotein Ibα; [f] Protease activated receptors; [g] Triply phosphorylated GpIbα.

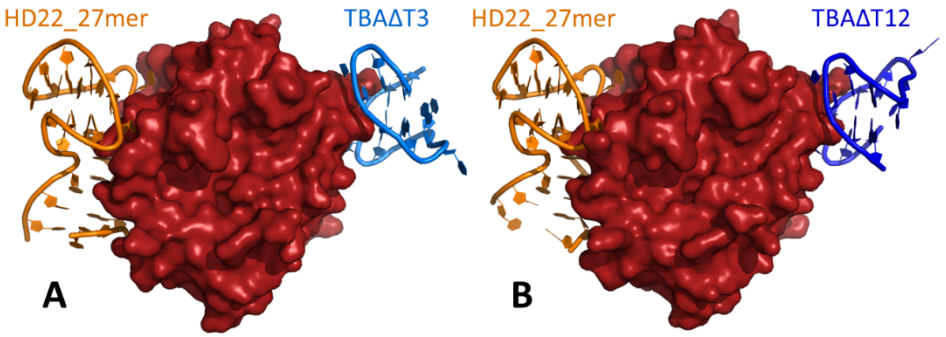

Figure 1.7. Cartoon/surface representation of the crystal structures of the two ternary complexes in which exosite II is bound to HD22_27mer and exosite I interacts with A) TBAΔT3 (PDB code: 5EW1)[95] or B) TBAΔT12 (PDB code: 5EW2)[95].

These structures, which are embedded in different packing organizations, display subtle but significant differences only in the conformation of HD22_27mer and in its interaction with thrombin surface. Indeed, despite the close similarity in the

overall organization of HD22_27mer with respect to the binary complex, in the TBA-thrombin-HD22_27mer ternary complexes the four bases of tetrad II (Gua5,Gua7,Gua12,Gua16), which in the binary complex show the non-canonical *anti-syn-anti-anti* conformational sequence, adopt a non-canonical *anti-anti-anti-anti* conformation (Figure 1.8).[95]

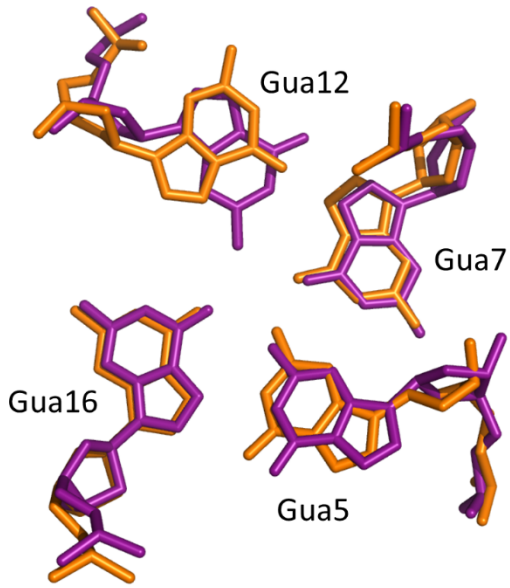

Figure 1.8. Top view of the HD22_27mer tetrad II as found in the crystal structures of the HD22_27mer-thrombin binary (orange, PDB code: 4I7Y)[83] and the TBAΔT3-thrombin-HD22_27mer ternary complexes (violet, PDB code: 5EW1)[95]. In TBAΔT12-thrombin-HD22_27mer, the tetrad II of HD22_27mer assumes the same conformation as in the other ternary complex.

This reorganization of tetrad II with a different orientation of Gua12 and the more massive presence of the sodium ion, which is present only at a very low level in the binary complex, slightly displaces the duplex region and causes the whole aptamer to improve the adhesion to exosite II. These effects can be associated with the presence of a TBA-like aptamer at exosite I. However, the presence in the protein active site of the covalently bound inhibitor PPACK, which is used in

crystallization experiments to avoid the heterogeneity of protein solution induced by autoproteolysis, influences the intrinsic mobility of the protein.[96,97] This prevents a more marked structural identification of an interplay between the two exosites.

1.4. Thrombin binding aptamer modifications

A disadvantage of aptamers is the short lifetime in blood that depends on the renal clearance and nuclease degradation.[20,27,98,99] Among the many strategies devised to overcome this long-standing limitation,[16,20,100] the chemical modification of the aptamer structure has been one of the most studied approaches,[101] involving changes in the sugar backbone,[102–108] the internucleotide linkages,[109–111] or sequence/length variations of key residues[112–117]. Generally, the post-SELEX modification is an established strategy to improve the affinity or the inhibitory properties of anticoagulant aptamers.[68,118]

1.4.1. TBA variants with N3-modified Thy3 and Thy12

Modified TBA analogues demonstrated high potential as promising anticoagulant drugs.[68,118] Modification of the guanines belonging to G-quadruplex was examined for several non-natural nucleoside analogues.[106,119–121] Generally, these modifications drastically affect the quadruplex stability. Although distal from the aptamer-protein interface, the TGT loop was successfully modified, improving the aptamer binding affinity towards thrombin, or increasing its thermal stability.[114,120,122–124] Regarding TT loops, nucleotides Thy4 and Thy13 are the most intolerant to modifications, a feature strictly related to the structural organization of the complex of TBA with thrombin.[103,123,125,126] Indeed, the nucleobases of Thy4 and Thy13 are linked to the guanidinium groups of Arg75 and Arg77A forming an hybrid tetrad, which stacks onto the guanines of the first quadruplex tetrad.[66] In contrast, Thy3 or Thy12 accept a variety of modifications without compromising the ability of the aptamer to bind thrombin.[71,103,122,126–128]

Based on these observations, the group of Dr. Edward Timofeev of the Engelhardt Institute of Molecular Biology (Russian Academy of Sciences, Russia) synthesized a panel of TBA variants with N3-modified Thy3 and Thy12, in order to identify TBA analogues with enhanced affinity and improved anticoagulant activity.[129] In particular, a two-step modification strategy was used. First, three non-natural thymidine precursors containing a functional side chain at the N3 position of the pyrimidine base were prepared. Then, further transformation of these partially modified thymidines with different chemical agents provided a library of 22 TBA variants with extended functionalities at Thy3 and Thy12. The aptamer library was diversified with a variety of substituents from three different chemical groups: amino acids, aromatic carboxylic acids, and carbohydrates. Due to the peripheral arrangement of the modified fragment with respect to the G-quadruplex core, TBA mutants demonstrated insignificant variations in their thermal stability. Conversely, a notable variation in the binding affinity and biochemical properties (anticoagulant activity) of mutants was observed. In particular, three aptamer variants (TBA-3L, TBA-3G, and TBA-3Leu) with enhanced affinity or improved anticoagulant activity were identified within the mutants containing the modification on Thy3 (Figure 1.9).[129]

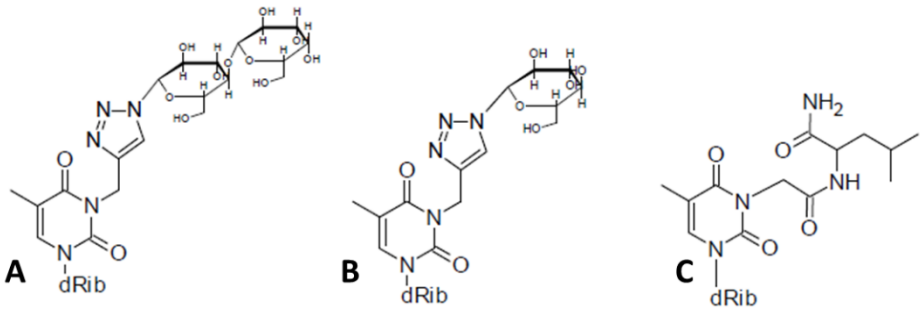

Figure 1.9. Chemical structures of A) the N3-(1-beta-D-lactopyranosyl-1,2,3-triazolylmethyl), B) the N3-(1-beta-D-glucopyranosyl-1,2,3-triazolylmethyl), and C) the N3-(N-(1-amino-4-methyl-1-oxopentan-2-yl)-2-amino-2-oxo-ethyl)thymidines contained at position 3 of TBA-3L, TBA-3G, and TBA-3Leu, respectively.

1.4.2. Cyclic and pseudo-cyclic TBA analogues

As a general strategy to improve the *in vivo* properties of anticoagulant aptamers, a cyclization approach involving the covalent connection, via a proper flexible linker, of the 5′- and 3′-ends of the oligonucleotide strand was proposed by the group of Prof. Daniela Montesarchio of the Department of Chemical Sciences, University of Naples Federico II (Italy), jointly to the group of Dr. François Morvan of the Institut des Biomolécules Max Mousseron, University of Montpellier (France).[130–132] In particular, cyclic TBA were obtained using two different strategies. In the first, they used a chemical cyclization based on the oxime ligation method. The second strategy was based on the Cu(I)-assisted azide-alkyne cycloaddition (CuAAC) protocol. The analysis of the cyclic variants showed that the absence of the 5′ and 3′ termini protect all TBA analogous from nuclease degradation. Moreover, the cyclic backbone forces in most cases a structural preorganisation of the mutated aptamer stabilising the G-quadruplex conformation. Unfortunately, only one mutant, named cycTBA II, showed a higher thrombin clotting inhibitory activity than the unmodified TBA. In particular, cycTBA II contains one triethylene glycol unit inserted at each end of the oligonucleotide, providing a 30-atom long linker (Figure 1.10A).[131]

Recently, as new strategy, the groups of Prof. D. Montesarchio and Dr. F. Morvan produced and studied TBA variants with naphthalene diimides and/or dansyl groups covalently bound at 5′- and/or 3′-ends. Considering the putative interactions between these groups, a *pseudo*-cyclic conformation is expected for these variants. Also in this case, some TBA mutants featured concomitantly increased thermal stability and nuclease resistance. In addition, due to the fluorescence properties of the terminal modification they are excellent candidates for diagnostic purposes. The most promising *pseudo*-cyclic TBA analogue, named TBA NN/DD, also showed an improved anticoagulant activity with respect to

TBA. It has two naphthalene diimides and two dansyl groups at 5′- and 3′-ends, respectively (Figure 1.10B).

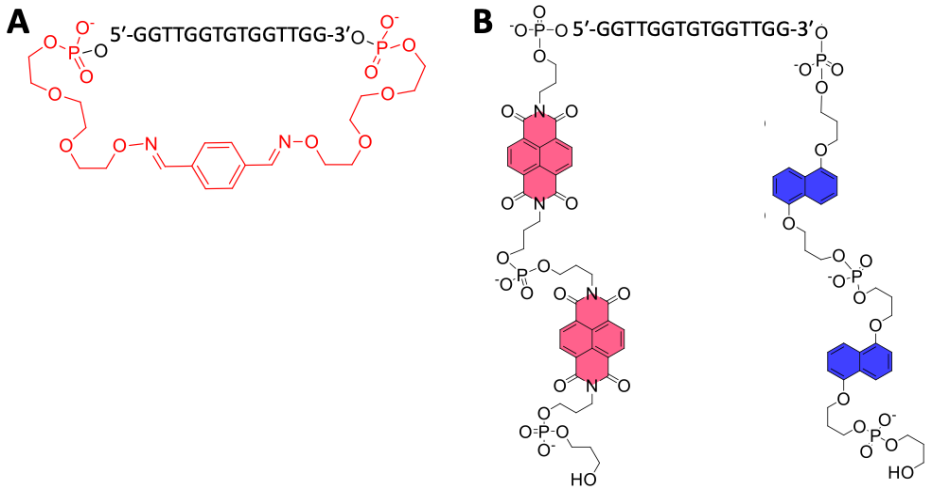

Figure 1.10. Schematic representation of A) cycTBA II and B) TBA NN/DD aptamers. The 30-atom long linker that covalently connects the 5′- and 3′-ends of cycTBA II is red. The two naphthalene diimides at 5′-end and the two dansyl groups at 3′-end of TBA NN/DD are pink and blue, respectively.

1.4.3. NU172 variants incorporating hexitol nucleotides

Although modifications were mainly focused on TBA,[68,118] only recently were reported changes in the structure of NU172.[132,133] In particular, the groups of Prof. Annalisa Guaragna of the Department of Chemical Sciences, University of Naples Federico II (Italy) and of Prof. Piet Herdewijn of the Rega Institute for Medical Research, Leuven (Belgium) produced NU172 variants incorporating unnatural nucleotides belonging to the class of Hexitol Nucleic Acids (HNA).[133] HNA are sugar-modified nucleic acids, in which native ribonucleotides are replaced by 1′,5′-anhydro-D-*arabino*-hexitol nucleotides. It was demonstrated to act as an A-type (RNA) mimic, as the $^{4}C_{1}$ sugar conformation of the hexitol ring resembles the C3′-*endo* (North) sugar ring pucker of natural (deoxy)ribonucleotides (Figure 1.11).[134]

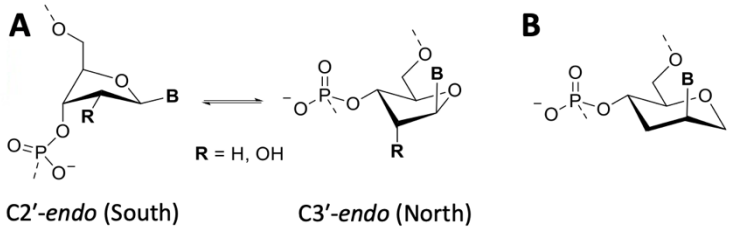

Figure 1.11. A) C2′-*endo* (South) and C3′-*endo* (North) conformations of (deoxy)ribonucleotides. B) 1′,5′ -anhydro-D-*arabino*-hexitol nucleotide conformation that resembles the North conformation of natural (deoxy)ribose.

It was reported that the hexitol moiety in HNA enhances the thermodynamic stability of both duplexes and quadruplexes when compared with unmodified oligonucleotides.[135,136] In addition, HNA exhibits high stability against nucleases.[137] The involvement of HNA in the development of thrombin binding aptamers takes place from the conformational analysis of NU172 nucleotides, as revealed by the crystal structure of the aptamer in complex with thrombin.[80] Differently from TBA, in which all nucleotides are reported to adopt South conformations,[102,104,118] two key nucleotides of NU172, both engaged in the interaction with thrombin, were found to have different conformational preferences. Particularly, Gua18, involved in H-bonds with Gua13, adopted a pure C3′-*endo* sugar ring pucker. On the other hand, Thy9 was arranged in a O4′-*endo* sugar conformation, which is intermediate between South and North forms. Based on these observations, the groups of Prof. A. Guaragna and Prof. P. Herdewijn incorporated hexitol nucleotides into these two positions (Gua18 and Thy9) and other three crucial positions (Thy10, Thy14, and Thy19), due to their involvement in the interaction with thrombin[80] or in nuclease digestion[111,138] (Table 1.2).

The mutant, named NU172-T^{H}9, containing the hexitol nucleotides in position Thy9 turned out to be the most interesting. Indeed, it exhibited a higher binding affinity toward thrombin than the native oligonucleotide. In addition, a significant enhancement of the half-life of the mutated oligonucleotide was estimated in 90% human serum.[133]

Table 1.2. NU172 variants containing hexitol nucleotides.

Name	Sequence (5′ → 3′)
NU172-T^H9	CGCCTAGG**T^H**TGGGTAGGGTGGTGGCG
NU172-T^H10	CGCCTAGGT**T^H**GGGTAGGGTGGTGGCG
NU172-T^H14	CGCCTAGGTTGGG**T^H**AGGGTGGTGGCG
NU172-G^H18	CGCCTAGGTTGGGTAGG**G^H**TGGTGGCG
NU172-T^H19	CGCCTAGGTTGGGTAGGG**T^H**GGTGGCG
NU172-T^H9T^H14	CGCCTAGG**T^H**TGGG**T^H**AGGGTGGTGGCG
NU172-T^H9G^H18	CGCCTAGG**T^H**TGGGTAGG**G^H**TGGTGGCG
NU172-T^H9T^H19	CGCCTAGG**T^H**TGGGTAGGG**T^H**GGTGGCG
NU172-G^H18T^H19	CGCCTAGGTTGGGTAGG**$G^H$$T^H$**GGTGGCG
NU172-T^H9T^H14G^H18	CGCCTAGG**T^H**TGGG**T^H**AGG**G^H**TGGTGGCG
NU172-T^H9G^H18T^H19	CGCCTAGG**T^H**TGGGTAGG**$G^H$$T^H$**GGTGGCG
NU172-T^H9T^H10G^H18T^H19	CGCCTAGG**$T^H$$T^H$**GGGTAGG**$G^H$$T^H$**GGTGGCG

N^H represents the modified hexitol nucleotide.

1.5. Inhibition of the prothrombin activation by aptamers

The proteolytic conversion of prothrombin to thrombin catalysed by prothrombinase is the only reaction not duplicated in the coagulation pathway and yields the critical regulatory end product of coagulation.[139]

Prothrombin, or clotting factor II, is a modular protein composed of 579 amino acids organized into the membrane-anchoring γ-carboxyglutamic acid (GLA) domain, kringle-1, kringle-2, and the protease domain, connected by three intervening linkers (Figure 1.12A).[140,141] The conversion of prothrombin to thrombin by the prothrombinase complex involves cleavage at two distinct sites, Arg271 and Arg320, along two alternative pathways that generate the zymogen precursor prethrombin-2 (Figure 1.12B) and the active enzyme meizothrombin (Figure 1.12C), respectively.[139,142] Although these intermediates do not accumulate under physiologically relevant conditions, selection of the pathway of activation is of mechanistic interest because it defines the rate of thrombin generation depending on the context.[143–145]

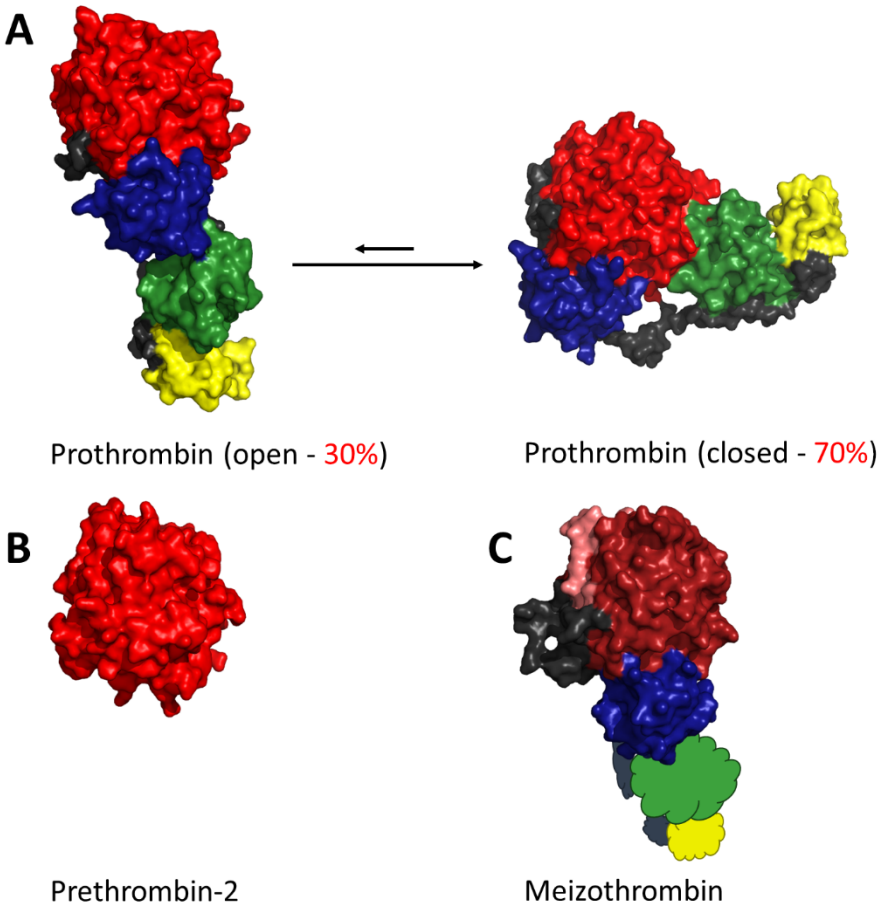

Figure 1.12. Surface representation of the crystal structures of A) prothrombin deletion mutant Δ154-167 (on the left, PDB code: 5EDM)[146], prothrombin mutant S101C/A470C (on the right, PDB code: 6C2W)[147], B) prethrombin-2 mutant S195A (PDB code: 4RN6)[148], and C) meizothrombin deletion mutant desF1 (PDB code: 3E6P)[149]. The GLA, kringle-1, kringle-2, and protease domains are yellow, green, blue, and red, respectively, while the linkers are grey. Prothrombin is involved in a conformational equilibrium in solution between an open (30%) and a closed (70%) conformation.[150] Prethrombin-2 and meizothrombin intermediates are generated after the cleavage of prothrombin at Arg271 or Arg320, respectively.[139] As in thrombin, after the cleavage in meizothrombin the protease domain is divided in heavy and light chain, that are connected via a disulphide bond. In the meizothrombin representation the fragment 1, F1 (GLA domain, kringle-1 and some linkers), that is absent in the crystal structure (PDB code: 3E6P), is schematically represented.

Prothrombinase, that activates prothrombin, is an enzyme complex composed of factor Xa (enzyme) and factor Va (cofactor) assembled on a cellular surface in the presence of calcium ions (Figure 1.13A).[151] Although factor Xa can independently catalyse the activation of prothrombin, the rate at which this reaction occurs is increased nearly 10^5-fold with complete assembly of the prothrombinase complex.[152] The membrane-bound prothrombinase recognizes and binds prothrombin through exosites on prothrombinase surface.[153] Conformational changes of the prothrombinase-prothrombin assembly subsequently enable the active site of factor Xa to sequentially recognize and cleave the two cleavage sites (Arg271 and Arg320) in the prothrombin to yield activated thrombin as product.[154] Efficient processing of prothrombin by the prothrombinase complex is required to form a stable blood clot at the site of tissue damage. Consequently, the inhibition of the prothrombin activation hampers the coagulation process. Several oral anticoagulants specifically targeting factor Xa recently shown remarkable efficacy in preventing stroke and managing venous thromboembolism, although none of these currently have an effective antidote approved for use.[155] Prothrombin pro-exosite I, the preformed exosite I, represents a potentially important new target for anticoagulant drug design, because it guides the prothrombin-factor Va interaction that has a controlling influence on the rate of prothrombin activation under physiological conditions (Figure 1.13B).[156]

Interestingly, studies conducted by Kretz *et al.*[157,158] demonstrated that TBA binds prothrombin at the pro-exosite I and attenuates prothrombin activation by prothrombinase by over 90%. Spiridonova *et al.*[72] showed the ability of a family of new generation duplex/quadruplex aptamers to interact with prothrombin. Furthermore, it was demonstrated that an RNA aptamer, named R9D-14T, is able to binds not only the thrombin exosite I but also the prothrombin pro-exosite I.[159] NU172 also provides an inhibitory action on prothrombin activation due to its binding to pro-exosite I of prothrombin.[160] Overall, these aptamers, inhibiting both

activity and generation of thrombin, represent effective dual targeting therapy agents that could provide a decrease of therapeutic doses and of bleeding rates.

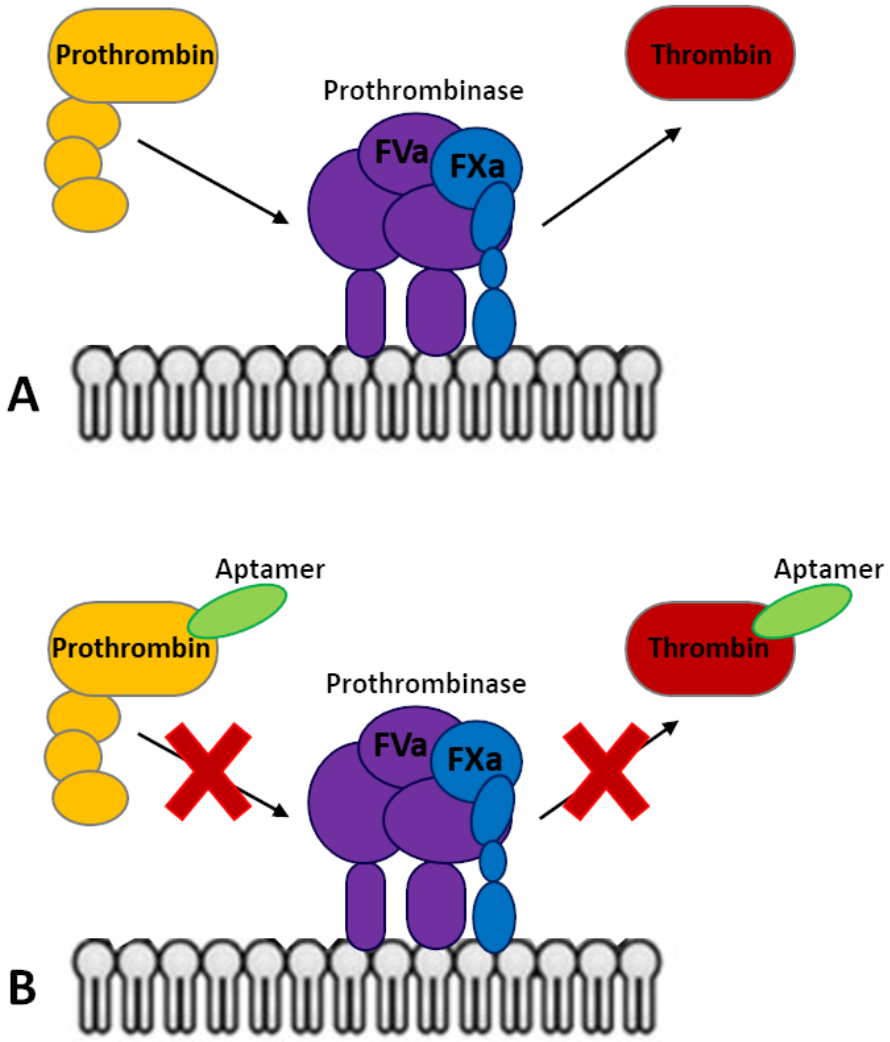

Figure 1.13. Schematic representation of A) the prothrombin activation to thrombin by prothrombinase complex and B) the possible inhibition of the process due to the binding of an aptamer to the prothrombin pro-exosite I. The prothrombin, thrombin, and aptamer are yellow, red, and green, respectively. The factors Xa and Va, assembled on membranes, are blue and violet, respectively.

Although studies on thrombin inhibitors are widely supported by structural information,[66,76,80,83] a detailed structural analysis of the interactions between prothrombin and aptamers is still absent in literature. This is due to the high conformational flexibility of some regions of the prothrombin and its tendency to assume two different conformations (closed and open) (Figure 1.12A),[150,161] which hinder the crystallization of the aptamer-prothrombin complexes, as well as of the free wild-type protein. Indeed, up to date, only the crystallographic structures of prothrombin mutants were solved.[141,146,147,161]

1.6. Aim of the project

In order to deeply understand the chemical and physical mechanisms by which the biological systems exploit their functions, a description of their structural, functional and dynamics properties is required.

The present study is part of a wider project on the structural definition of protein-aptamer recognition process. Specifically, in the group where this thesis work has been carried out, a structural characterization of several G-quadruplex-based aptamers free and in complex with their target was performed, both in solution and in the crystalline state.[66,67,69,70,76,80,83,95] Accordingly, this thesis project has been focused on three intriguing aspects of the interaction between thrombin or its zymogen prothrombin and aptamers adopting a G-quadruplex or a mixed duplex/quadruplex structure (Table 1.3).

Table 1.3. Anti-thrombin G-quadruplex-based aptamers studied in this PhD thesis. For each sequence, the name and the observed or putative thrombin binding site are reported. In TBA, RE31, HD22_27mer, and NU172, the guanines forming G-tetrads are red, while the nucleotides involved in duplex domain are green. In the other oligonucleotides, the nucleotides supposed to be involved in G-tetrads and duplex domain are magenta and blue, respectively. The variations with respect to the parent aptamer are in bold.

Name	Binding site	Sequence (5′ → 3′)
TBA	exosite I	GGTTGGTGTGGTTGG
TBA-3L	exosite I	GG**T^{L}**TGGTGTGGTTGG
TBA-3G	exosite I	GG**T^{G}**TGGTGTGGTTGG
TBA-3Leu	exosite I	GG**T^{Leu}**TGGTGTGGTTGG
cycTBA II	exosite I	**Linker-**GGTTGGTGTGGTTGG**-Linker**
TBA NN/DD	exosite I	**NN-**GGTTGGTGTGGTTGG**-DD**
RE31	exosite I	GTGACGTAGGTTGGTGTGGTTGGGGCGTCAC
HD22_27mer	exosite II	GTCCGTGGTAGGGCAGGTTGGGGTGAC
NU172	exosite I	CGCCTAGGTTGGGTAGGGTGGTGGCG
NU172-T^{H}9	exosite I	CGCCTAGG**T^{H}**TGGGTAGGGTGGTGGCG
NU172-T^{H}10	exosite I	CGCCTAGGTT**T^{H}**GGGTAGGGTGGTGGCG
NU172-T^{H}14	exosite I	CGCCTAGGTTGGG**T^{H}**AGGGTGGTGGCG
NU172-G^{H}18	exosite I	CGCCTAGGTTGGGTAGG**G^{H}**TGGTGGCG
NU172-T^{H}19	exosite I	CGCCTAGGTTGGGTAGGG**T^{H}**GGTGGCG
NU172-T^{H}9T^{H}14	exosite I	CGCCTAGG**T^{H}**TGGG**T^{H}**AGGGTGGTGGCG
NU172-T^{H}9G^{H}18	exosite I	CGCCTAGG**T^{H}**TGGGTAGG**G^{H}**TGGTGGCG
NU172-T^{H}9T^{H}19	exosite I	CGCCTAGG**T^{H}**TGGGTAGGG**T^{H}**GGTGGCG
NU172-G^{H}18T^{H}19	exosite I	CGCCTAGGTTGGGTAGG**G^{H}T^{H}**GGTGGCG
NU172-T^{H}9T^{H}14G^{H}18	exosite I	CGCCTAGG**T^{H}**TGGG**T^{H}**AGG**G^{H}**TGGTGGCG
NU172-T^{H}9G^{H}18T^{H}19	exosite I	CGCCTAGG**T^{H}**TGGGTAGG**G^{H}T^{H}**GGTGGCG
NU172-T^{H}9T^{H}10G^{H}18T^{H}19	exosite I	CGCCTAGG**T^{H}T^{H}**GGGTAGG**G^{H}T^{H}**GGTGGCG

T^{L}, T^{G} and **T^{Leu}** represent the N3-modified nucleotides; **Linker** represents the 30-atom long linker that covalently connects the 5′- and 3′-ends of cycTBA II; **NN** and **DD** represent the two naphthalene diimides at 5′-end and the two dansyl groups at 3′-end of TBA NN/DD; **T^{H}** and **G^{H}** represent the modified hexitol nucleotides.

First, a structural and dynamics analysis of the simultaneous binding between thrombin and two aptamers was performed in order to complete the atomic level description of the inter-exosites communication in thrombin. In particular, the crystal structure of the ternary complex in which the thrombin is sandwiched between two duplex/quadruplex aptamers (NU172 and HD22_27mer) was solved. Moreover, a series of molecular dynamics simulations of thrombin in different binding states (free thrombin; TBA-, NU172- and HD22_27mer-thrombin binary complexes; TBA- and NU172-thrombin-HD22_27mer ternary complexes) was performed.

Secondly, structural studies on intriguing new analogues of thrombin binding aptamers were carried out. In particular, the crystal structures of the complexes between thrombin and three TBA mutants with N3-modified Thy3 (TBA-3L, TBA-3G and TBA-3Leu) were analysed. In addition, the complexes of thrombin with cycTBA II and TBA NN/DD, cyclic and *pseudo*-cyclic TBA mutants, respectively, was studied in the crystalline state. Conversely, the structural and biochemical properties of NU172 variants incorporating hexitol nucleotides were investigated in solution.

Thirdly, a preliminary investigation of the interaction between prothrombin and some anti-thrombin aptamers recognizing exosite I was carried out. In particular, a complete comparative thermodynamic analysis of the binding of TBA, RE31 and NU172 aptamers to thrombin and prothrombin was performed by means of ITC experiments. Furthermore, the ability of prothrombin to act as molecular chaperone of aptamers was revealed by CD experiments. To raise the possibility to obtain crystallographic information on aptamer-prothrombin complexes, considering the high flexibility of the wild-type protein, two deletion mutants of prothrombin and the prethrombin-2 intermediate were recombinantly produced. These expression and purification experiments were conducted (1st February - 30th

September 2020) at the Institute of Structural Biology of the Helmholtz Zentrum München (Munich, Germany) under the supervision of Dr. Grzegorz Popowicz.

SECTION 2:

Results and discussion

2. RESULTS AND DISCUSSION

The results achieved in this thesis are presented and discussed in three different subsections. In particular, in the subsection 2.1 the structural and dynamics studies on the simultaneous binding of two aptamers to thrombin are examined. The subsection 2.2 is focused on the structural studies of novel modified anti-thrombin aptamers in the free or bound state. A preliminary analysis of the interaction between aptamer and prothrombin is reported in the subsection 2.3. In the latter, the strategies to produce recombinant prethrombin-2 and prothrombin mutants are presented. Finally, the conclusions and the future perspective are jointly discussed in the final subsection 2.4.

2.1. Simultaneous binding of two aptamers to thrombin exosites

Ligand binding to thrombin exosites allosterically modulates the enzyme activity via long-range effects.[90] In this scenario, the impact that the binding of an aptamer at the exosite II has on the binding and/or on the anticoagulant activity of another aptamer at the exosite I, and *vice versa*, was investigated.[93,94,162]

In this subsection, the crystal structure of the ternary complex formed by the thrombin with two duplex/quadruplex aptamers, NU172 and HD22_27mer, is reported. Moreover, extensive molecular dynamics simulations of thrombin in different binding contexts are discussed. Finally, anticoagulant activity experiments that provide a clear picture of the cooperative action between NU172 and HD22_27mer are presented.

The results reported in this subsection are the object of the following publications:[163,164]

- Troisi, R., Balasco, N., Vitagliano, L. & Sica, F. Molecular dynamics simulations of human α-thrombin in different structural contexts: evidence for an aptamer-guided cooperation between the two exosites. *J Biomol Struct Dyn.* **39**, 2199-2209 (2021).

- Troisi, R., Balasco, N., Santamaria, A., Vitagliano, L. & Sica, F. Structural and functional analysis of the simultaneous binding of two duplex/quadruplex aptamers to human α-thrombin. *Int J Biol Macromol.* **181**, 858-867 (2021).

2.1.1. NU172-thrombin-HD22_27mer crystal structure

The impact of the simultaneous binding of NU172 and HD22_27mer on thrombin structure was investigated by determining the crystallographic structure of the ternary complex in which thrombin is sandwiched between the two duplex/quadruplex aptamers, NU172 and HD22_27mer.

The NU172-thrombin-HD22_27mer ternary complex was crystallized by adapting and fine-tuning the experimental conditions used for other aptamer-thrombin complexes.[66,69–71,76,80,83,95] To avoid protein autodigestion and consequently guarantee the homogeneity of the sample, the crystallization experiments were performed using a thrombin sample in which the active site was blocked by the covalent inhibitor PPACK. Crystals of NU172-thrombin-HD22_27mer complex belong to the monoclinic space group $P2_1$ and diffract X-rays up to 3.10 Å resolution. They contain two ternary complexes (1 and 2) in the asymmetric unit, in which NU172 binds thrombin exosite I, while HD22_27mer binds exosite II on the opposite side of thrombin. Detailed statistics on data collection and refinement are reported in Table 2.1. The final model lacks in both complexes some residues at the light chain termini (Thr1h-Gly1d and Asp14l-Arg15), Gly246 and Glu247 of heavy chain C-terminal and γ-autolysis loop (Thr147-Lys149e). NU172 and HD22_27mer aptamers were entirely built in both complexes.

Table 2.1. Crystallographic statistics for the NU172-thrombin-HD22_27mer complex. Values in brackets refer to the highest resolution shell.

	NU172-thrombin-HD22_27mer
Crystal data	
Space group	$P2_1$
Unit-cell parameters	
a, b, c (Å)	84.93, 77.62, 95.41
α, β, γ (deg)	90.00, 103.47, 90.00
V_M ($Å^3$ Da^{-1})	2.87
No. of complexes in the asymmetric unit	2
Solvent content (%)	60.6
Data Collection	
Resolution limits (Å)	60.00 - 3.10 (3.21 - 3.10)
Unique reflections	22065 (2150)
Completeness (%)	99.8 (99.8)
Average multiplicity	3.7 (3.7)
$\langle I/\sigma(I) \rangle$	6.6 (2.2)
$CC_{1/2}$	1.0 (0.8)
Refinement	
Resolution limits (Å)	26.77 - 3.10
No. of reflections	20946
R_{factor}/R_{free}	0.200/0.257
No. of atoms	6893
Average B factors ($Å^2$)	36.82
R.m.s. deviations	
Bond lengths (Å)	0.002
Bond angles (deg)	1.067
Ramachandran plot, residues in (%)	
Favoured regions	91.0
Allowed regions	9.0
Outliers	0
PDB code	7NTU

The two complexes in the asymmetric unit present a similar architecture, as also shown by the value of the root-mean-square deviation (RMSD, 0.42 Å) calculated after the superposition of the C^{α} protein atoms and all oligonucleotide atoms. Hence, complex 1 will be referred to throughout the text (Figure 2.1) unless stated otherwise.

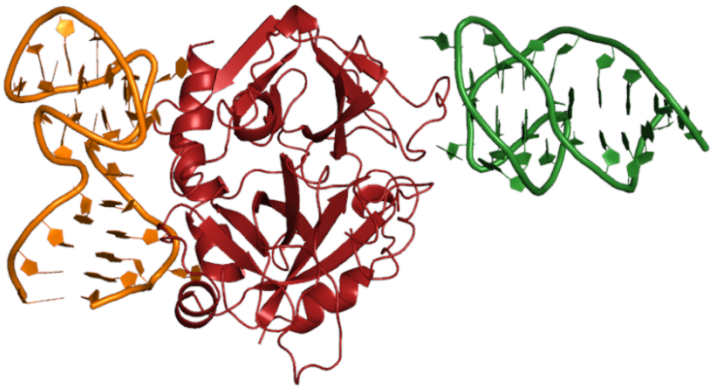

Figure 2.1. Cartoon representation of the crystal structure of the NU172-thrombin-HD22_27mer ternary complex (complex 1). Thrombin, NU172, and HD22_27mer are red, green, and orange, respectively.

Thrombin folding has been carefully examined and compared with that adopted in the unbound state and in the NU172-thrombin and HD22_27mer-thrombin binary complexes. In particular, the RMSD values after the superposition of all the C^{α} thrombin atoms with those of the aptamer-free protein (PDB code: 1PPB)[60,61], NU172-bound protein (PDB code: 6GN7)[80] and HD22_27mer-bound protein (PDB code: 4I7Y)[83] resulted 0.48 Å, 0.51 Å, and 0.45 Å, respectively, suggesting that the protein in the ternary complex does not present overall relevant modifications with respect to the other cases. In particular, residues of the two exosites adopt similar conformations to those found in the other crystallographic models of both free and liganded thrombin, although the different binding states of protein.

NU172 assumes a compact mixed duplex/quadruplex architecture very similar to that found previously in the NU172-thrombin binary complex (Figure 2.2A).[80] Although retaining a duplex/quadruplex folding (Figure 2.2B), HD22_27mer presents some small conformational variations with respect to the aptamer in HD22_27mer-thrombin binary complex.[83]

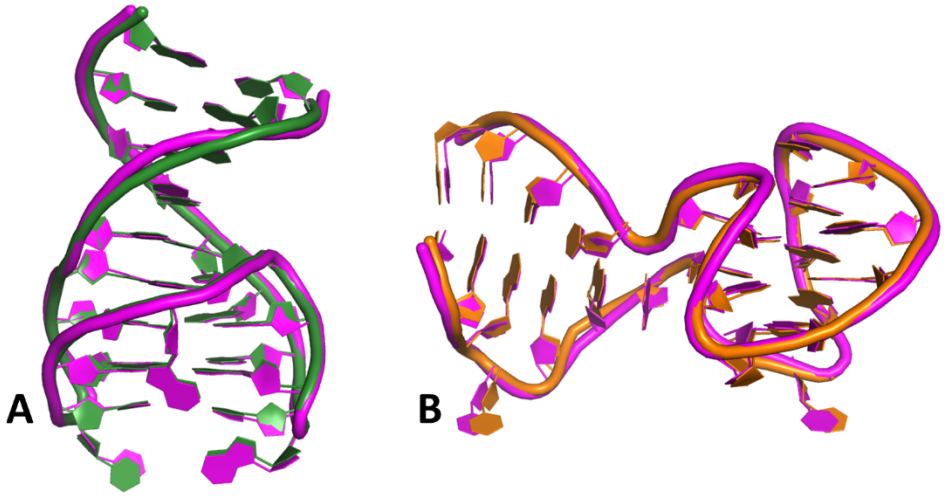

Figure 2.2. Superposition of A) NU172 and B) HD22_27mer as found in NU172-thrombin (green, PDB code: 6GN7)[80], HD22_27mer-thrombin (orange, PDB code: 4I7Y)[83] and NU172-thrombin-HD22_27mer (magenta) crystallographic structures.

In particular, the tetrad II of HD22_27mer G-quadruplex domain adopts a non-canonical organization, where all guanines are in the *anti*-conformation (Figure 2.3). This organization differs from that found in the binary complex[83] and is similar to that observed for the two previous reported ternary complexes[95] where exosite I was bound to TBA variants (Figure 1.8). This organization allows a higher occupancy of a sodium ion between the two tetrads of HD22_27mer G-quadruplex domain (Figure 2.3), which is present only at a very low level, if any, in the HD22_27mer-thrombin binary complex. The Gua13 and Cyt14 nucleobases that stack on HD22_27mer G-quadruplex tetrad II are flipped with respect to all the other previously reported crystal structures of HD22_27mer (Figure 2.3).

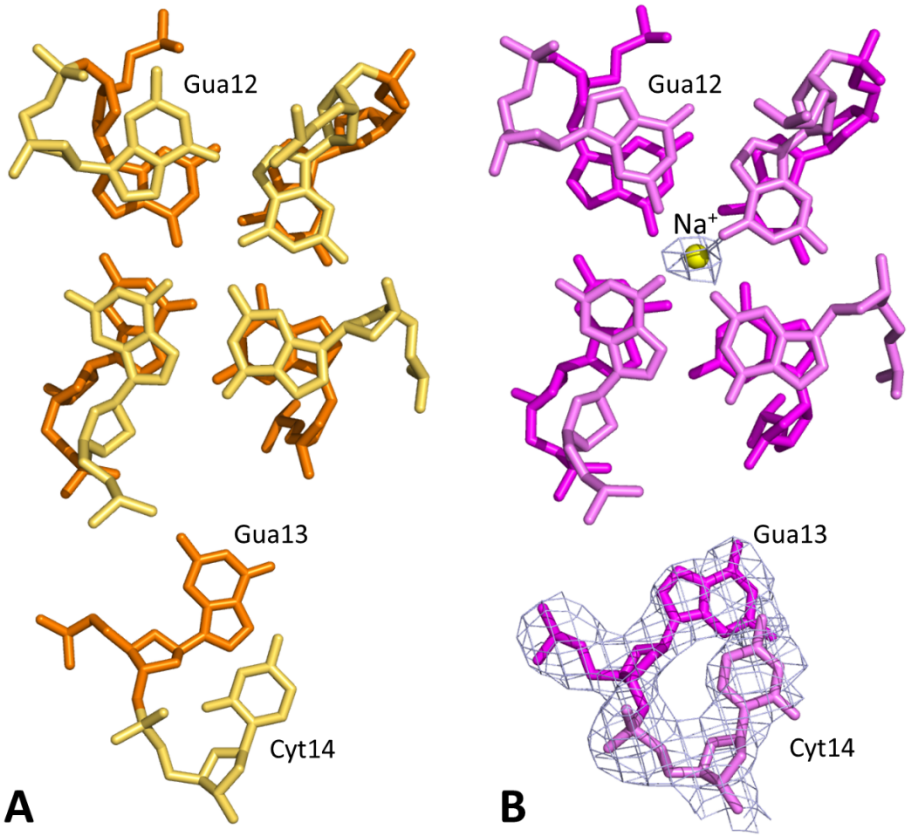

Figure 2.3. View along the G-quadruplex axis of the two tetrads and of Gua13 and Cyt14 of HD22_27mer aptamer in A) HD22_27mer-thrombin binary complex (PDB code: 4I7Y)[83] and B) NU172-thrombin-HD22_27mer ternary complex. In the upper panels, dark and light colours refer to tetrad I and II, respectively. The $2F_o$-F_c electron density map of the sodium ion (yellow) and Gua13-Cyt14 segment in ternary complex is contoured at 1.5 and 1.0 σ level, respectively. The electron density of the G-tetrad guanines is not reported for clarity of representation.

All these features underline the different nature of the two aptamers. NU172 is able to fold in a very packed structure thanks to a continuous stacking between the duplex and the quadruplex domains. On the contrary, HD22_27mer is a more flexible aptamer and its conformation is strongly influenced by the boundary conditions. This is also supported by the finding that some residues (Gua23-

Thy24-Gua25) of HD22_27mer assume two alternative conformations in the complex 2 of the NU172-thrombin-HD22_27mer crystal structure (Figure 2.4).

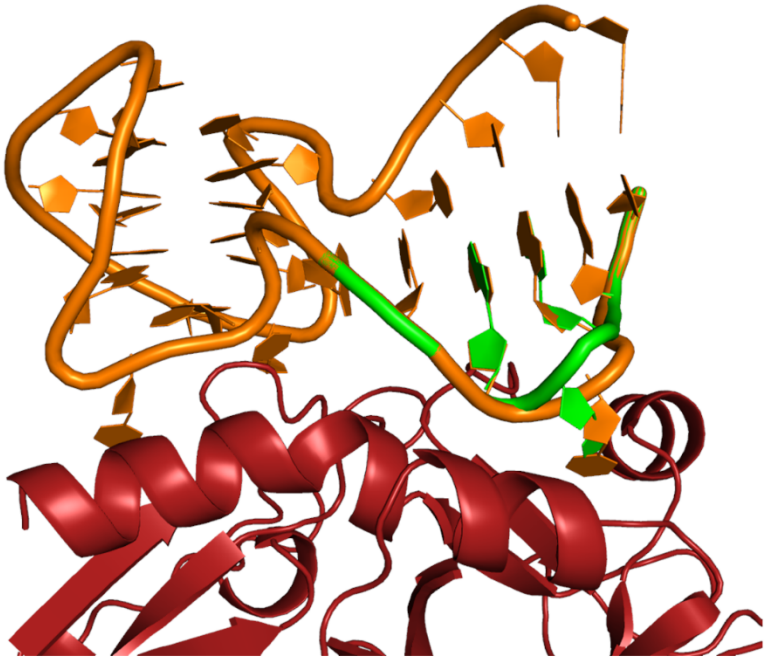

Figure 2.4. Cartoon representation of HD22_27mer in the complex 2 of the NU172-thrombin-HD22_27mer crystal structure. The two alternative conformations of the Gua23-Thy24-Gua25 segment are in different colours.

Overall, the interaction mechanism of the two aptamers with thrombin is conserved with respect to the two binary complexes. A comparison of the buried areas, the hydrogen bonds, and the hydrophobic interactions is reported in Table 2.2.

Table 2.2. Comparison of interface interactions and areas among NU172-thrombin, HD22_27mer-thrombin (PDB codes: 6GN7 and 4I7Y)[80,83], and NU172-thrombin-HD22_27mer ternary complex.

Binary complexes		Ternary complex	
NU172	**HD22_27mer**	**NU172**	**HD22_27mer**
Buried Area (Å^2)			
589	1080	591	1095
Hydrogens bonds			
Thy10^{O2}-Arg75^{Nε}	Thy9^{N3}-Pro92^{O}	Thy10^{O2}-Arg75^{Nη1}	Thy9^{N3}-Pro92^{O}
Thy10$^{O4'}$-Tyr76^{N}	Thy9^{OP1}-Asn95^{Nδ2}	Thy10$^{O4'}$-Tyr76^{N}	Thy9^{OP1}-Asn95^{Nδ2}
Thy10^{O4}-Arg77A^{Nη1}	Thy9^{OP2}-Arg97^{Nη1}		
Gua13^{O6}-Arg75^{Nη1}	Thy18^{O2}-Trp237^{Nε1}	Gua13^{O6}-Arg75^{Nε}	Thy18^{O2}-Trp237^{Nε1}
		Gua13^{O6}-Arg75^{Nη2}	Thy18^{OP2}-Gln244^{Nε2}
		Gua18^{O6}-Arg75^{Nη2}	Thy19^{OP1}-Lys240^{Nζ}
Gua18^{N1}-Glu77^{Oε1}	Gua20^{OP1}-Arg93^{Nη1}	Gua18^{N1}-Glu77^{Oε2}	Gua20^{OP1}-Arg93^{Nε}
Gua18^{N2}-Glu77^{Oε1}	Gua20$^{O4'}$-Arg93^{Nη1}		Gua20$^{O4'}$-Arg93^{Nη2}
Thy19^{O4}-Arg75^{Nη1}	Gua20$^{O5'}$-Arg93^{Nη1}	Thy19^{O4}-Arg75^{Nη1}	Gua20$^{O5'}$-Arg93^{Nη2}
Thy19^{O4}-Arg75^{Nη2}	Gua21^{O6}-Arg93^{Nη1}		
	Gua21^{O6}-Arg101^{Nη2}	Thy19$^{O3'}$-Asn78^{Nδ2}	Gua21^{O6}-Arg101^{Nη2}
	Gua23$^{O5'}$-Arg126^{Nε}	Gua20$^{O4'}$-Arg77A^{Nη1}	
		Gua20^{OP1}-Asn78^{Nδ2}	Gua23^{N2}-Asp178^{Oδ2}
			Gua23^{N3}-Arg233^{Nη1}
	Thy24^{OP1}-His230^{Nε2}		Thy24^{OP1}-His230^{Nε2}
	Thy24^{OP1}-Arg233^{Nη1}		
	Gua25^{OP2}-Arg126^{Nη2}		
	Cyt27^{OP1}-Lys169^{Nζ}		
Hydrophobic interactions			
Thy9-Tyr76	Thy9-Arg93	Thy9-Tyr76	Thy9-Arg93
Thy10-Tyr76	Thy9-Asn95	Thy10-Tyr76	Thy9-Asn95
Gua18-Ile24	Thy9-Trp96	Gua18-Ile24	Thy9-Trp96
Gua18-Ile79	Thy9-Arg97	Gua18-Ile79	Thy9-Arg97
Gua18-Tyr117	Thy18-Tyr89	Gua18-Tyr117	Thy18-Tyr89
Thy19-Ile79	Thy18-Pro92	Thy19-Ile79	Thy18-Pro92
	Thy18-Trp237		Thy18-Trp237
	Thy18-Val241		
	Thy18-Phe245		
	Thy19-His91		Thy19-His91
	Thy19-Pro92		Thy19-Pro92
	Thy19-Arg93		Thy19-Arg93
	Thy19-Trp237		Thy19-Trp237
	Thy24-His230		Thy24-His230
	Ade26-Arg165		Ade26-Arg165

Eventually, attention should be paid to the peculiar crystal packing observed in the NU172-thrombin-HD22_27mer X-ray structure. Instead, the two complexes in the asymmetric unit form an intricate pattern of contacts with symmetry-related mates mediated by the aptamers that generates a crystal-wide array of interacting complexes (Figure 2.5).

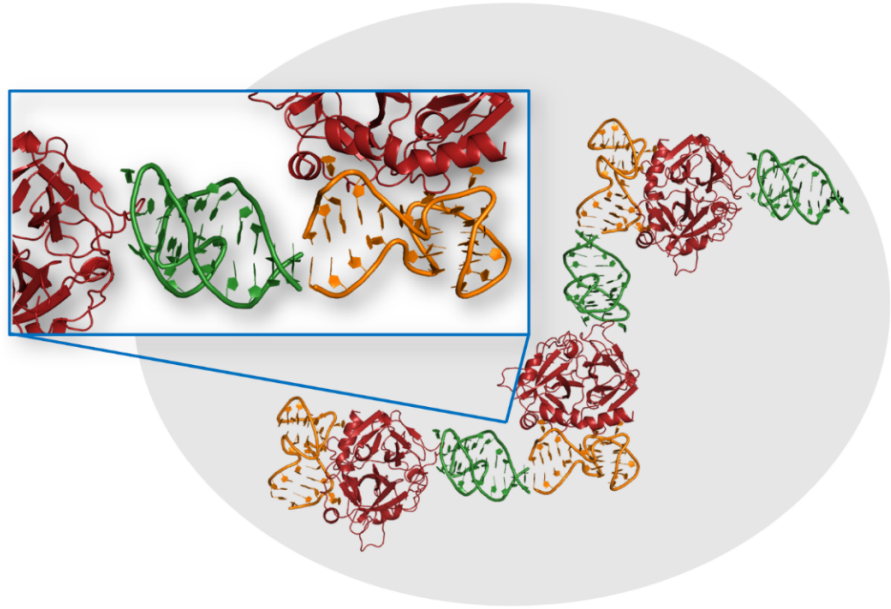

Figure 2.5. Details of the interaction between aptamers in the crystal packing of NU172-thrombin-HD22_27mer ternary complex. Thrombin, NU172, and HD22_27mer are red, green, and orange, respectively.

2.1.2. Aptamer-guided cooperation between the two exosites revealed by molecular dynamics simulations

In order to achieve a dynamic view of the recognition between thrombin and its aptamers and to obtain an atomic level description of the exosites intercommunication, a series of molecular dynamics (MD) simulations of thrombin in different binding states was performed. In particular, the structural and dynamic properties of the free thrombin and of its complexes with aptamers were investigated in a crystal-free context through MD simulations performed in

explicit solvent. In addition to the unbound protein, simulations were carried out on the three binary complexes formed by the protein with TBA, NU172 or HD22_27mer and on the ternary complexes (TBA-thrombin-HD22_27mer, NU172-thrombin-HD22_27mer) whose structures were determined by X-ray crystallography.

Structural stability of the systems in the MD simulations

To assess the structural stability of the complexes in the crystal-free environment, the time evolution of several indicators commonly used in MD studies as the RMSD values of trajectory structures compared to the starting models, the gyration radius, and specific structural parameters including distances and angles were monitored. The systems reached a stable state within 50 ns of the simulation timescale with average RMSD values in the range 2.5-3.5 Å (Figure 2.6).

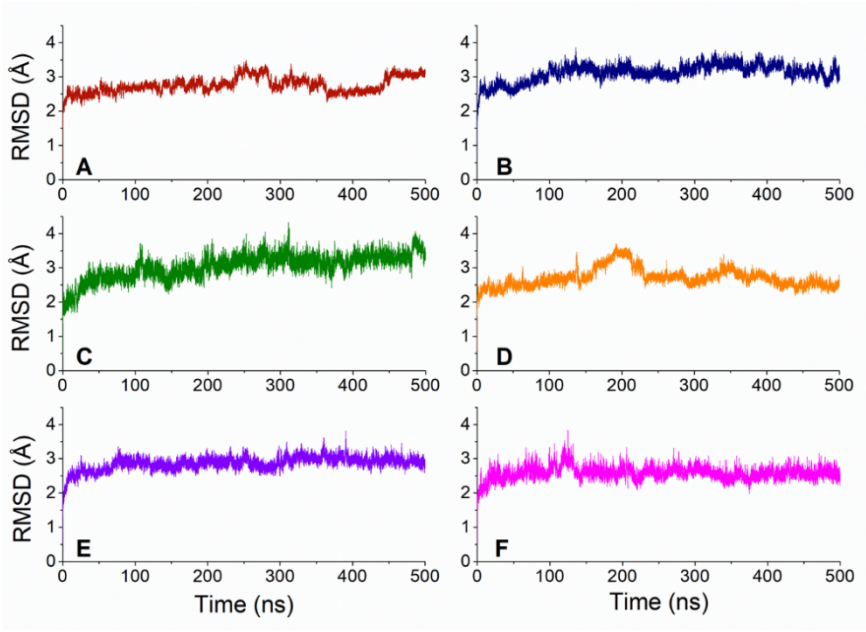

Figure 2.6. RMSD values computed on all atoms of the trajectory structures against the starting crystallographic models for A) free thrombin and B) TBA-thrombin, C) NU172-thrombin, D) HD22_27mer-thrombin, E) TBA-thrombin-HD22_27mer, and F) NU172-thrombin-HD22_27mer complexes.

As frequently observed in MD studies, the rapid increase of the RMSD values observed in Figure 2.6 can be attributed to a slight relaxation of the systems that are transferred from the crystal state to a solution-like environment. Despite this expected initial rearrangement, the systems do not show significant variations (< 1 Å) in their gyration radius (Figure 2.7).

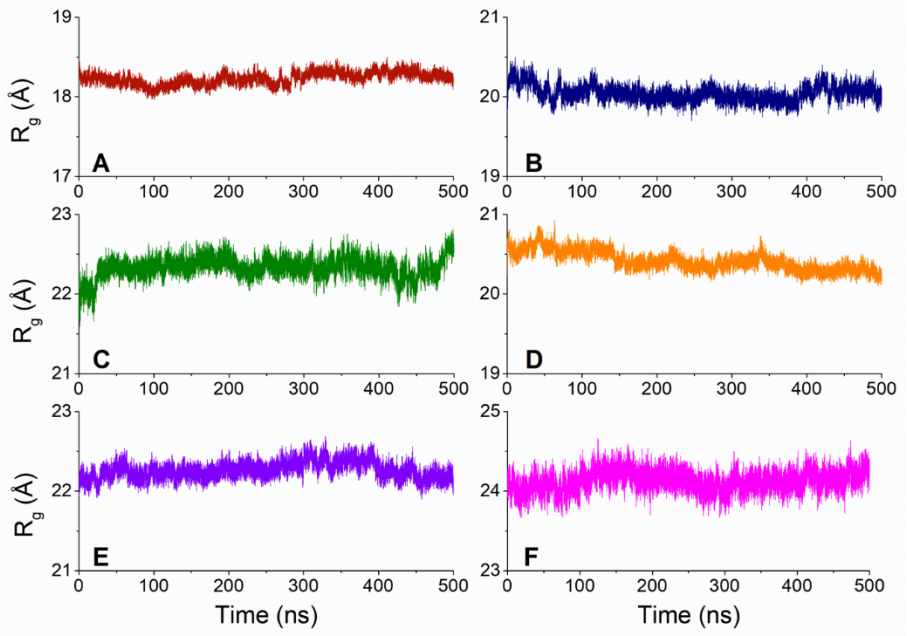

Figure 2.7. Gyration radius (R_g) of trajectory structures in the simulations of A) free thrombin and B) TBA-thrombin, C) NU172-thrombin, D) HD22_27mer-thrombin, E) TBA-thrombin-HD22_27mer, and F) NU172-thrombin-HD22_27mer complexes.

Moreover, despite some limited fluctuations (< 2.5 Å), the distance between the centres of mass of the protein and the aptamer(s) is well-preserved in the binary/ternary complexes (Figure 2.8). In addition, no significant variations (< 10°) in the angle between the centres of mass of the partners in the ternary complexes are observed (Figure 2.9).

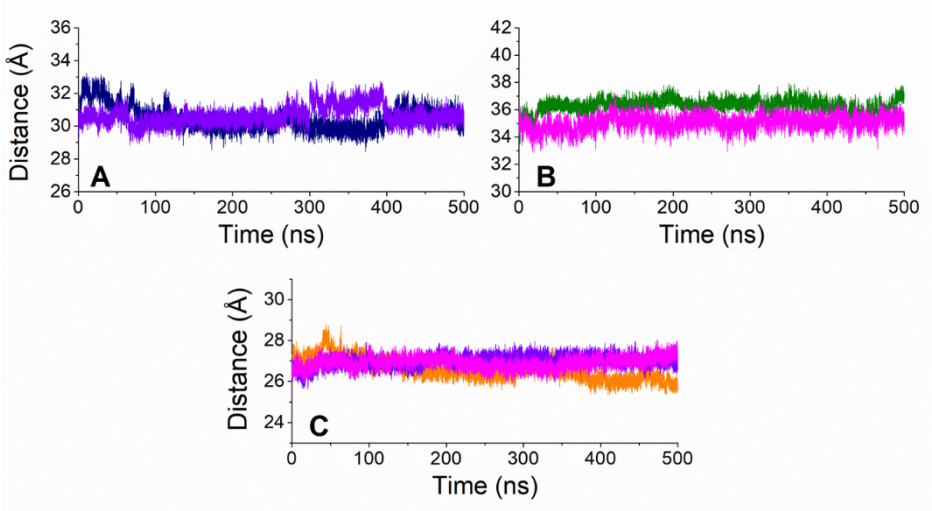

Figure 2.8. A) Distance between the centres of mass of thrombin and TBA in the TBA-thrombin (blue) and TBA-thrombin-HD22_27mer (violet) complexes. B) Distance between the centres of mass of thrombin and NU172 in the NU172-thrombin (green) and NU172-thrombin-HD22_27mer (magenta) complexes. C) Distance between the centres of mass of thrombin and HD22_27mer in the HD22_27mer-thrombin (orange), TBA-thrombin-HD22_27mer (violet), and NU172-thrombin-HD22_27mer (magenta) complexes.

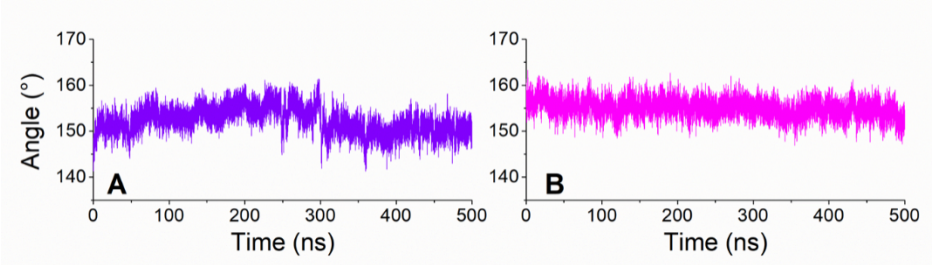

Figure 2.9. Angle between the centres of mass of thrombin and the two aptamers in the A) TBA-thrombin-HD22_27mer and B) NU172-thrombin-HD22_27mer complexes.

Altogether these data indicate that no major structural reorganizations of these complexes are observed when they are analysed in a crystal-free context.

This result is also corroborated by the analysis of specific features of the protein and of the aptamers in these simulations. The structural stability of thrombin is confirmed by the preservation of its secondary structure elements in the trajectory

structures. Indeed, with the exception of the α-helix encompassing protein residues 159-166 (CS 126-130) (for the correspondence between the MD notation, used in the dynamics simulations, and CS notation, used in the crystal structures, see Experimental section, Table 3.3), which is transient and tends to assume the 3_{10} helical conformation, all other secondary structures are well-preserved throughout the simulations (Figure 2.10 and Figure 2.11).

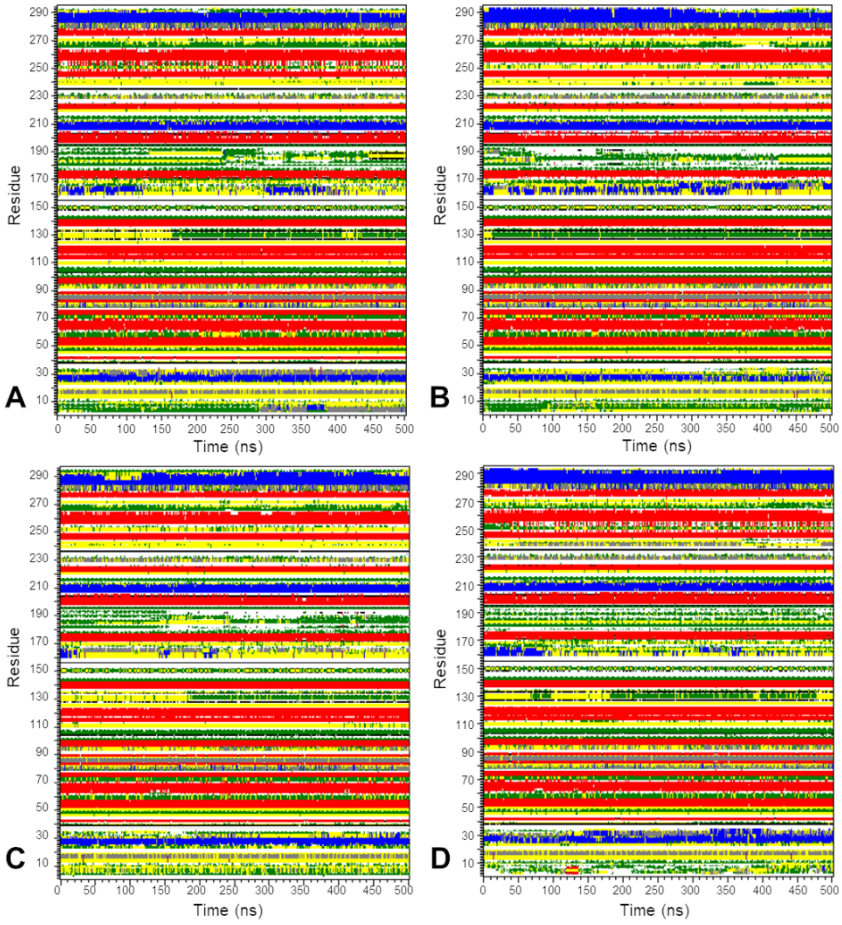

Figure 2.10. Time evolution of thrombin secondary structure elements in the simulations of A) free thrombin and B) TBA-thrombin, C) NU172-thrombin, and D) HD22_27mer-thrombin binary complexes. The colour code, as defined by the DSSP program, is the following: white for coil, red for β-sheet, black for β-bridge, green for bend, yellow for turn, blue for α-helix, purple for π-helix, and grey for 3_{10}-helix.

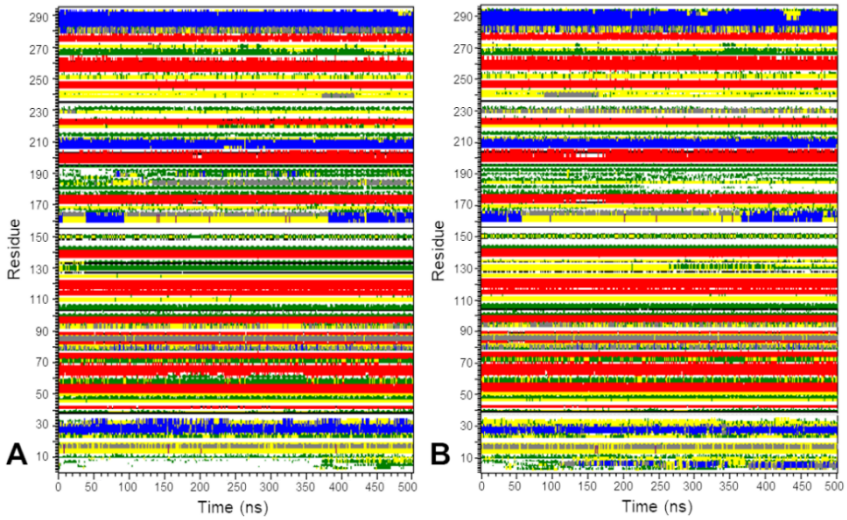

Figure 2.11. Time evolution of thrombin secondary structure elements in the simulations of A) TBA-thrombin-HD22_27mer and B) NU172-thrombin-HD22_27mer ternary complexes. The colour code, as defined by the DSSP program, is the following: white for coil, red for β-sheet, black for β-bridge, green for bend, yellow for turn, blue for α-helix, purple for π-helix, and grey for 3_{10}-helix.

Furthermore, the protein/aptamer gyration radius values of the trajectory frames are in line with those detected in the crystallographic structures of thrombin (~ 18 Å), TBA (~ 10 Å), NU172 (~ 12 Å), and HD22_27mer (~ 14 Å) (Figure 2.12 and Figure 2.13). Also, the number of intramolecular H-bonds (~ 230 for thrombin, ~ 17 for TBA, ~ 35 for NU172, and ~ 33 for HD22_27mer) is well-preserved throughout the MD simulations.

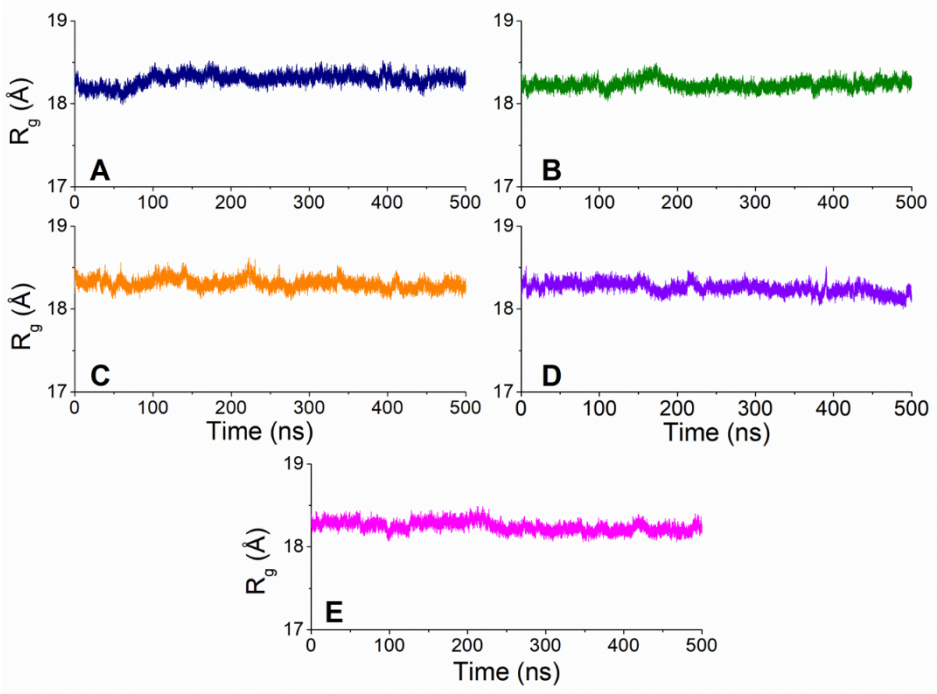

Figure 2.12. Thrombin gyration radius in the simulations of A) TBA-thrombin, B) NU172-thrombin, C) HD22_27mer-thrombin, D) TBA-thrombin-HD22_27mer, and E) NU172-thrombin-HD22_27mer complexes.

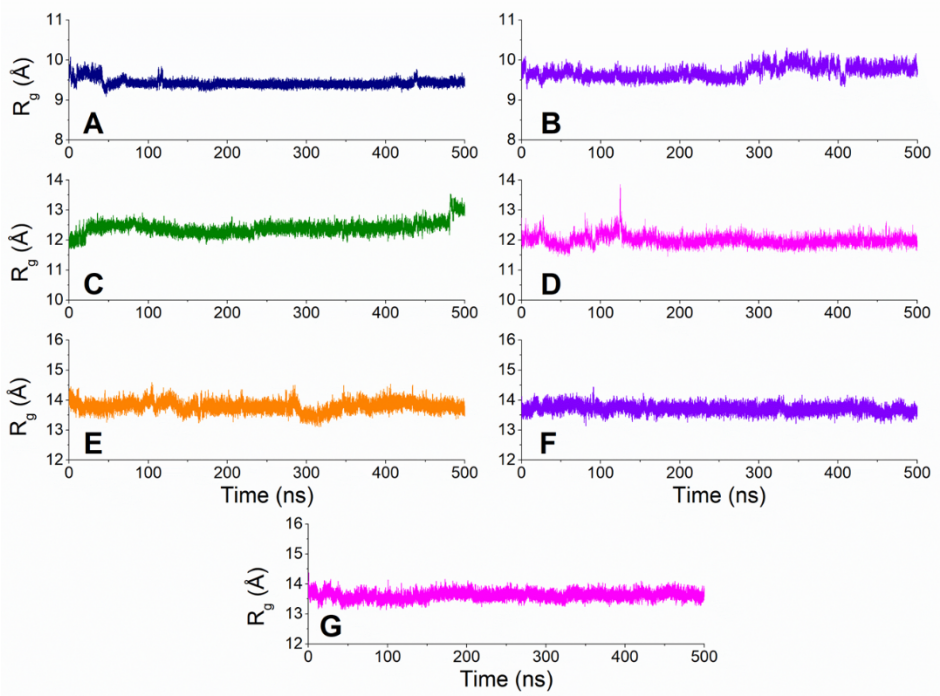

Figure 2.13. TBA gyration radius in the simulations of A) TBA-thrombin and B) TBA-thrombin-HD22_27mer complexes. NU172 gyration radius in the simulations of C) NU172-thrombin and D) TBA-thrombin-HD22_27mer complexes. HD22_27mer gyration radius in the simulations of E) HD22_27mer-thrombin, F) TBA-thrombin-HD22_27mer, and G) NU172-thrombin-HD22_27mer complexes.

Dynamic view of the protein-thrombin interactions in the binary and ternary complexes

The protein-aptamer interactions, both hydrophilic and hydrophobic, that were found to stabilize the crystallographic structures of the binary and ternary complexes were analysed from a dynamic point of view.

Most of the H-bonding interactions detected in the starting crystallographic models are either permanent or transient in the simulations of the binary and ternary complexes. It is also worth noting that some H-bonds, which are not present in the crystal structure of the binary complex but were found to stabilize the ternary complex, are formed throughout the MD simulation of the binary

complexes. *Vice versa*, interactions that are not detected in the crystal structure of the ternary complex but found in the crystal structure of binary complexes are formed in the simulation of the ternary ones. This observation indicates that some of the differences emerged from the comparison of the crystal structures are due to the different packing environment and not to the different binding state of the thrombin. The preservation of the hydrophobic interactions that stabilize the aptamer-thrombin interface in the complexes has been also evaluated by computing the distances between the centres of mass of the residues/nucleotides involved in these contacts in the trajectory structures. Their time evolution indicates that a good level of preservation is achieved in all simulations.

Structural flexibility of the thrombin in the MD simulations

The identification and characterization of thrombin flexible regions as function of context (free or bound) was preceded by the analysis of the residues that exhibit large displacements in the simulations. The inspection of the deviations of the average MD structure from the crystallographic starting model in terms of RMSD *per* residue values (Figure 2.14) indicates that, as expected, highest displacements (RMSD values > 4 Å) are exhibited by the terminal residues of the protein chains and by the unstructured regions, in particular the γ-autolysis loop (MD residues 184-191; CS residues 148-150). On the other hand, residues belonging to the secondary structure elements do not display significant deviations (RMSD values < 1 Å).

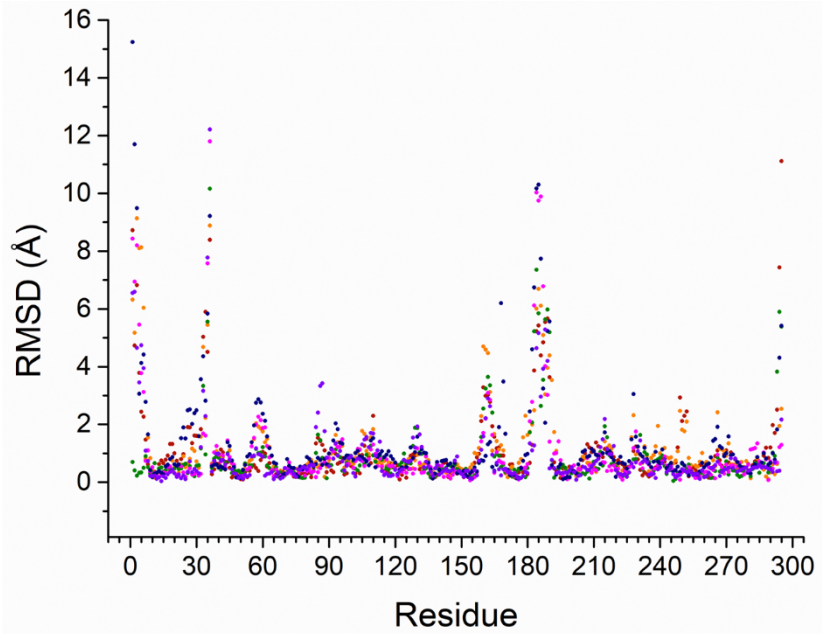

Figure 2.14. The RMSD *per* residue values of the average structures computed in the 100-500 ns region of the MD trajectories of free thrombin (red) and TBA-thrombin (blue), NU172-thrombin (green), HD22_27mer-thrombin (orange), TBA-thrombin-HD22_27mer (violet), and NU172-thrombin-HD22_27mer (magenta) complexes *versus* the crystallographic starting models. RMSD values are computed on the C^{α} atoms of thrombin.

The regions showing large RMSD *per* residue values exhibit also large root-mean-square fluctuations (RMSF) (Figure 2.15). As expected on the basis of the involvement of some mobile regions of the free thrombin in the aptamer anchoring, the highest fluctuations are exhibited by the unbound protein. Interestingly, a limited mobility of the free exosites in the binary complexes was observed. Specifically, in HD22_27mer-thrombin, where the HD22_27mer is bound to exosite II, the exosite I residues are less flexible compared to the unbound thrombin. Similarly, residues of exosite II of TBA-thrombin and NU172-thrombin display lower fluctuations compared to the free protein.

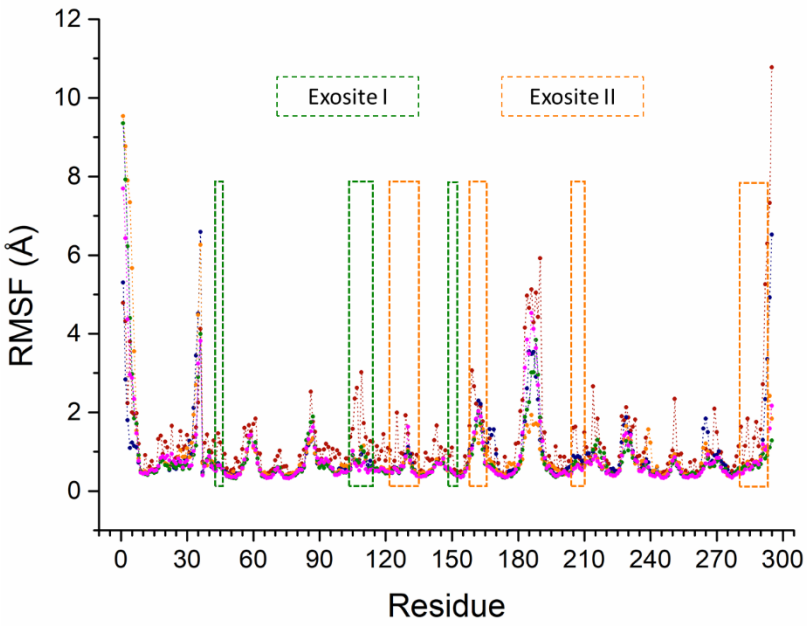

Figure 2.15. RMSF values computed on thrombin C^{α} atoms in the 100–500 ns region of the MD trajectories in the simulations of free thrombin (red) and TBA-thrombin (blue), NU172-thrombin (green), HD22_27mer-thrombin (orange), TBA-thrombin-HD22_27mer (violet), and NU172-thrombin-HD22_27mer (magenta) complexes. Green and orange dashed boxes identify residues of exosites I and II, respectively.

To gain further insights into this issue, the dynamical behaviour of the two thrombin exosite was monitored. Although the different binding states of thrombin, residues of exosite I adopt similar conformations in the crystallographic models of both free and liganded thrombin (Figure 2.16A). On the other hand, the superimposition of the average protein structures computed in the equilibrated regions of MD trajectories shows a conformational reorganization of exosite I residues in the case of free thrombin (Figure 2.16B). The inspection of the trajectory structures of the exosite I in the unbound thrombin unravels a rather dynamic behaviour of this region as indicated by the relatively high RMSF values (Figure 2.15).

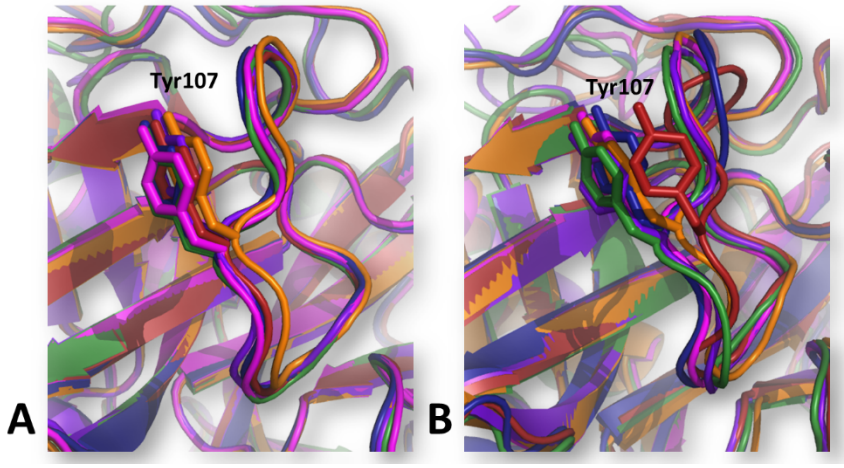

Figure 2.16. Detail of the exosite I in the superimposition of A) the starting crystallographic structures and B) the average structures computed in the region 100–500 ns of the MD simulations of free thrombin (red) and TBA-thrombin (blue), NU172-thrombin (green), HD22_27mer-thrombin (orange), TBA-thrombin-HD22_27mer (violet), and NU172-thrombin-HD22_27mer (magenta) complexes.

To analyse the structure and the dynamics of the exosite I, the C^{α}-C^{α} distance of two residues, Arg104 (CS 73) and Asn110 (CS 78), that are part of the main segment of the site, was monitored. This distance, which is 15.7 Å in the starting crystallographic model, assumes a range of values centred at 15.0 Å in the simulation of the free thrombin (Figure 2.17). This distance presents a similar distribution of values in the simulations of the aptamer(s)-thrombin complexes with the most populated state at 16.0 Å, independently of the binding state of the exosite I (Figure 2.17). In line with the analysis of the RMSF values reported above, the flexibility of the unbound exosite I of HD22_27mer-thrombin is significantly more similar to that observed in the complexes where the site is bound (TBA-thrombin, NU172-thrombin, TBA-thrombin-HD22_27mer, and NU172-thrombin-HD22_27mer) compared to free thrombin. These observations suggest a cross-talk between the two exosites.

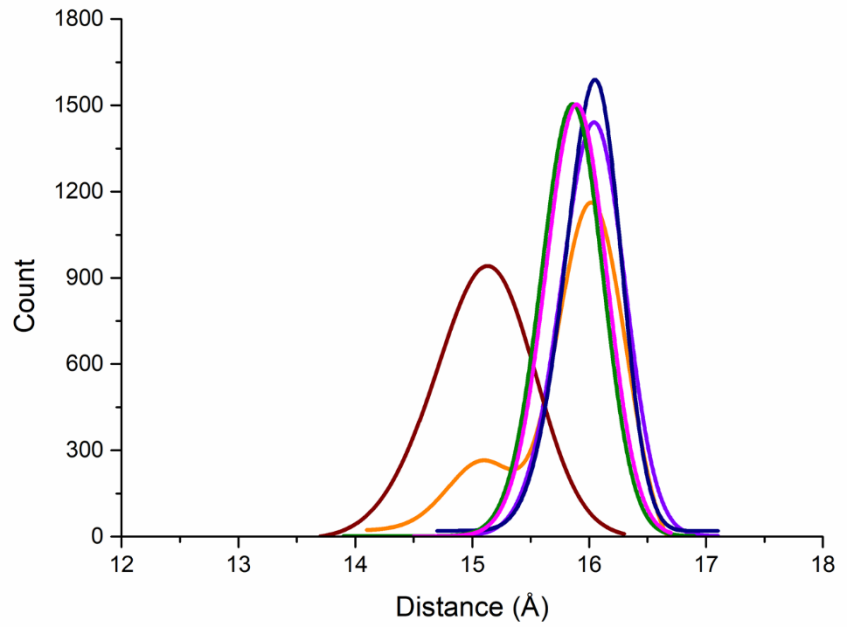

Figure 2.17. Distribution of the C^a-C^a distance of the exosite I residues Arg104 (CS 73) and Asn110 (CS 78) in the simulations of free thrombin (red) and TBA-thrombin (blue), NU172-thrombin (green), HD22_27mer-thrombin (orange), TBA-thrombin-HD22_27mer (violet), and NU172-thrombin-HD22_27mer (magenta) complexes.

Thrombin exosite II covers a significantly much larger protein surface than exosite I and involves the peptide segments: 121-134 (CS 89-101), 159-166 (CS 126-130), 205-210 (CS 164-169) and 280-293 (CS 232-245). As shown in Figure 2.15, the RMSF values of the free thrombin are generally higher than those found in the simulations carried out on the complexes, which present very similar trends independently of the binding state of the exosite II. It is worth mentioning that the exosite II fragment 159-166 (CS 126-130) keeps a significant mobility also in the complexes. Of particular interest is the behaviour of the thrombin heavy chain C-terminal region (MD residues 280-293, CS residues 232-245). As shown in Figure 2.18A, this region adopts the conformation of the free thrombin in the starting models of the TBA- and NU172-thrombin binary complexes.

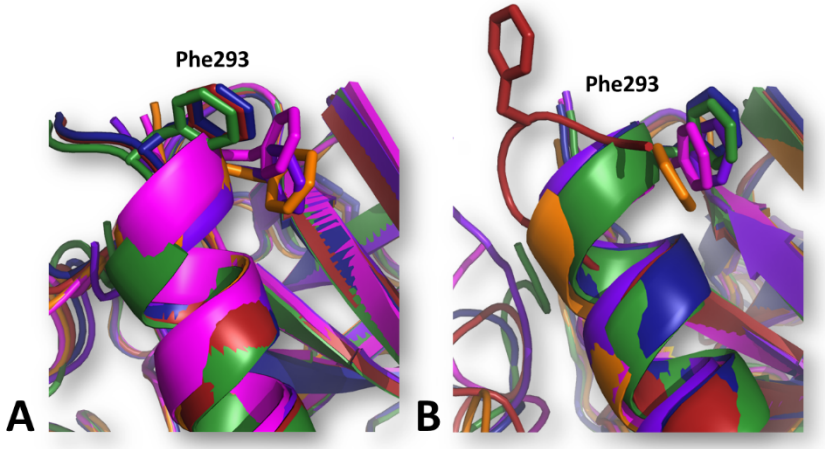

Figure 2.18. Detail of the exosite II in the superimposition of A) the starting models and B) the average structures computed in the region 100–500 ns of the MD simulations of free thrombin (red) and TBA-thrombin (blue), NU172-thrombin (green), HD22_27mer-thrombin (orange), TBA-thrombin-HD22_27mer (violet), and NU172-thrombin-HD22_27mer (magenta) complexes.

On the other hand, a structural variation is observed in the X-ray models of the ternary complexes as shown by the position of the side chain of residue Phe293 (CS Phe245). To monitor the conformational behaviour of this portion the C^{α}-C^{α} distance between two residues, Phe280 (CS 232) and Phe293 (CS 245), that delimitate this exosite II segment, was computed in the MD simulations (Figure 2.19). This distance assumes a wide range of values (18-26 Å) in the trajectory frames of the unbound protein. Conversely, it is interesting to note that in TBA- and NU172-thrombin trajectory structures the distance preferentially adopts the values (19-21 Å) observed in the MD structures of the ternary complexes with the exosite II bound by HD22_27mer (Figure 2.19). These data suggest that the binding of TBA or NU172 at the exosite I favours a conformational state of the exosite II that is prone to the anchoring of the other aptamer. The superimposition of the MD average structures in Figure 2.18B clearly shows that in the simulation of the binary complexes the Phe293 evolves toward the state observed in the structure of the ternary complexes where the exosite II is occupied.

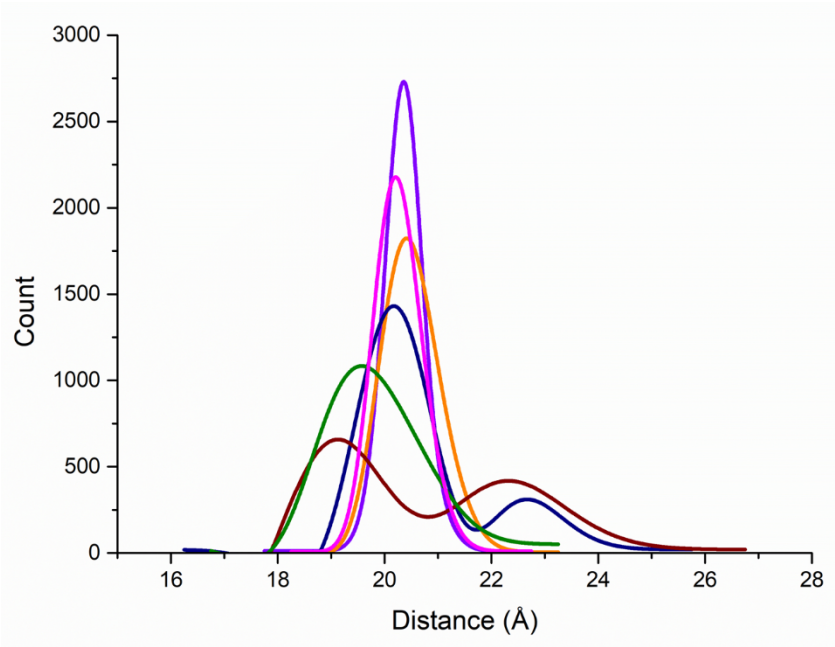

Figure 2.19. Distribution of the C^{α}-C^{α} distance of the exosite II residues Phe280 (CS 232) and Phe293 (CS 245) in the simulations of free thrombin (red) and TBA-thrombin (blue), NU172-thrombin (green), HD22_27mer-thrombin (orange), TBA-thrombin-HD22_27mer (violet), and NU172-thrombin-HD22_27mer (magenta) complexes.

Altogether these observations suggest that the binding of the TBA or NU172 at the exosite I favours a conformational state of the exosite II prone to the aptamer binding, and *vice versa*.

Structural flexibility of the aptamers in the MD simulations

The comparison of the crystal structures of TBA, NU172, and HD22_27mer have disclosed a different dynamic behaviour of the three aptamers. Indeed, while the structure of TBA and NU172 appears to be highly invariant as function of the context, on the other hand, Gua12 and Gua13 nucleobases of HD22_27mer are significantly reoriented in NU172-thrombin-HD22_27mer when compared to their state in the HD22_27mer-thrombin binary complex[83] (Figure 2.3) and form different intramolecular interactions (Table 2.3).

Table 2.3. List of contacts involving the Gua12 and Gua13 nucleobases of HD22_27mer detected in the crystallographic structures of HD22_27mer-thrombin (PDB code: 4I7Y)[83], TBA-thrombin-HD22_27mer (PDB code: 5EW1)[95], and NU172-thrombin-HD22_27mer complexes. The green/red colour denotes the presence/absence of the specific interaction.

Distance (Å)	HD22_27mer-thrombin	TBA-thrombin-HD22_27mer	NU172-thrombin-HD22_27mer
$Gua12^{O6}$-$Gua7^{N7}$	2.32	2.83	3.33
$Gua12^{N2}$-$Gua13^{N1}$	3.07	7.29	4.98
$Gua12^{N2}$-$Gua16^{O6}$	9.48	2.69	3.17
$Gua12^{N1}$-$Gua7^{N7}$	4.40	2.76	2.93
$Gua12^{N2}$-$Gua7^{O6}$	8.55	2.84	3.13
$Gua13^{O6}$-$Gua7^{OP1,2}$	2.73/2.93	3.51/3.28	3.78/5.84
$Gua13^{N7}$-$Gua7^{OP2}$	2.86	3.30	6.48
$Gua13^{N1}$-$Gua7^{OP1}$	4.80	5.48	3.17
$Gua13^{N2}$-$Thy6^{O3'}$	9.04	9.57	2.89

These nucleobases assume an intermediate state in the TBA-thrombin-HD22_27mer ternary complex (Figure 2.20).[95] Analysing the three MD simulation where HD22_27mer was bound to thrombin, the dynamic behaviour of these different states of HD22_27mer was evaluated.

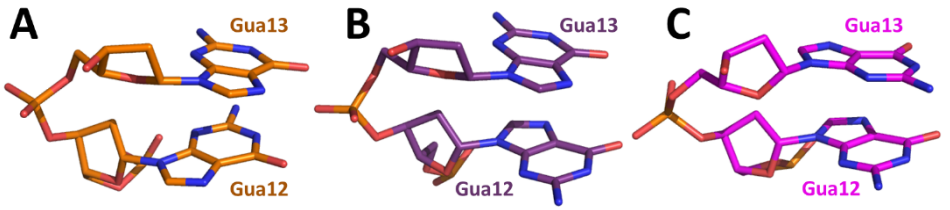

Figure 2.20. View of the conformations adopted by Gua12 and Gua13 nucleobases of HD22_27mer in the crystallographic structures of A) HD22_27mer-thrombin binary complex (PDB code: 4I7Y)[83], B) TBA-thrombin-HD22_27mer ternary complex (PDB code: 5EW1)[95], and C) NU172-thrombin-HD22_27mer ternary complex.

The inspection of the total number of intramolecular H-bonds indicate that the HD22_27mer state detected in NU172-thrombin-HD22_27mer is, on average, stabilized by a significantly higher number of bonds (Figure 2.21).

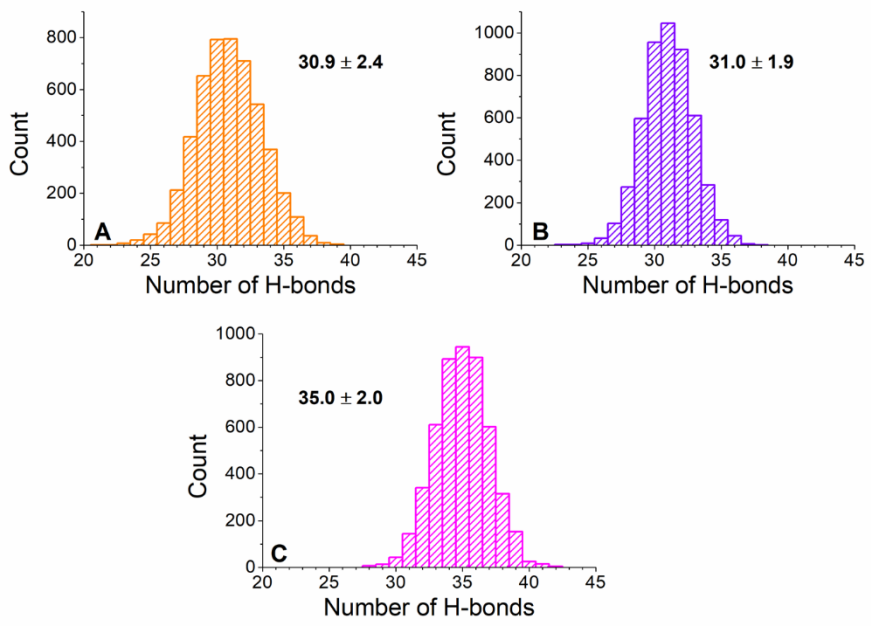

Figure 2.21. Distribution of the number of HD22_27mer intramolecular H-bonds in the simulations of A) HD22_27mer-thrombin, B) TBA-thrombin-HD22_27mer, and C) NU172-thrombin-HD22_27mer complexes. The average values with standard deviations are reported.

In particular, the inspection of the preservation of the interactions made by Gua12 and Gua13 clearly indicates that the mobility of the first nucleobase in the ternary complexes is significantly lower than that found in HD22_27mer-thrombin (Figure 2.22), whereas the flexibility of the second nucleobase decreases only in the NU172-thrombin-HD22_27mer complex (Figure 2.22).

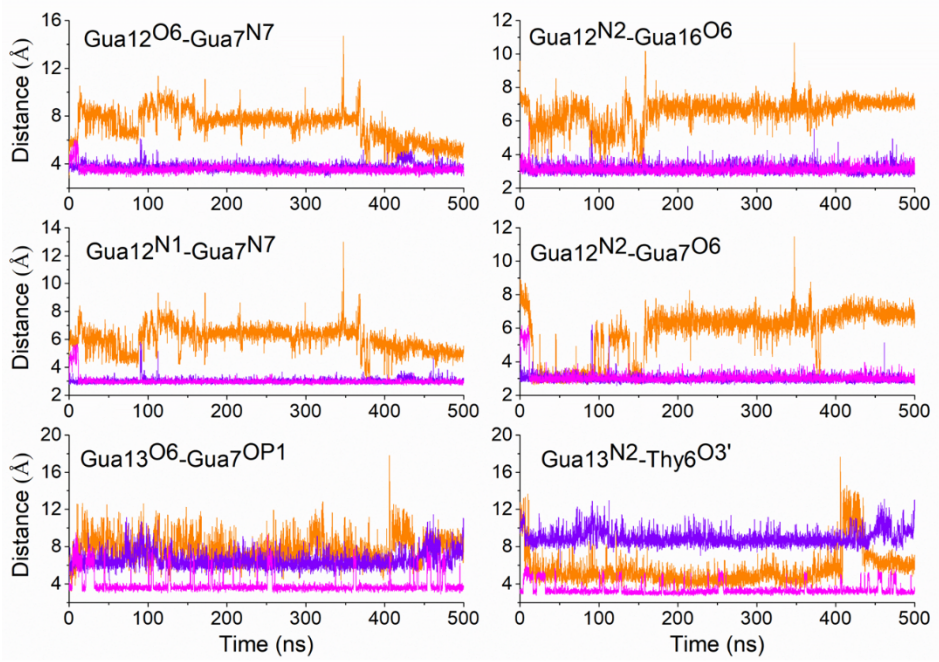

Figure 2.22. Representative examples of interactions involving Gua12 or Gua13 nucleobases of HD22_27mer (see Table 2.3) in the simulations of HD22_27mer-thrombin (orange), TBA-thrombin-HD22_27mer (violet), and NU172-thrombin-HD22_27mer complexes (magenta).

2.1.3. Anticoagulant activity of NU172 in the ternary complex

The positive effect on the binding affinity and/or anticoagulant activity of TBA when HD22 aptamers are bound to the exosite II has been widely discussed in the literature.[93,94,162,165] Considering the limited functional data on NU172 and the indications emerged from the MD studies, the ability of the NU172 to compete with fibrinogen for thrombin exosite I in either the absence or the presence on exosite II of HD22_27mer was evaluated by performing a spectrophotometric fibrinogen clotting assay.

Interestingly, when HD22_27mer was bound to thrombin exosite II, a net enhancement of the anticoagulant activity of NU172 was revealed (Figure 2.23). While no variation of the anticoagulant activity of NU172 was detected in the

presence of an equimolar amount of IGA3, an insulin binding aptamer that adopts a parallel G-quadruplex structure,[166] which was used as negative control. It must be underlined that both HD22_27mer and IGA3 are not able to inhibit the cleavage of fibrinogen by thrombin, showing a clotting time comparable to the basal value determined in the absence of oligonucleotides.

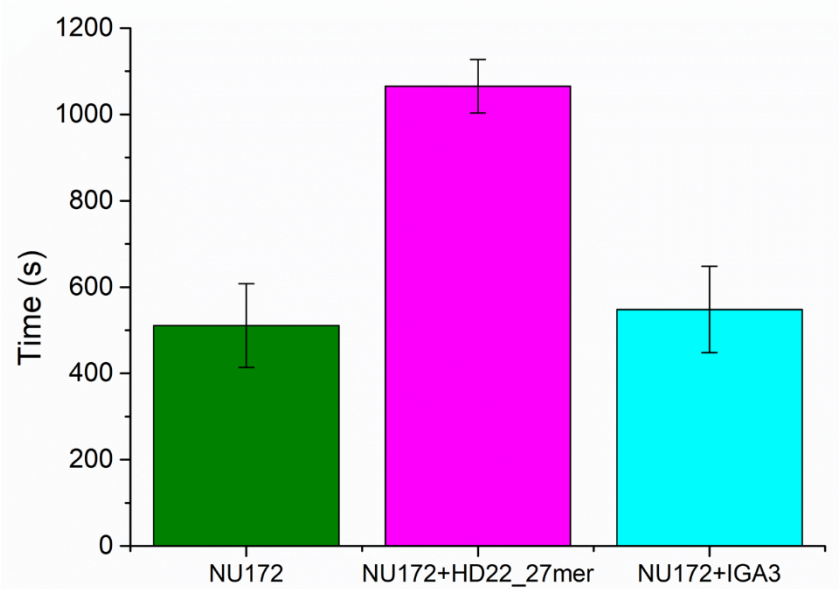

Figure 2.23. Prolonged fibrinogen clotting times measured in PBS in the presence of fibrinogen (1.8 mg mL^{-1}), thrombin (5 nM), and aptamer(s) (40 nM).

2.2. Modified thrombin binding aptamers

The application of chemical modifications to protect oligonucleotide aptamers from being degraded by endogenous, ubiquitous nucleases and from being rapidly cleared through glomerular filtration has been valuable to optimize aptamer performances.[167–169]

In this subsection, the crystal structures of the complexes between thrombin and three TBA mutants with N3-modified Thy3 (TBA-3L, TBA-3G, and TBA-3Leu) are described. Moreover, a preliminary analysis of the X-ray structures of the thrombin complexes with cyclic- and *pseudo*-cyclic TBA analogues (cycTBA II

and TBA NN/DD) is reported. Finally, the spectroscopic studies performed on NU172 variants incorporating hexitol nucleotides are presented.

The results reported in the paragraphs 2.2.1 and 2.2.3 are, respectively, part of the two following publications:[129,133]

- Smirnov, I., Kolganova, N., Troisi, R., Sica, F. & Timofeev, E. Expanding the recognition interface of the thrombin-binding aptamer HD1 through modification of residues T3 and T12. *Mol Ther Nucleic Acids.* **23**, 863-871 (2021).
- De Fenza, M., Eremeeva, E., Troisi, R., Yang, H., Esposito, A., Sica, F., Herdewijn, P., D'Alonzo, D. & Guaragna, A. Structure-activity relationship study of a potent α-thrombin binding aptamer incorporating hexitol nucleotides. *Chem Eur J.* **26**, 9589-9597 (2020).

2.2.1. Crystal structures of TBA-3L, -3G, and -3Leu in complex with thrombin

As part of a collaboration with the group of Dr. Edward Timofeev, the effects of Thy3 N3-modification on the TBA folding and on its interaction with thrombin was investigated (see Introduction, paragraph 1.4.1). In particular, a structural characterization of thrombin complexes with the three TBA variants (TBA-3L, TBA-3G and TBA-3Leu; Figure 1.9) with the highest affinities was carried out.
Isomorphous trigonal $P3_221$ crystals with one 1:1 aptamer-protein complex in the asymmetric unit were grown for the three complexes. Detailed statistics on data collection and refinement are reported in Table 2.4, Table 2.5, and Table 2.6.
As expected, the TBA variants binding does not substantially modify the thrombin structure. After superposition of the C^{α} heavy chain of the present structures with that of the PPACK inhibited enzyme (PDB code: 1PPB)[60,61] the value of RMSD is in the range 0.44-0.57 Å.

Table 2.4. Crystallographic statistics for the TBA-3L-thrombin complex. Values in brackets refer to the highest resolution shell.

	TBA-3L-thrombin
Crystal data	
Space group	$P3_221$
Unit-cell parameters	
a, b, c (Å)	94.92, 94.92, 125.40
α, β, γ (deg)	90.00, 90.00, 120.00
V_M ($Å^3$ Da^{-1})	3.90
No. of complexes in the asymmetric unit	1
Solvent content (%)	68.5
Data Collection	
Resolution limits (Å)	82.20 - 1.58 (1.76 - 1.58)
Unique reflections	54291 (2718)
Completeness (%)	95.9 (81.2)
Average multiplicity	19.6 (10.6)
$\langle I/\sigma(I) \rangle$	23.2 (2.0)
$CC_{1/2}$	1.0 (0.8)
Refinement	
Resolution limits (Å)	82.20 - 1.58
No. of reflections	51616
R_{factor}/R_{free}	0.180/0.206
No. of atoms	2828
Average B factors ($Å^2$)	27.47
R.m.s. deviations	
Bond lengths (Å)	0.015
Bond angles (deg)	2.220
Ramachandran plot, residues in (%)	
Favoured regions	97.2
Allowed regions	2.8
Outliers	0
PDB code	6Z8V

Table 2.5. Crystallographic statistics for the TBA-3G-thrombin complex. Values in brackets refer to the highest resolution shell.

	TBA-3G-thrombin
Crystal data	
Space group	$P3_221$
Unit-cell parameters	
a, b, c (Å)	94.80, 94.80, 125.33
α, β, γ (deg)	90.00, 90.00, 120.00
V_M (Å^3 Da^{-1})	3.90
No. of complexes in the asymmetric unit	1
Solvent content (%)	68.5
Data Collection	
Resolution limits (Å)	125.33 - 1.73 (1.94 – 1.73)
Unique reflections	41910 (2097)
Completeness (%)	94.4 (72.0)
Average multiplicity	20.1 (15.6)
$\langle I/\sigma(I)\rangle$	19.0 (1.9)
$CC_{1/2}$	1.0 (0.7)
Refinement	
Resolution limits (Å)	82.10 - 1.73
No. of reflections	39863
R_{factor}/R_{free}	0.178/0.207
No. of atoms	2796
Average B factors (Å^2)	32.95
R.m.s. deviations	
Bond lengths (Å)	0.016
Bond angles (deg)	2.304
Ramachandran plot, residues in (%)	
Favoured regions	97.1
Allowed regions	2.9
Outliers	0
PDB code	6Z8W

Table 2.6. Crystallographic statistics for the TBA-3Leu-thrombin complex. Values in brackets refer to the highest resolution shell.

	TBA-3Leu-thrombin
Crystal data	
Space group	$P3_221$
Unit-cell parameters	
a, b, c (Å)	94.67,94.67, 124.69
α, β, γ (deg)	90.00, 90.00, 120.00
V_M ($Å^3$ Da^{-1})	3.88
No. of complexes in the asymmetric unit	1
Solvent content (%)	68.3
Data Collection	
Resolution limits (Å)	81.99 - 2.53 (2.96 - 2.53)
Unique reflections	6793 (341)
Completeness (%)	91.5 (77.8)
Average multiplicity	19.2 (18.1)
$\langle I/\sigma(I)\rangle$	10.7 (1.8)
$CC_{1/2}$	1.0 (0.7)
Refinement	
Resolution limits (Å)	81.99 - 2.53
No. of reflections	6123
R_{factor}/R_{free}	0.245/0.291
No. of atoms	2511
Average B factors ($Å^2$)	69.54
R.m.s. deviations	
Bond lengths (Å)	0.002
Bond angles (deg)	0.764
Ramachandran plot, residues in (%)	
Favoured regions	87.0
Allowed regions	13.0
Outliers	0
PDB code	6Z8X

Similarly to the unmodified TBA,[66] the refined models of the aptamers adopt a G-quadruplex structure with a chair-like antiparallel fold. A potassium ion is sandwiched between G-tetrad I and II, which are formed by guanines 2, 5, 11, 14 and 1, 6, 10, 15, respectively. Thy3(modified)-Thy4, Thy12-Thy13 and Thy7-Gua8-Thy9 are involved in the formation of the three edge-wise loops. Resembling TBA,[66] the TT loops of the G-quadruplex domain act as a pincer-like system that captures the protruding region of exosite I (Figure 2.24).

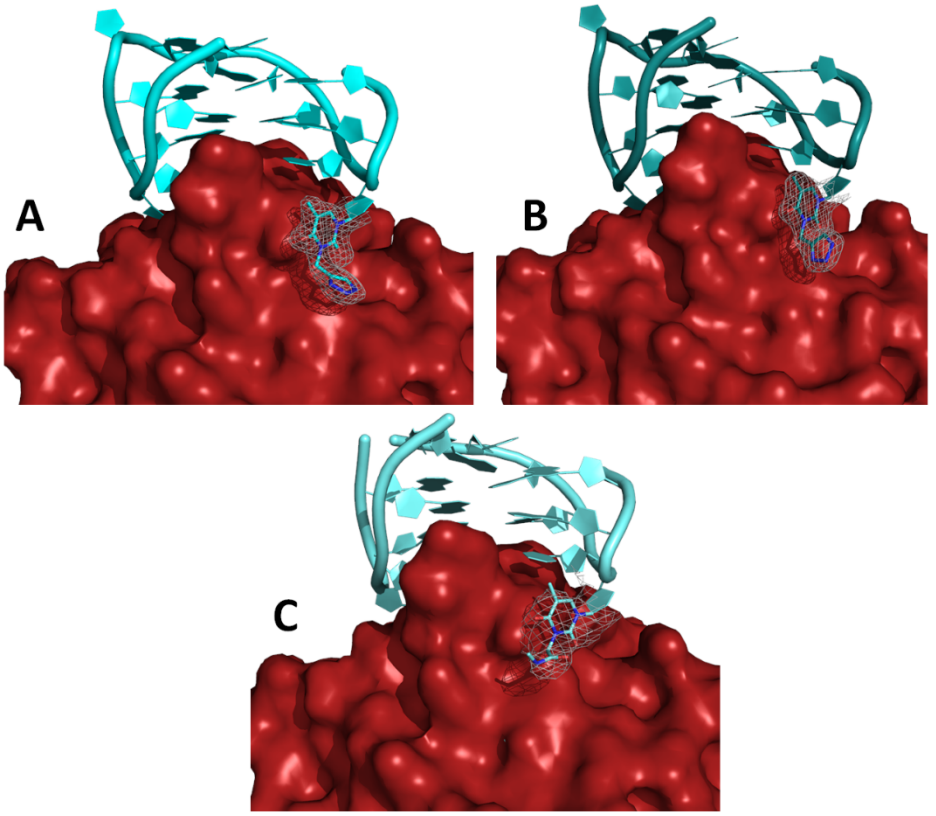

Figure 2.24. Cartoon/surface views of the A) TBA-3L-thrombin, B) TBA-3G-thrombin, and C) TBA-3Leu-thrombin interfaces. The $2F_o–F_c$ electron density maps of the modified nucleobases contoured at the 1.0 σ level are highlighted. Thrombin is coloured in red, and TBA-3L, -3G, and -3Leu are coloured in cyan, dark cyan, and light cyan, respectively.

It has to be recalled that exosite I is actually split into two regions: A, formed by Arg75, Glu77, Arg77A, Asn78 and Ile79, and B, formed by Arg75 and Tyr76. The binding of TBA at the A-region of the thrombin engages a higher contact area compared with the B-region.[70]

Interestingly, due to the steric hindrance of Thy3 modifications that could hamper the interactions with exosite I A-region, in the three complexes the modified thymine interacts through a π-π stacking with Tyr76 belonging to the exosite I B-region (Figure 2.25).

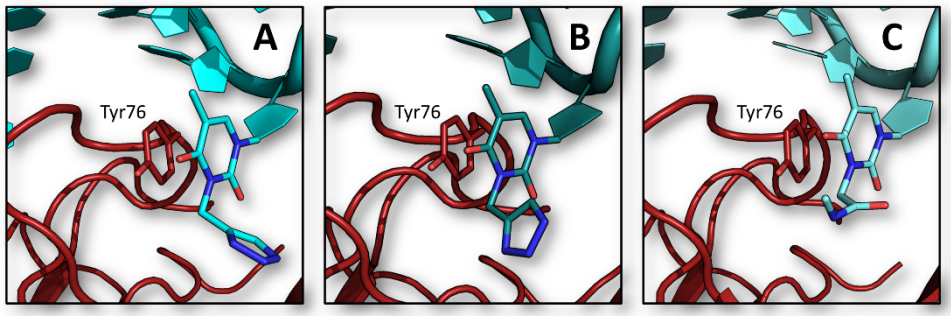

Figure 2.25. Cartoon views of the stacking interaction between the Tyr76 in the B-region of thrombin exosite I and the modified thymine bases of A) TBA-3L, B) TBA-3G, and C) TBA-3Leu. Thrombin is coloured in red, and TBA-3L, -3G, and -3Leu are coloured in cyan, dark cyan, and light cyan, respectively.

Being the A-region well modelled to host a native loop, chemical modifications of one of the two TT loops modulate the binding affinity of the parent aptamer by increasing or decreasing the contacts of the oligonucleotide with the exosite I B-region.[70] This, indeed, has been observed in the crystal structures of the three complexes, although only a part of the chemical substituents of Thy3 is detectable in the electron density. Indeed, the visible part of the Thy3 substituents shields a protein hydrophobic patch, including the side chain of Ile82, from water contact thus extending the contact area between the aptamer and the thrombin surface.

Moreover, albeit crystallized in the presence of potassium ions, the structures of the mutated TBAs are more similar to that of TBA observed in the presence of

Na^+ (TBA-Na, PDB code: 4DIH)[66] than that in the presence of K^+ (TBA-K, PDB code: 4DII)[66] (Figure 2.26), as indicated by the RMSD values reported in Table 2.7.

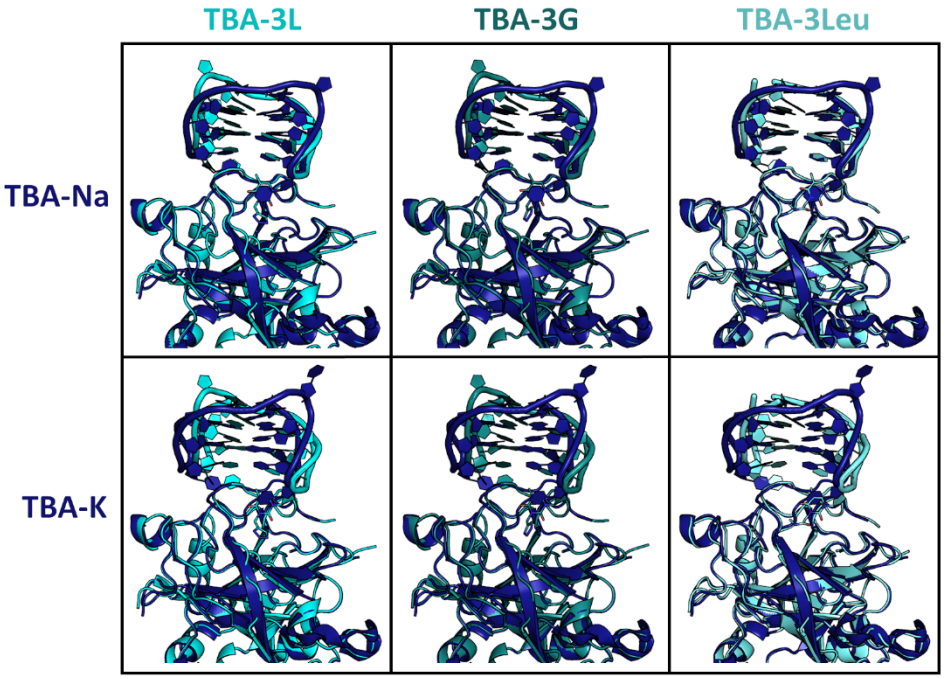

Figure 2.26. Comparison between the crystal structures of TBA-Na-thrombin (PDB code: 4DIH)[66] and TBA-K-thrombin (PDB code: 4DII)[66] with those of TBA-3L-thrombin, TBA-3G-thrombin, and TBA-3Leu-thrombin, after the superposition of the protein.

Table 2.7. RMSD values obtained by the superposition of all atoms of the TBA structures (PDB codes: 4DIH and 4DII)[66] and the TBA-3L, TBA-3G, and TBA-3Leu structures. The nucleotides of the TGT loop were not considered in the analysis because the unmodified and modified TBAs rotate 180° around the G-quadruplex axis.

	TBA-Na	**TBA-K**
TBA-K	0.67 Å	-
TBA-3L	0.43 Å	0.80 Å
TBA-3G	0.44 Å	0.79 Å
TBA-3Leu	0.64 Å	0.69 Å

It has been reported that in the presence of sodium the flexibility of unmodified aptamer increases, allowing a better fit on the thrombin surface and an

optimization of the intermolecular contacts.[66] A similar effect has been observed in the complexes of thrombin with the modified TBAs which show an increase in the number of aptamer-protein interactions and in the interface area (Table 2.8) with respect to TBA-K-thrombin complex.

Table 2.8. Interface interactions and areas of the complexes between thrombin and TBA in the presence of sodium ions (PDB code: 4DIH)[66] or potassium ions (PDB code: 4DII)[66], TBA-3L, TBA-3G, and TBA-3Leu.

	TBA-Na	**TBA-K**	**TBA-3L**	**TBA-3G**	**TBA-3Leu**
Thy A (in A-region)	Ile24 Arg75 Glu77 Ile79 Tyr117	Ile24 His71 Ile79 Tyr117	Ile24 Arg75 Glu77 Ile79 Tyr117	Ile24 Arg75 Glu77 Ile79 Tyr117	Ile24 His71 Glu77 Ile79 Tyr117
Thy B (in A-region)	Arg75 Arg77A Asn78 Ile79	Arg75 Arg77A Asn78 Ile79	Arg75 Arg77A Asn78 Ile79	Arg75 Arg77A Asn78 Ile79	Arg75 Arg77A Asn78 Ile79
Thy C (in B-region)	Tyr76 Ile82	Tyr76	Tyr76 Ile82	Tyr76 Ile82	Tyr76 Ile82
Thy D (in B-region)	Arg75 Tyr76 Arg77A	Thr74 Arg75 Tyr76 Arg77A	Thr74 Arg75 Tyr76 Arg77A	Thr74 Arg75 Tyr76 Arg77A	Arg75 Tyr76 Arg77A
Gua (G-quadruplex)	Thr74 Arg75 Arg77A	Arg75 Arg77A Asn78	Thr74 Arg75 Arg77A Asn78	Thr74 Arg75 Arg77A Asn78	Thr74 Arg75 Arg77A Asn78
Interface area (Å^2)	565	543	606	606	592

Interestingly, the contact areas between thrombin and the modified TBAs are even slightly greater than those found in the TBA-Na-thrombin complex (Table 2.8). This finding could be interpreted in terms of a significant increase of the aptamer flexibility induced by the modification on the Thy3. The modified aptamers are indeed able to overcome the stiffness of the two tetrads, due to the binding of the

potassium ion, thus optimizing their adhesion to the thrombin exosite I. In addition, it can be surmised that the modified residues could be involved in transient interactions with the protein surfaces providing a further contribution to the binding.

Altogether, these results could explain the observed increase in binding affinity toward thrombin for TBA-3L, TBA-3G, and TBA-3Leu variants with respect to the parent aptamer.

2.2.2. Crystal structures of cycTBA II and TBA NN/DD in complex with thrombin

In order to gain insight in the effects of 5′ and 3′ terminal modifications (see Introduction, paragraph 1.4.2) on the folding of TBA and on its interaction with thrombin, the crystal structures of a cyclic (cycTBA II) and a *pseudo*-cyclic (TBA NN/DD) oligonucleotide (Figure 1.10) in complex with thrombin were solved. Here, a preliminary presentation of the obtained structures is reported, while further refinements and validations are needed to analyse them in-depth.

CycTBA II-thrombin complex

Crystals of cycTBA II-thrombin complex belong to the $C222_1$ space group and diffract X-ray up to 2.45 Å resolution. They contain an aptamer-thrombin complex, in which cycTBA II binds thrombin exosite I, in the asymmetric unit (Figure 2.27). Detailed statistics on data collection are reported in Table 2.9.

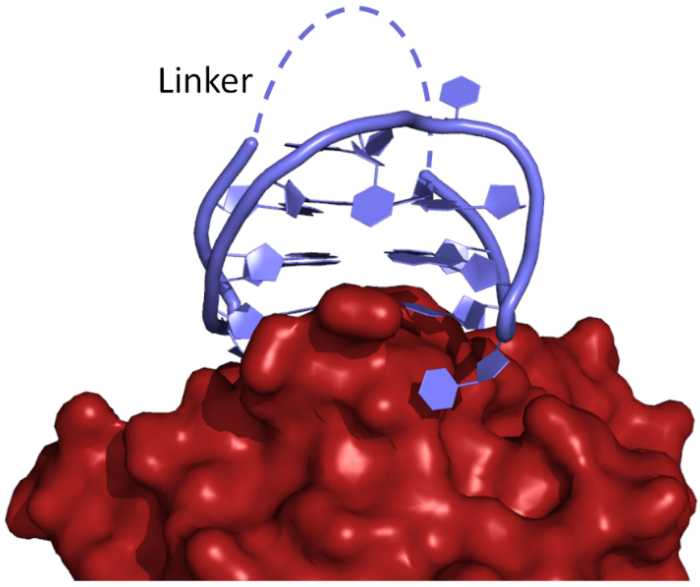

Figure 2.27. Cartoon/surface view of the cycTBA II-thrombin interface. The linker, not visible in the electron density, is represented in dashed line. Thrombin and cycTBA II are coloured in red and light violet, respectively.

Table 2.9. Data collection statistics for the cycTBA II-thrombin complex. Values in brackets refer to the highest resolution shell.

	cycTBA II-thrombin
Crystal data	
Space group	$C222_1$
Unit-cell parameters	
a, b, c (Å)	67.39, 158.60, 119.28
α, β, γ (deg)	90.00, 90.00, 90.00
V_M ($Å^3$ Da^{-1})	3.79
No. of complexes in the asymmetric unit	1
Solvent content (%)	70.2
Data Collection	
Resolution limits (Å)	79.30 - 2.45 (2.55 – 2.45)
Unique reflections	23269 (2529)
Completeness (%)	97.5 (95.9)
Average multiplicity	11.0 (10.3)
$\langle I/\sigma(I) \rangle$	7.0 (0.8)
$CC_{1/2}$	1.0 (0.6)

CycTBA II, that has been cyclized by introducing at the 3′- and 5′-ends of the oligonucleotide a triethylene glycol unit and connecting these terminal units by a 30-atom long linker,[131] adopts an antiparallel G-quadruplex structure similar to that of unmodified TBA.[66] In particular, the structure includes a core of two stacked G-tetrads and three edge-wise loops, Thy3-Thy4, Thy12-Thy13 and Thy7-Gua8-Thy9. The 30-atom long linker that covalently connects the 5′- and 3′-ends of the aptamer is not visible in the electron density, due to its intrinsic flexibility. The only electron density trace of the connecting loop presence regards the phosphate group of the linker at 5′-end, that interacts via hydrogen bonds with the Gua8 nucleobase (Figure 2.28), that is firmly positioned on the Gua6 of the G-tetrad II (Gua1,Gua6,Gua10,Gua15).

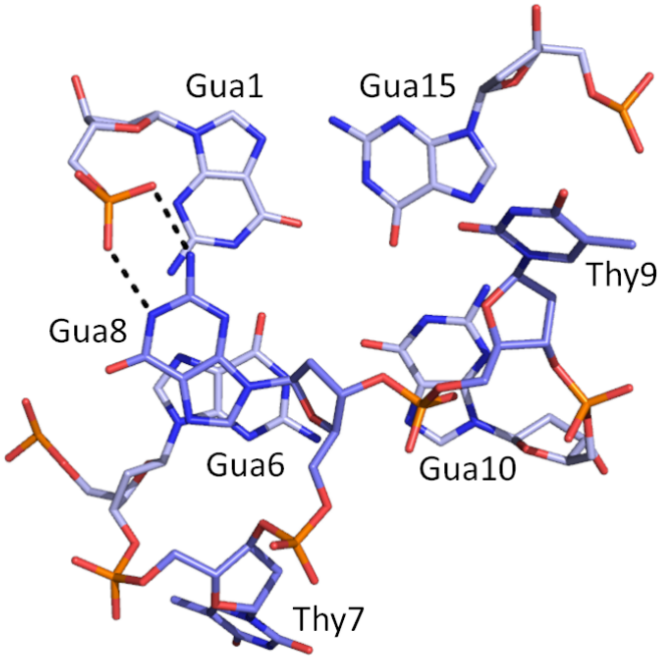

Figure 2.28. Top view of the tetrad II and TGT loop of cycTBA II as found in the crystal structure of its complex with thrombin. The hydrogen bonds formed between the Gua8 of TGT loop and the phosphate group of the linker at 5′-end are represented as black dashed lines.

Interestingly, it is worth to underline that the aptamer forms crystal packing interactions with another cycTBA II of a symmetry-related complex, by swapping the Thy7 of the TGT loop (Figure 2.29). In this arrangement, the 5′-3′ linker is exposed in the solvent channels. From a structural point of view, the TBA cyclization does not affect the aptamer-thrombin interaction mechanism.

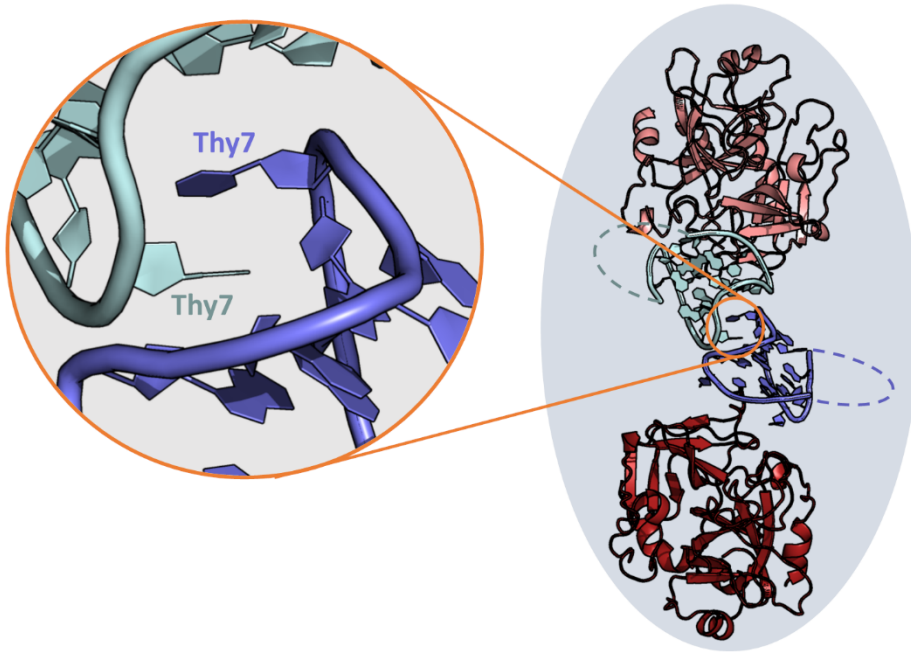

Figure 2.29. Details of the interaction between aptamers in the crystal packing of cycTBA II-thrombin complex. Thrombin is red and the aptamer violet. The symmetric molecule x, -y, -z is represented with light colours.

TBA NN/DD-thrombin complexes

The crystallization trials of the complex formed by thrombin and the TBA variant (TBA NN/DD), containing two naphthalene diimides at 5′-end and the two dansyl groups at 3′-end, provided three different crystal forms, A, B, and C (see Table 3.2 in the Experimental section). The crystals respectively belong to $P3_121$, $P2_1$, and $P6_4$ space groups and diffract X-ray up to 2.00, 3.03 and 3.18 Å. Detailed

statistics on data collections are reported in Table 2.10, Table 2.11, and Table 2.12.

Table 2.10. Data collection statistics for the TBA NN/DD-thrombin complex (condition A). Values in brackets refer to the highest resolution shell.

	TBA NN/DD-thrombin (A)
Crystal data	
Space group	$P3_121$
Unit-cell parameters	
a, b, c (Å)	76.60, 76.60, 129.38
α, β, γ (deg)	90.00, 90.00, 120.00
V_M (Å^3 Da^{-1})	2.20
No. of complexes in the asymmetric unit	1
Solvent content (%)	48.6
Data Collection	
Resolution limits (Å)	59.03 - 2.00 (2.04 – 2.00)
Unique reflections	30224 (1486)
Completeness (%)	99.8 (100.0)
Average multiplicity	18.1 (18.9)
$\langle I/\sigma(I)\rangle$	23.7 (2.2)
$CC_{1/2}$	1.0 (0.8)

Table 2.11. Data collection statistics for the TBA NN/DD-thrombin complex (condition B). Values in brackets refer to the highest resolution shell.

	TBA NN/DD-thrombin (B)
Crystal data	
Space group	$P2_1$
Unit-cell parameters	
a, b, c (Å)	76.62, 114.86, 83.44
α, β, γ (deg)	90.00, 117.25, 90.00
V_M (Å^3 Da^{-1})	3.28
No. of complexes in the asymmetric unit	2
Solvent content (%)	65.5
Data Collection	
Resolution limits (Å)	68.04 - 3.03 (3.09 – 3.03)
Unique reflections	24860 (1266)
Completeness (%)	99.6 (99.8)
Average multiplicity	6.6 (6.9)
$\langle I/\sigma(I)\rangle$	11.2 (2.2)
$CC_{1/2}$	1.0 (0.8)

Table 2.12. Data collection statistics for the TBA NN/DD-thrombin complex (condition C). Values in brackets refer to the highest resolution shell.

	TBA NN/DD-thrombin (C)
Crystal data	
Space group	$P6_4$
Unit-cell parameters	
a, b, c (Å)	152.91, 152.91, 79.49
α, β, γ (deg)	90.00, 90.00, 120.00
V_M (Å^3 Da^{-1})	6.20
No. of complexes in the asymmetric unit	1
Solvent content (%)	81.8
Data Collection	
Resolution limits (Å)	76.45 - 3.18 (3.24 – 3.18)
Unique reflections	17902 (872)
Completeness (%)	100.0 (100.0)
Average multiplicity	19.5 (19.9)
$\langle I/\sigma(I)\rangle$	23.7 (2.1)
$CC_{1/2}$	1.0 (0.7)

Crystals of condition C contain an aptamer-thrombin complex in the asymmetric unit, in which, as expected, TBA NN/DD binds thrombin exosite I (Figure 2.30).

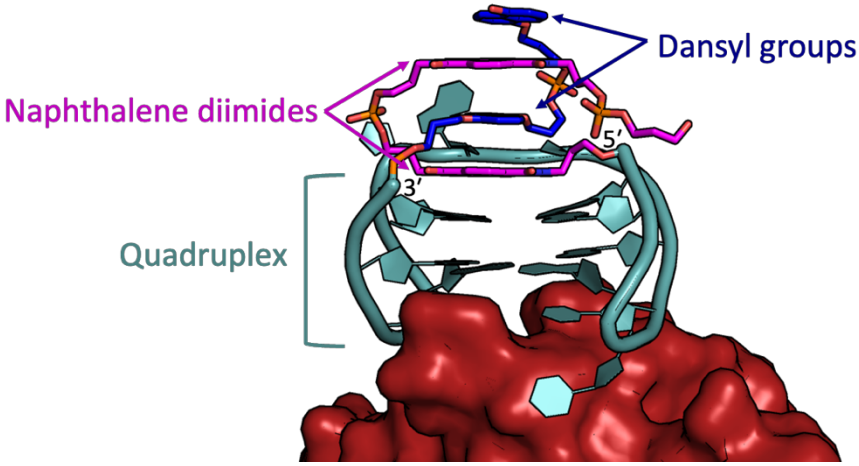

Figure 2.30. Cartoon/surface view of the TBA NN/DD-thrombin interface in the condition C. Thrombin, oligonucleotide domain of TBA NN/DD, naphthalene diimides at 5′-end, and dansyl groups at 3′-end are red, dark cyan, magenta, and blue, respectively.

The oligonucleotide domain of TBA NN/DD adopts the same structural organization of the unmodified aptamer[66] (Figure 2.30), a chair-like quadruplex structure consisting of two G-tetrads connected by two TT loops and a single TGT loop. The two naphthalene diimides (N) at 5′-end and the two dansyl groups (D) at 3′-ends alternately stack on top of each other, forming a N/D/N/D motif. The first naphthalene diimide at 5′-ends in turn stacks on the G-tetrad II of the G-quadruplex domain. This continuous stacking between oligonucleotide domain and terminal groups generates a compact architecture that resembles that of a duplex/quadruplex oligonucleotide.[76,80] It must be underlined that, as supposed, the modification interactions determine a *pseudo*-cyclization of the aptamer.
Surprisingly, one or two ternary complexes (Figure 2.31), in which thrombin is bound to two TBA NN/DD molecules, were found in the asymmetric units of crystals grown in conditions A and B, respectively.

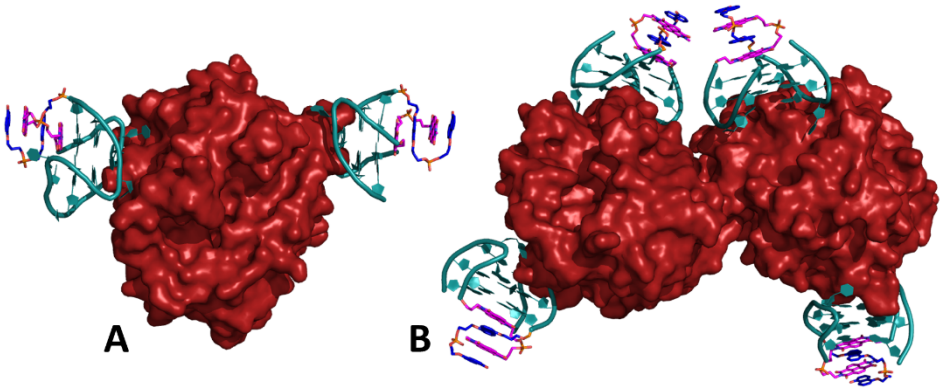

Figure 2.31. Cartoon/surface representation of ternary complex between thrombin and two TBA NN/DD molecules in the A) condition A and B) condition B. In the crystals of condition B, two ternary complexes are in the asymmetric unit. Thrombin, oligonucleotide domain of TBA NN/DD, naphthalene diimides at 5′-end, and dansyl groups at 3′-end are red, dark cyan, magenta, and blue, respectively.

In particular, in addition to the aptamer bound canonically to exosite I, another TBA NN/DD molecule is present on the exosite II in both the conditions. All the aptamers adopt the same structural organization observed in condition C (Figure

2.30), regardless of the binding site. In each ternary complex the second TBA NN/DD molecule interacts by means of the two TT loops with a localized protruding region of the extended exosite II (Figure 2.32). This region is formed by thrombin residues 89-101 and 232-245.

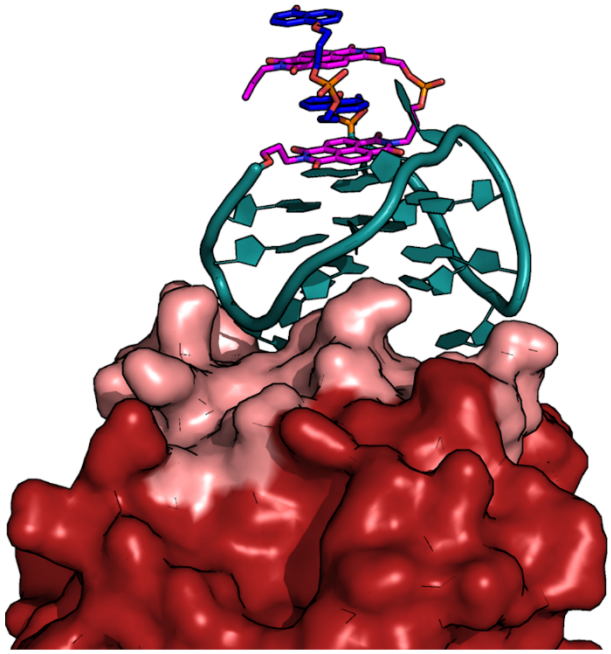

Figure 2.32. Cartoon/surface view of the interface between TBA NN/DD and thrombin exosite II in the condition A. Thrombin, oligonucleotide domain of TBA NN/DD, naphthalene diimides at 5′-end, and dansyl groups at 3′-end are red, dark cyan, magenta, and blue, respectively. The residues Tyr89-Arg101 and Phe232-Phe245 of the exosite II are coloured in pink.

Further analyses are required to verify if the ability of TBA NN/DD to bind thrombin exosite II is relevant in solution or is facilitated in the solid state by modification-guided intermolecular interactions.

2.2.3. Spectroscopic and functional studies of NU172 incorporating hexitol nucleotides

Spectroscopic analysis

To evaluate the effects of the hexitol nucleotide substitutions at one or more positions on the structure and the thermal stability of NU172 aptamer, an extensive analysis of its variants (see Table 1.2 in the Introduction) was carried out by means of circular dichroism (CD) and UV spectroscopies.

In first studies, the biomimetic potential of HNA was explored by CD analysis. As previously reported,[67] the CD spectrum (Figure 2.33) of NU172 in the presence of potassium ions displays two positive signals at 295 and 245 nm and one negative signal at 265 nm, which are distinctive of the antiparallel G-quadruplex structure.

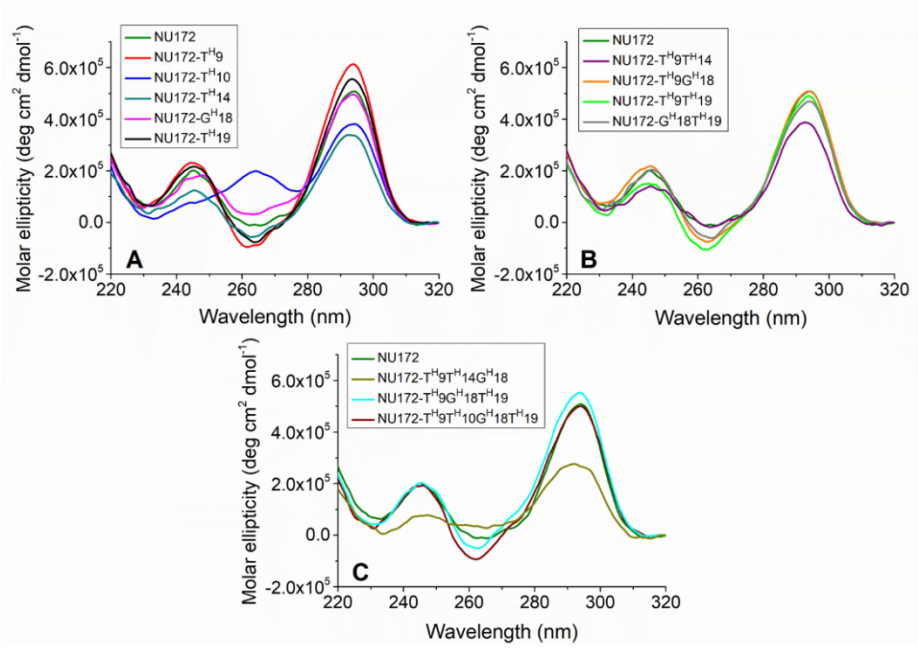

Figure 2.33. CD spectra of NU172 and its variants containing A) one mutation, B) two mutations, C) three or four mutations. Spectra were recorded at 10 °C on oligonucleotide samples (10 μM) previously annealed in 10 mM potassium phosphate pH 7.4 and 100 mM KCl.

Accordingly, changes in the profile of the CD spectra were analysed for each mutant with respect to the unmodified aptamer. Single incorporations were first considered (Figure 2.33A). The T^H14 mutation had a detrimental effect on the conformational integrity of the oligonucleotide, as estimated by the reduced intensity of the signals at 295, 265, and 245 nm. The modified oligonucleotide carrying the T^H10 nucleotide displayed a fully different CD spectrum compared with NU172, as it exhibited two positive bands at 295 and 265 nm, suggesting conformational heterogeneity. Conversely, the NU172-T^H19 and NU172-G^H18 mutants showed a CD profile substantially superimposable to that of NU172, strongly indicating that the presence of the unnatural deoxyguanosine and thymidine at these positions did not produce differences in the conformational behaviour of the parent aptamer. Additionally, the CD spectrum of the NU172-T^H9 mutant displayed an enhancement in the intensity of all bands, indicating a more pronounced propensity than NU172 to adopt an antiparallel G-quadruplex architecture.

Multiple incorporations were also considered (Figure 2.33B and Figure 2.33C). In line with data on single incorporations, the presence of T^H14 in NU172-T^H9T^H14 and NU172-$T^H9T^H14G^H18$ mutants significantly destabilized the structure of the oligonucleotides. On the other hand, NU172-T^H9G^H18, NU172-T^H9T^H19, NU172-G^H18T^H19, NU172-$T^H9G^H18T^H19$, or NU172-$T^H9T^H10G^H18T^H19$ oligonucleotides displayed broadly unchanged intensities of the CD signals compared to NU172.

CD analysis was also conducted to provide indications on the thermal stability of the modified oligonucleotides by plotting the fraction of folded oligonucleotides as a function of temperature (Figure 2.34).

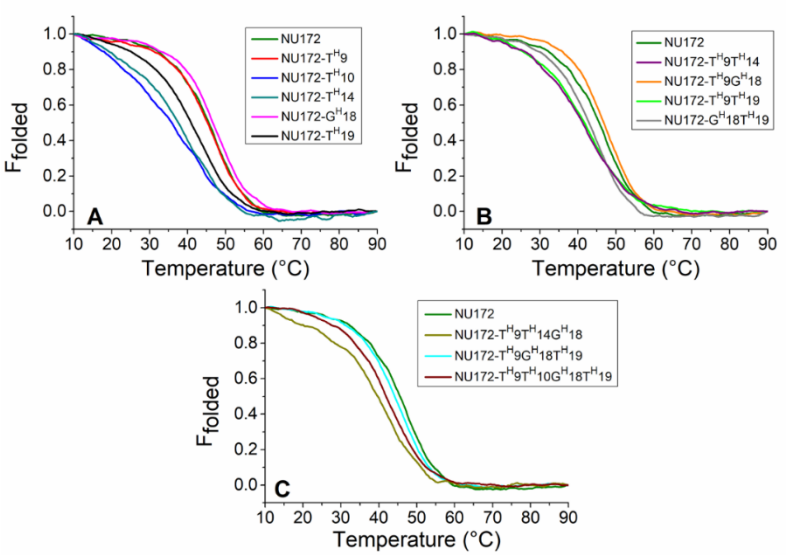

Figure 2.34. CD melting profiles of NU172 and its variants having A) one mutation, B) two mutations, and C) three or four mutations. Melting profiles were recorded on 10 μM oligonucleotide samples previously annealed in the presence of 10 mM potassium phosphate buffer pH 7.4 and 100 mM KCl.

Melting temperature (T_m) values (Table 2.13) obtained for most NU172 mutants were lower than that reported for the unmodified aptamer, indicating that incorporations of hexitol nucleotides perturb the thermal stability of the parent aptamer. Conversely, NU172-T^H9, NU172-G^H18, and NU172-T^H9G^H18 essentially retained the thermal denaturation temperature of NU172.

Table 2.13. Melting temperatures of NU172 and its variants obtained by temperature-dependent CD and UV measurements.

Oligonucleotide	T_m (°C) (CD at 295 nm)[a]	T_m (°C) (UV at 297 nm)[a]	T_m (°C) (UV at 260 nm)[a]
NU172	47	48	52
NU172-T^H9	48	49	53
NU172-T^H10	n.d.[b]	47	n.d.[b]
NU172-T^H14	41	43	n.d.[b]
NU172-G^H18	48	49	52
NU172-T^H19	44	45	52
NU172-T^H9T^H14	43	-	-
NU172-T^H9G^H18	48	-	-
NU172-T^H9T^H19	44	-	-
NU172-G^H18T^H19	45	-	-
NU172-T^H9T^H14G^H18	42	-	-
NU172-T^H9G^H18T^H19	46	-	-
NU172-T^H9T^H10G^H18T^H19	42	-	-

[a]Temperatures were calculated as the average of two independent measurements: errors range between 0.5 and 1.0 °C.
[b]The melting curve trends hamper a correct determination of T_m value.

Except for NU172-T^H10, the superimposition of CD spectra obtained during denaturation experiments provided isodichroic points at about 279 and 253 nm (Figure 2.35 and Figure 2.36), which is an indication of a two-state unfolding process. Moreover, the reversibility of the thermal unfolding process of all samples was confirmed by the full recovery of spectral features after cooling to 10 °C upon heat denaturation.

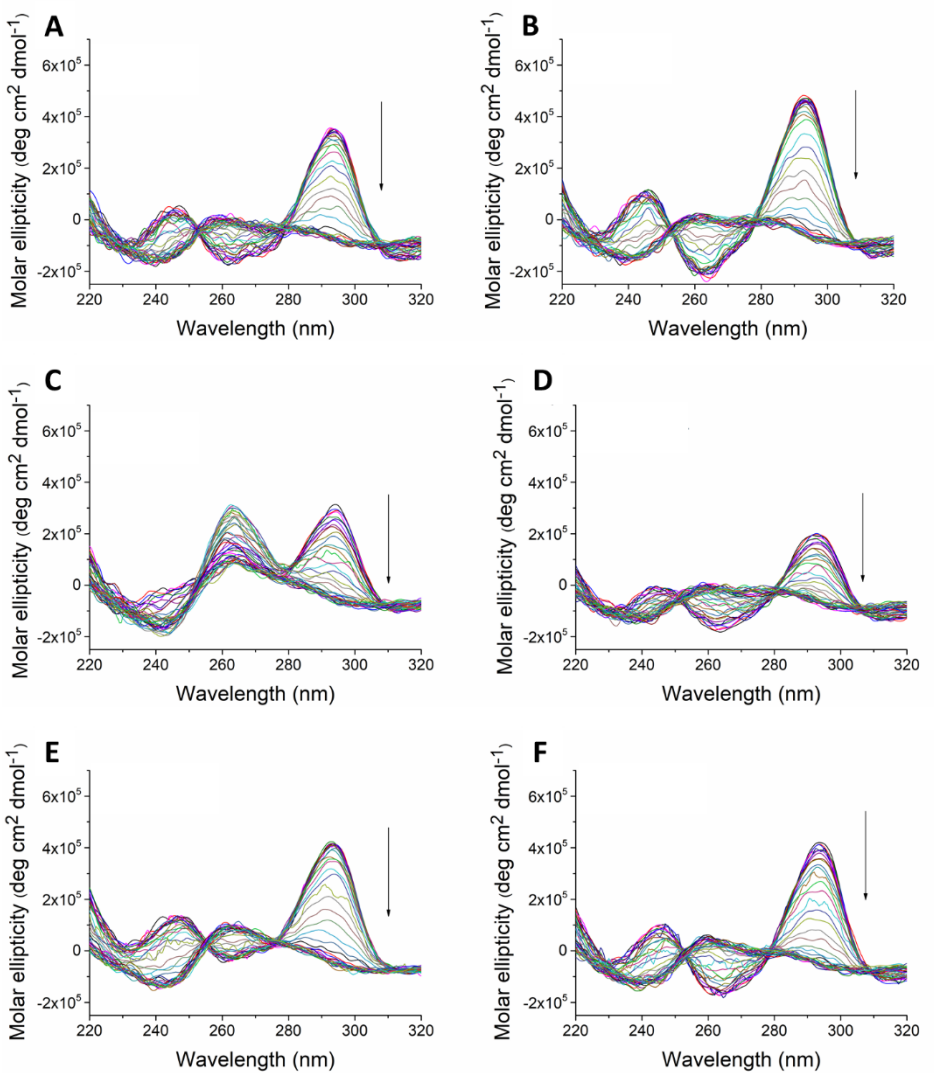

Figure 2.35. Superimposition of CD spectra collected in the 10-90 °C range with 2 °C steps for A) NU172, B) NU172-T^{H}9, C) NU172-T^{H}10, D) NU172-T^{H}14, E) NU172-G^{H}18, and F) NU172-T^{H}19 in 10 mM potassium phosphate pH 7.4 and 100 mM KCl.

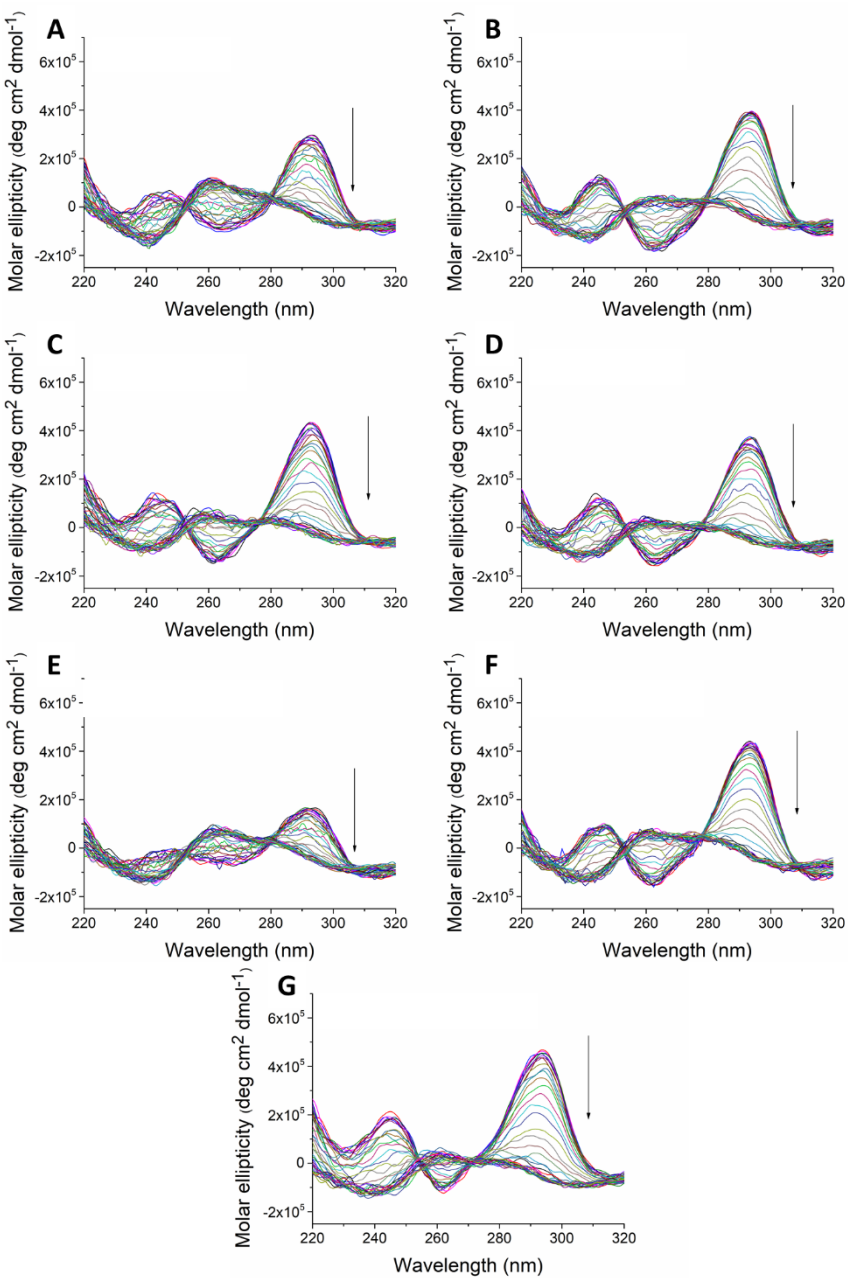

Figure 2.36. Superimposition of CD spectra collected in the 10-90 °C range with 2 °C steps for A) NU172-T^{H}9T^{H}14, B) NU172-T^{H}9G^{H}18, C) NU172-T^{H}9T^{H}19, D) NU172-G^{H}18T^{H}19, E) NU172-T^{H}9T^{H}14G^{H}18, F) NU172-T^{H}9G^{H}18T^{H}19, and G) NU172-T^{H}9T^{H}10G^{H}18T^{H}19 in 10 mM potassium phosphate buffer pH 7.4 and 100 mM KCl.

The $\Delta H_{v.H}$ and $\Delta S_{v.H}$ values obtained by the van't Hoff analysis of the melting curves (Table 2.14) together with the CD spectra clearly suggest that the insertion of the hexitol moiety in Thy9 or Gua18 does not impair a full acquisition of a quadruplex organization similar to NU172. Indeed, within the limits of experimental errors, both the thermodynamic parameters obtained for the unfolding process of NU172-T^{H}9, NU172-G^{H}18, and NU172-T^{H}9G^{H}18 are comparable to those found for the unmodified aptamer. On the contrary, most analogues with the modifications at T^{H}14 and T^{H}19 positions show slightly lower $\Delta H_{v.H}$ and $\Delta S_{v.H}$ values with respect to those of NU172, suggesting a moderate reduction of the rigidity of their G-quadruplex structures.

Table 2.14. Thermodynamic parameters for the unfolding process of NU172 and its variants as followed by means of CD measurements. Errors on thermodynamic parameters are within 10%.

Oligonucleotide	$\Delta H_{v.H}$ (kJ mol^{-1})	$\Delta S_{v.H}$ (kJ mol^{-1} K^{-1})
NU172	180	0.56
NU172-T^{H}9	191	0.60
NU172-T^{H}14	142	0.45
NU172-G^{H}18	194	0.60
NU172-T^{H}19	162	0.51
NU172-T^{H}9T^{H}14	133	0.42
NU172-T^{H}9G^{H}18	193	0.60
NU172-T^{H}9T^{H}19	150	0.47
NU172-G^{H}18T^{H}19	178	0.56
NU172-T^{H}9T^{H}14G^{H}18	171	0.54
NU172-T^{H}9G^{H}18T^{H}19	185	0.58
NU172-T^{H}9T^{H}10G^{H}18T^{H}19	168	0.53

The effect of the incorporation of a single hexitol nucleotide on the thermal stability of NU172 was also investigated by temperature-dependent UV studies (Table 2.13 and Figure 2.37), which allow to evaluate independently the stability of quadruplex and duplex domains, by following the absorbance variations at 297 and 260 nm, respectively.

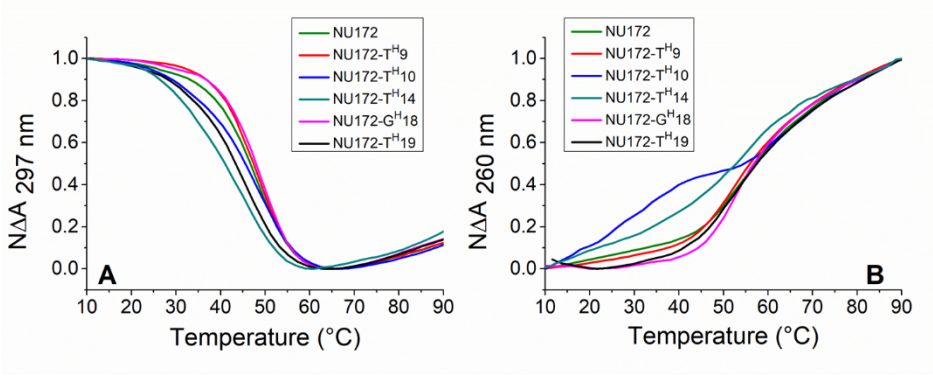

Figure 2.37. UV melting profiles at A) 297 nm and B) 260 nm of NU172 and its variants having single incorporations of hexitol nucleotides. Melting profiles were obtained by annealing 20 μM oligonucleotide samples in 10 mM potassium phosphate pH 7.4 and 100 mM KCl.

Indeed, in the case of the double helix structure during the unfolding process the absorbance at 260 nm increases by about 25% on denaturation.[67,170] In the case of the G-quadruplex structure, there is only a small (4%) change in absorbance at 260 nm upon unfolding. On the contrary, a 50-80% decrease in absorbance associated with G-quadruplex melting can be observed in the 290-300 nm spectral region.[171,172] Single incorporations of hexitol nucleotides generally led to slight to marked reductions in the stability of the oligonucleotides. As exceptions, modifications at positions Thy9 and Gua18 did not perturb the stability of either the quadruplex or the duplex of the parent aptamer. $\Delta H_{v.H}$ and $\Delta S_{v.H}$ values from UV melting curves (Table 2.15) show the same trend shown by CD data.

Table 2.15. Thermodynamic parameters for the unfolding process of NU172 and some of its variants as followed by means of UV measurements. Errors on thermodynamic parameters are within 10%.

Oligonucleotide	$\Delta H_{v.H}$ (kJ mol^{-1})	$\Delta S_{v.H}$ (kJ mol^{-1} K^{-1})	$\Delta H_{v.H}$ (kJ mol^{-1})	$\Delta S_{v.H}$ (kJ mol^{-1} K^{-1})
	UV at 297 nm		UV at 260 nm	
NU172	183	0.57	172	0.53
NU172-T^{H}9	191	0.59	170	0.52
NU172-T^{H}14	125	0.39	-	-
NU172-G^{H}18	203	0.63	190	0.58
NU172-T^{H}19	150	0.47	127	0.39

The spectroscopic analysis of NU172 mutants correlates well with the conformational preferences of native nucleotides in NU172 and with the biomimetic properties of hexitol nucleotides. The NU172-G^{H}18 mutant keeps the structural properties of the parent aptamer, as expected owing to the ability of the $^{4}C_{1}$ sugar chair in Gua18 to faithfully resemble the C3′-*endo* conformation adopted by the same nucleotide in NU172. Conversely, the incorporation of hexitol nucleotides at positions Thy10, Thy14, and Thy19 negatively affects the conformational properties and/or the thermal stability of the corresponding oligonucleotides. This can be easily rationalized, as these nucleotide residues adopt a C2′-*endo* sugar puckering in the unmodified aptamer. The highly destabilizing effect is especially apparent for NU172-T^{H}14, considering that in NU172 the Thy14 residue is involved in a tight junction between duplex and quadruplex domains.[80] Concerning the NU172-T^{H}9 mutant, the ability of the hexitol nucleotide to not interfere with the structural and thermal properties of NU172 suggests that the hexitol moiety can be properly accommodated in the oligonucleotide, even though the modified nucleotide does not closely reproduce the O4′-*endo* form of Thy9 in NU172. The spectral features of NU172-T^{H}9G^{H}18, which are superimposable with those of the unmodified aptamer, also suggest that both modified nucleotides do not perturb the integrity of the duplex/quadruplex architecture of the parent aptamer.

Anticoagulant activity experiments

The ability of NU172 variants to compete with fibrinogen for thrombin exosite I was evaluated by performing a spectrophotometric fibrinogen clotting assay (Figure 2.38).

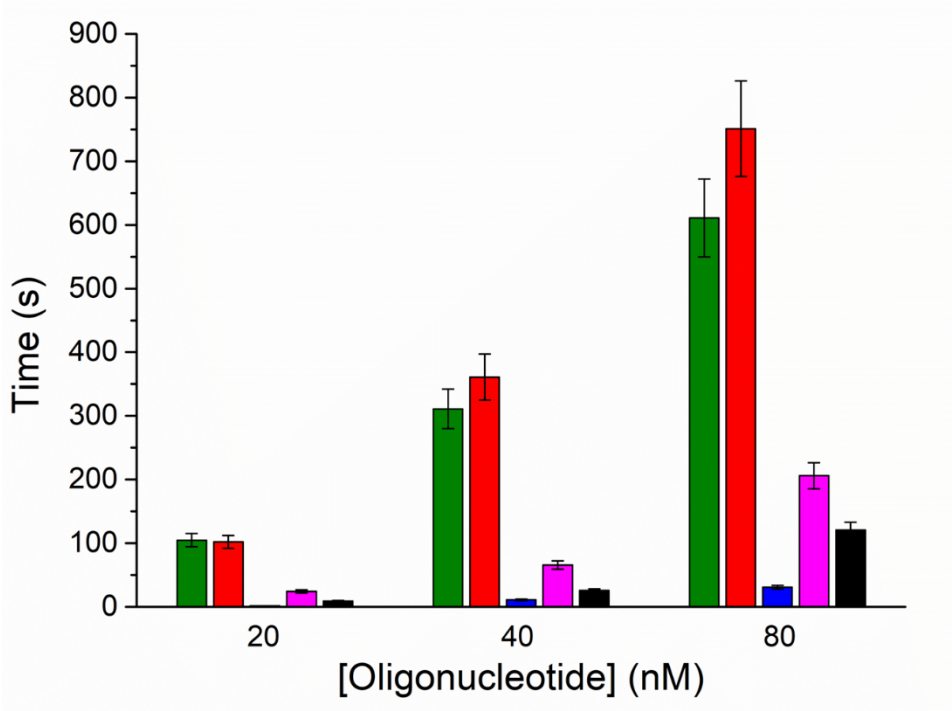

Figure 2.38. Prolonged fibrinogen clotting times measured in PBS buffer in the presence of fibrinogen (1.8 mg mL^{-1}), thrombin (5 nm), and either NU172 (green) or oligonucleotides carrying mutations T^H9 (red), T^H10 (blue), G^H18 (magenta), or T^H19 (black) at concentrations of 20, 40, and 80 nM.

Modifications at Thy10 and Thy19 of NU172 had a detrimental effect on the anticoagulant activity, leading to a significant decrease of the clotting times compared with the unmodified aptamer over the explored concentration range (20–80 nM). In the case of the NU172-G^H18 mutant, the clotting time was slightly longer than for previous oligonucleotides, although its anticoagulant activity was much lower than NU172. Finally, NU172-T^H9 is the only oligonucleotide that

retained the anticoagulant activity of NU172 at low dosage, although this was slightly enhanced at high concentrations, with a 1.2-fold increase at 80 nM (Figure 2.38).

2.3. Aptamer/prothrombin interaction

The structural features of the interaction between thrombin and oligonucleotide aptamers are well documented in literature.[66,69–71,76,80,83,95,129,164] On the contrary, up to date, a detailed structural characterization of the recognition mechanism between anticoagulant aptamers and the pro-exosite I of prothrombin is still lacking.

In this subsection, the thermodynamic analysis of the binding between three of the most effective aptamers and commercial thrombin or prothrombin is discussed. The effect of prothrombin on the aptamer folding, analysed by means of CD experiment, is also illustrated. Finally, the protocols to produce recombinant prethrombin-2 and prothrombin mutants for crystallization experiments are presented.

2.3.1. ITC analysis

The thermodynamic parameters of the binding between the prothrombin and anti-thrombin aptamers were obtained by Isothermal Titration Calorimetry (ITC) experiments. For comparison, the binding between the thrombin and the same aptamers was likewise investigated. The analysis was only focused on thrombin binding aptamers that recognize the exosite I, as in prothrombin the exosite II region is involved in intramolecular interactions with the kringle-2 domain (Figure 2.39). In particular, the aptamers used in these investigations were the basal TBA, that adopts an antiparallel G-quadruplex structure, and the two duplex quadruplex aptamers, RE31 and NU172.

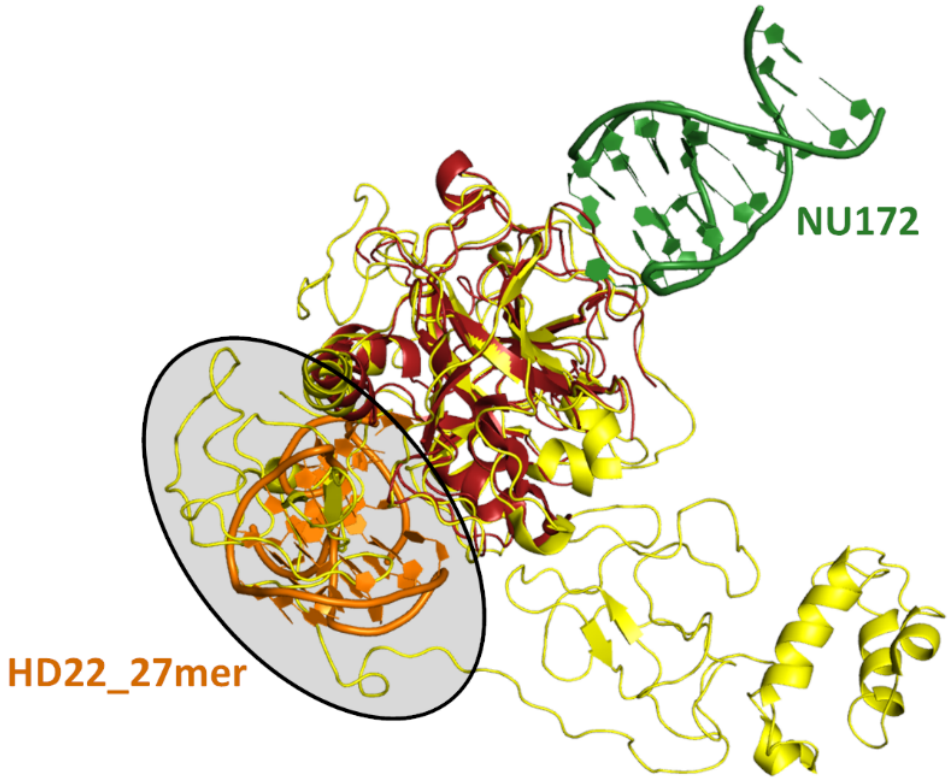

Figure 2.39. Superposition of the prothrombin mutant S101C/A470C (closed conformation, PDB code: 6C2W)[147] and the NU172-thrombin-HD22_27mer ternary complex (see paragraph 2.1.1). Prothrombin, thrombin, NU172, and HD22_27mer are yellow, red, green, and orange, respectively. The inability of HD22_27mer to bind prothrombin due to the presence of kringle-2 domain is shown in the circle.

In agreement with previous suggestions,[66,76,80] the results strongly indicate that TBA (Figure 2.40A), RE31 (Figure 2.41A), and NU172 (Figure 2.42A) form with thrombin a 1:1 complex. The same stoichiometry is observed in the case of the interaction of these aptamers with prothrombin (Figure 2.40B, Figure 2.41B, and Figure 2.42B), suggesting a thrombin-like interaction with the pro-exosite I on prothrombin surface.

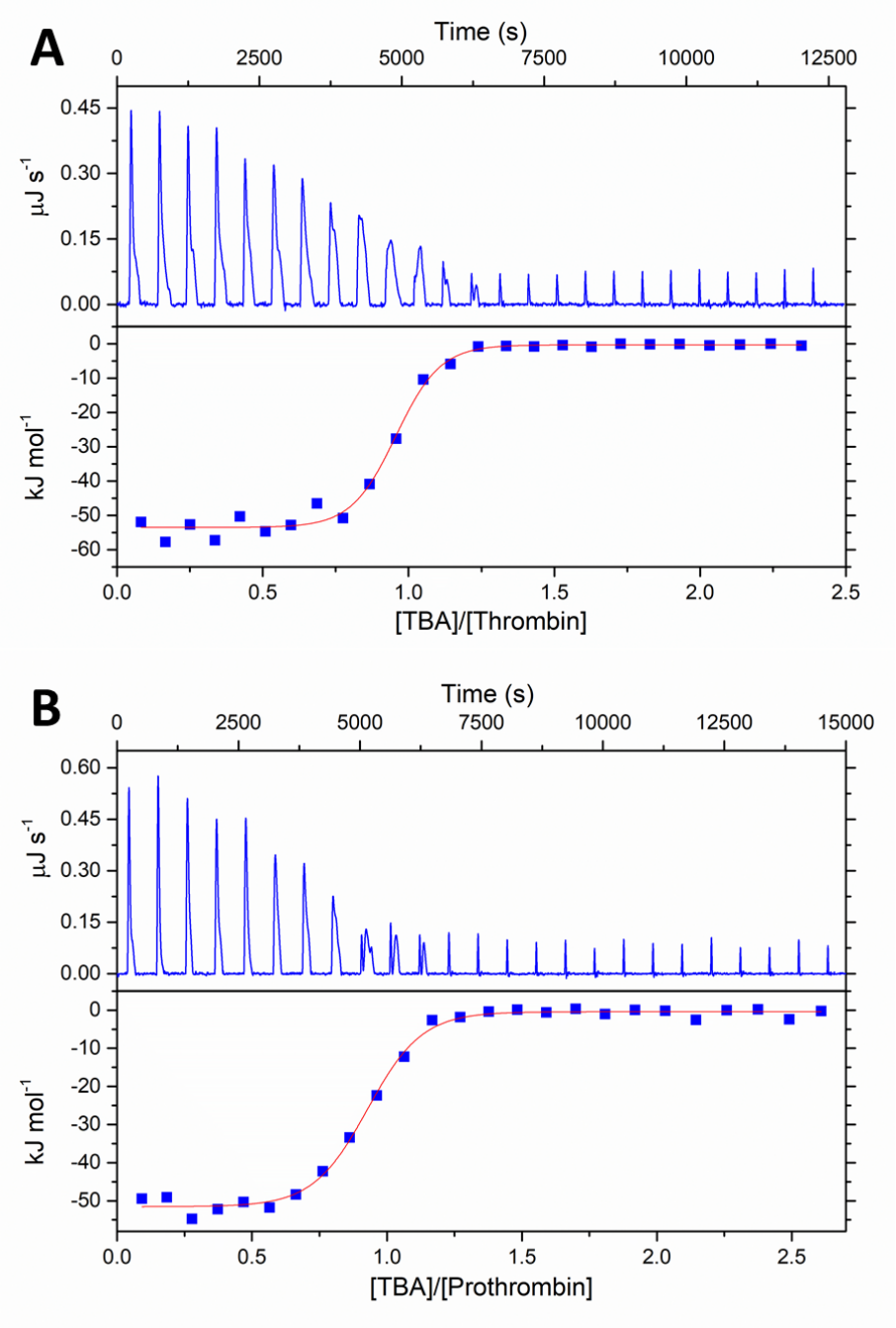

Figure 2.40. ITC binding isotherms for the interaction of TBA with A) thrombin or B) prothrombin in 10 mM potassium phosphate pH 7.4 and 100 mM KCl at 25 °C.

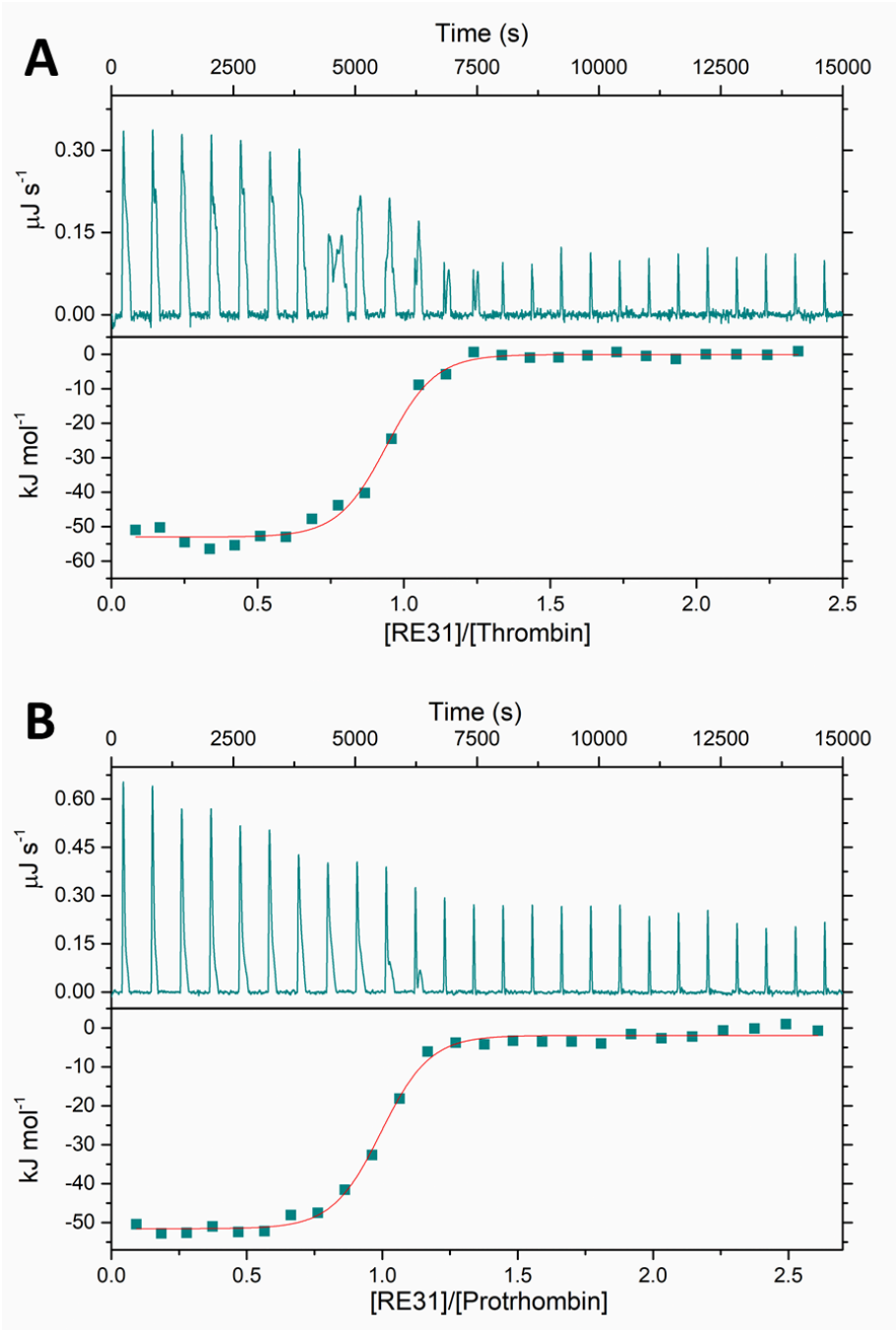

Figure 2.41. ITC binding isotherms for the interaction of RE31 with A) thrombin or B) prothrombin in 10 mM potassium phosphate pH 7.4 and 100 mM KCl at 25 °C.

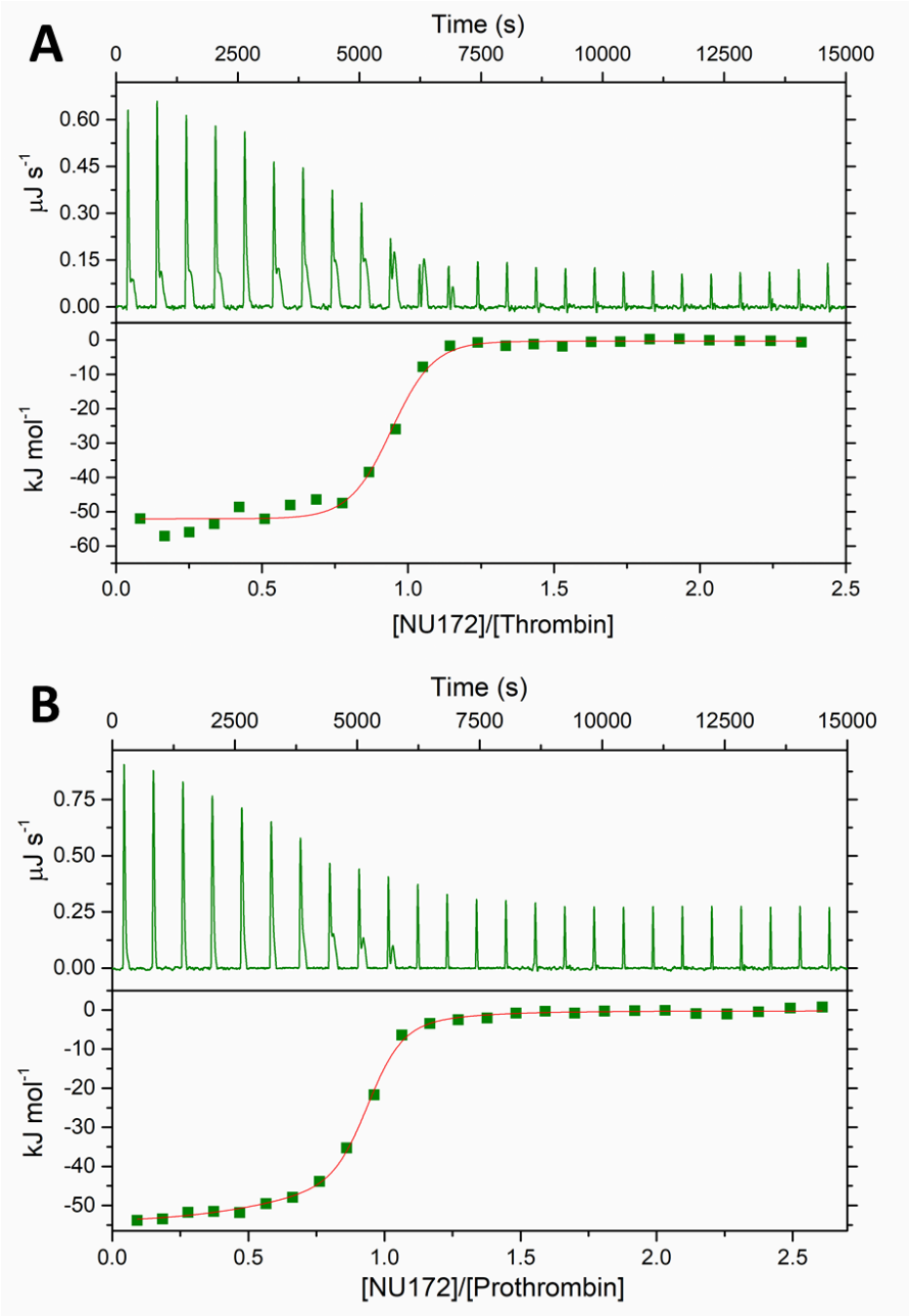

Figure 2.42. ITC binding isotherms for the interaction of NU172 with A) thrombin or B) prothrombin in 10 mM potassium phosphate pH 7.4 and 100 mM KCl at 25 °C.

The binding constants, K_b, (Table 2.16) obtained for the interaction of TBA, RE31, and NU172 aptamers with thrombin are quite similar each other and with those obtained for the interaction with prothrombin, although they seem to suggest a slightly lower affinity of these oligonucleotides towards prothrombin than thrombin. As far as the binding thermodynamic parameters (Δ_bH, Δ_bS, Δ_bG) are concerned (Table 2.16), very subtle are the differences in the various experiments both with thrombin and with prothrombin.

Table 2.16. Thermodynamic parameters for the interaction of TBA, RE31, and NU172 with thrombin or prothrombin.

Aptamer	Protein	K_b (10^7 M^{-1})	Δ_bH (kJ mol^{-1})	$-T\Delta_bS$ (kJ mol^{-1})	Δ_bG (kJ mol^{-1})
TBA	Thrombin	3.4 ± 1.4	-54 ± 1	11 ± 1	-43 ± 1
	Prothrombin	2.0 ± 0.6	-52 ± 1	11 ± 1	-42 ± 1
RE31	Thrombin	3.1 ± 1.2	-54 ± 1	11 ± 1	-43 ± 1
	Prothrombin	2.0 ± 0.7	-53 ± 1	11 ± 1	-42 ± 1
NU172	Thrombin	3.6 ± 1.5	-53 ± 1	10 ± 1	-43 ± 1
	Prothrombin	2.5 ± 0.5	-53 ± 1	10 ± 1	-42 ± 1

The finding that TBA and RE31 have similar Δ_bH, Δ_bS, and Δ_bG values agrees with the crystallographic data of the complex of each aptamer with thrombin: the two oligonucleotides, which share the G-quadruplex domain, show the same recognition motif of exosite I.[66,76] As concerns NU172, the finding that the enthalpy contribution to the binding is similar to that observed for TBA and RE31 is almost unexpected. Indeed, the value of the aptamer-thrombin contact area is slightly higher for NU172 than for the other aptamers.[80] This could be the result of the higher conformational flexibility in solution of NU172 in comparison to TBA and RE31, as revealed by means of spectroscopic and differential scanning calorimetry studies.[67] Some conformers would have to undergo to small structural changes to be able to tightly bind thrombin or prothrombin with probably an enthalpy penalty.

Overall, these results, that represent the first complete comparative thermodynamic analysis of the binding of each aptamer to thrombin and to its zymogen, clearly indicate the ability of the examined aptamers to recognize pro-exosite I with an affinity similar to that shown for exosite I and lay the foundations for a structural characterization of the aptamer-prothrombin complexes.

2.3.2. Prothrombin as molecular chaperone of aptamers

It is widely reported in literature that thrombin has the ability to act as molecular chaperone of its aptamers, inducing the structural reorganization of the TBA or its mutants to facilitate their binding even in the absence of ions.[66,80,173]

In order to verify if also the prothrombin can act as chaperone of aptamers, CD spectra of TBA, RE31, and NU172 aptamers were recorded before and after the addition of the protein. Indeed, since the CD spectra of proteins do not show relevant signals above 260 nm,[174] the change and/or the stabilization of these aptamer folding induced by the binding with the prothrombin can be easily revealed spectroscopically. The experiments were performed in the completely absence of K^+ or Na^+ ions, which could mask the effect of the prothrombin interaction with the aptamer. Indeed, the CD spectra of the unbound TBA (Figure 2.43A), RE31 (Figure 2.43B), and NU172 (Figure 2.43C) clearly indicate that in absence of ions they poorly adopt the G-quadruplex (TBA) or the duplex/quadruplex (RE31 and NU172) architecture observed in K^+-rich solutions.

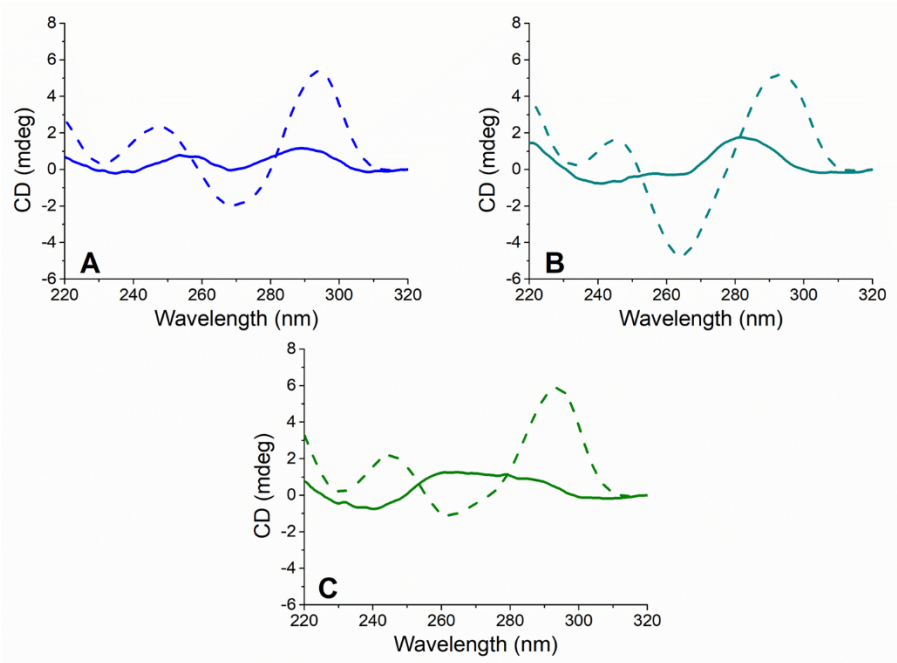

Figure 2.43. CD spectra of A) TBA, B) RE31, and C) NU172 in the absence (solid line) and in the presence (dashed line) of potassium ions. The spectra were recorded at 10 °C in 10 mM Tris-HCl pH 7.4 (solid line) or 10 mM potassium phosphate pH 7.4 and 100 mM KCl (dashed line), using an aptamer concentration of 1 μM.

In particular, the CD profile of NU172 in the absence of ions is very different from that of the duplex/quadruplex structure adopted in the presence of K^+ or thrombin,[80] suggesting a great conformational heterogeneity.

In the CD spectra of 1:2 aptamer-prothrombin solutions (Figure 2.44) the positive signal around 295 nm typical of the antiparallel G-quadruplex structure greatly increases, suggesting that the interaction of the protein with the three aptamers promotes their correct folding.

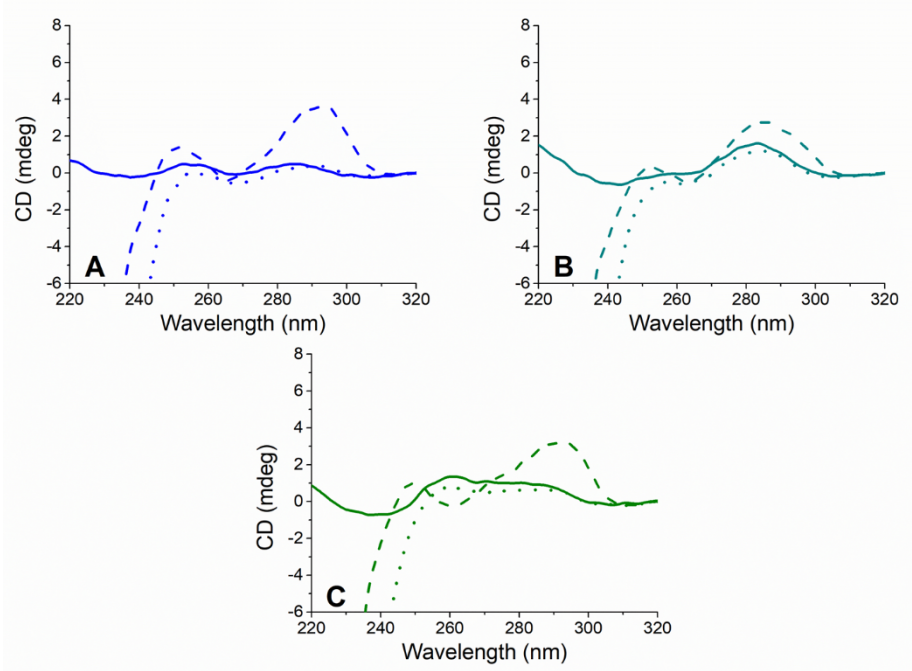

Figure 2.44. CD spectra of A) TBA, B) RE31, and C) NU172 in the absence (solid line) and in the presence of the native (dashed line) or denatured (dotted line) prothrombin. The spectra were recorded at 20 °C in 10 mM Tris-HCl pH 7.4, using an aptamer concentration of 1 μM. The prothrombin was added up to a concentration of 2 μM and denatured by heating the samples to 95 °C after the addition of 300 μM TCEP.

As negative control, the CD spectra (Figure 2.44) of these solutions were recorded after the denaturation of the protein induced by heating the samples to 95 °C after the addition of a reducing agent (300 μM TCEP). The CD profiles clearly lose the antiparallel G-quadruplex band observed upon aptamer binding with the protein. Due to the high conformational heterogeneity of NU172 in the absence of ions, the change of the folding upon binding of prothrombin occurs more slowly compared to other aptamers, allowing to follow the phenomenon kinetically (Figure 2.45). In particular, the variation of the folding after the addition of two equivalents of prothrombin reaches the maximum value after ~ 40 min.

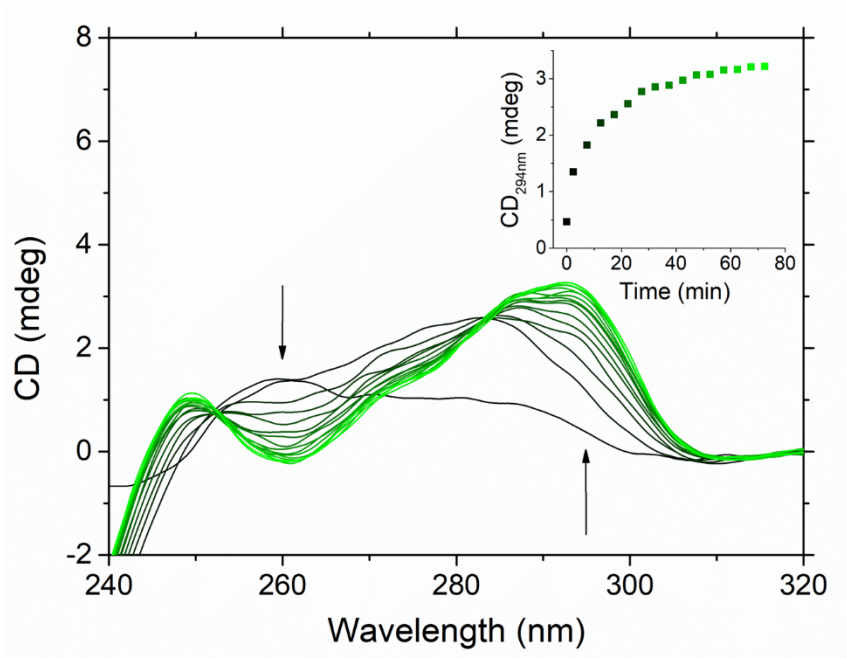

Figure 2.45. CD spectra of the NU172-prothombin binding. The first spectrum corresponds to NU172 in the absence of the protein and the following spectra were collected over time after the addition of two equivalents of prothrombin. The spectra were recorded at 20 °C in 10 mM Tris-HCl pH 7.4, using an aptamer concentration of 1 μM. The inset shows the changes in the CD signal at 294 nm over time.

Overall, these data not only confirm the binding between prothrombin and the three examined aptamers, but also underline the prothrombin ability to act as molecular chaperone, stabilizing and even promoting the quadruplex formation independent of the presence of cations.

2.3.3. Crystallization trials of the complexes between wild-type prothrombin and aptamers

An extensive search of the crystallization conditions of aptamer-prothrombin complexes was performed with the same commercial human wild-type prothrombin (Haematologic Technologies, USA) used for the ITC and CD experiments above reported. The complexes between prothrombin and TBA,

RE31, or NU172 were prepared in 10 mM potassium phosphate pH 7.4 and 100 mM KCl and concentrated to about 12 mg mL^{-1}, following the protocol usually used for the preparation of aptamer-thrombin complexes (see Experimental section, paragraph 3.2.1).[66,69,70,76,80] Initial crystallization screenings were carried out by using a commercial kit (Hampton Research Index) and reproducing the conditions reported in the literature for the crystallization of aptamer-thrombin complexes.[66,69–71,76,80,83,95] An optimization of the most interesting conditions was performed by hanging drop method and by fine-tuning of several parameters: precipitant type, precipitant concentration, addition of various salts, and pH. Crystals grew after several months in two conditions only for the RE31-prothrombin complex (Figure 2.46). Unfortunately, they diffracted X-ray very poorly and did not allow a high-resolution data collection and the structure solution.

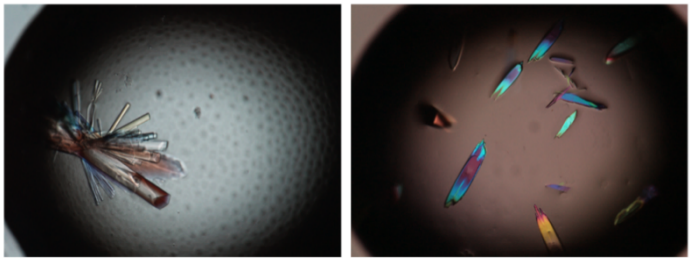

Figure 2.46. Crystals of the RE31-prothrombin complex grown in two different conditions.

2.3.4. Design of prethrombin-2 and prothrombin mutants

It is worth to note that prothrombin, due to the long intervening linkers connecting its four domains, possesses a great conformational flexibility that has hampered the crystallization of the free wild-type protein (see Introduction, paragraph 1.5). Indeed, up to date, only prothrombin mutants lacking its more flexible regions (PDB codes: 3NXP, 4HZH, 4NZQ, 4O03, 5EDK, 5EDM)[141,146,161,175] or locked in a specific conformation (PDB codes: 6BJR, 6C2W)[147] were characterized by means of X-ray crystallography. As a consequence, the production of prothrombin

variants could assist the structural characterization of the interaction between the aptamers and the prothrombin. Based on the sequences of the prothrombin deletion mutants in the Protein Data Bank, two variants lacking the residues 154-167 (ProT_Δ154-167) or 146-167 (ProT_Δ146-167) of the linker 2 connecting the kringle-1 and kringle-2 domains of prothrombin were designed (Figure 2.47).

```
wt-ProT       ANTFLEEVRKGNLERECVEETCSYEEAFEALESSTATDVFWAKYTACE 48
ProT_Δ154-167 ---------------------------------SSTATDVFWAKYTACE 16
ProT_Δ146-167 ---------------------------------SSTATDVFWAKYTACE 16
                                                ***************

wt-ProT       TARTPRDKLAACLEGNCAEGLGTNYRGHVNITRSGIECQLWRSRYPHK 96
ProT_Δ154-167 TARTPRDKLAACLEGNCAEGLGTNYRGHVNITRSGIECQLWRSRYPHK 64
ProT_Δ146-167 TARTPRDKLAACLEGNCAEGLGTNYRGHVNITRSGIECQLWRSRYPHK 64
              **************************************************

wt-ProT       PEINSTTHPGADLQENFCRNPDSSTTGPWCYTTDPTVRRQECSIPVCG 144
ProT_Δ154-167 PEINSTTHPGADLQENFCRNPDSSTTGPWCYTTDPTVRRQECSIPVCG 112
ProT_Δ146-167 PEINSTTHPGADLQENFCRNPDSSTTGPWCYTTDPTVRRQECSIPVCG 112
              **************************************************

wt-ProT       QDQVTVAMTPRSEGSSVNLSPPLEQCVPDRGQQYQGRLAVTTHGLPCL 192
ProT_Δ154-167 QDQVTVAMT--------------EQCVPDRGQQYQGRLAVTTHGLPCL 146
ProT_Δ146-167 Q----------------------EQCVPDRGQQYQGRLAVTTHGLPCL 138
              *                      ************************

wt-ProT       AWASAQAKALSKHQDFNSAVQLVENFCRNPDGDEEGVWCYVAGKPGDF 240
ProT_Δ154-167 AWASAQAKALSKHQDFNSAVQLVENFCRNPDGDEEGVWCYVAGKPGDF 194
ProT_Δ146-167 AWASAQAKALSKHQDFNSAVQLVENFCRNPDGDEEGVWCYVAGKPGDF 186
              **************************************************

wt-ProT       GYCDLNYCEEAVEEETGDGLDEDSDRAIEGRTATSEYQTFFNPRTFGS 288
ProT_Δ154-167 GYCDLNYCEEAVEEETGDGLDEDSDRAIEGRTATSEYQTFFNPRTFGS 242
ProT_Δ146-167 GYCDLNYCEEAVEEETGDGLDEDSDRAIEGRTATSEYQTFFNPRTFGS 234
              **************************************************

wt-ProT       GEADCGLRPLFEKKSLEDKTERELLESYIDGRIVEGSDAEIGMSPWQV 336
ProT_Δ154-167 GEADCGLRPLFEKKSLEDKTERELLESYIDGRIVEGSDAEIGMSPWQV 290
ProT_Δ146-167 GEADCGLRPLFEKKSLEDKTERELLESYIDGRIVEGSDAEIGMSPWQV 282
              **************************************************

wt-ProT       MLFRKSPQELLCGASLISDRWVLTAAHCLLYPPWDKNFTENDLLVRIG 384
ProT_Δ154-167 MLFRKSPQELLCGASLISDRWVLTAAHCLLYPPWDKNFTENDLLVRIG 338
ProT_Δ146-167 MLFRKSPQELLCGASLISDRWVLTAAHCLLYPPWDKNFTENDLLVRIG 330
              **************************************************
```

Continued on next page →

```
wt-ProT       KHSRTRYERNIEKISMLEKIYIHPRYNWRENLDRDIALMKLKKPVAFS 432
ProT_Δ154-167 KHSRTRYERNIEKISMLEKIYIHPRYNWRENLDRDIALMKLKKPVAFS 386
ProT_Δ146-167 KHSRTRYERNIEKISMLEKIYIHPRYNWRENLDRDIALMKLKKPVAFS 378
              *********************************************

wt-ProT       DYIHPVCLPDRETAASLLQAGYKGRVTGWGNLKETWTANVGKGQPSVL 480
ProT_Δ154-167 DYIHPVCLPDRETAASLLQAGYKGRVTGWGNLKETWTANVGKGQPSVL 434
ProT_Δ146-167 DYIHPVCLPDRETAASLLQAGYKGRVTGWGNLKETWTANVGKGQPSVL 426
              *********************************************

wt-ProT       QVVNLPIVERPVCKDSTRIRITDNMFCAGYKPDEGKRGDACEGDSGGP 528
ProT_Δ154-167 QVVNLPIVERPVCKDSTRIRITDNMFCAGYKPDEGKRGDACEGDAGGP 482
ProT_Δ146-167 QVVNLPIVERPVCKDSTRIRITDNMFCAGYKPDEGKRGDACEGDAGGP 474
              *******************************************:***

wt-ProT       FVMKSPFNNRWYQMGIVSWGEGCDRDGKYGFYTHVFRLKKWIQKVIDQ 576
ProT_Δ154-167 FVMKSPFNNRWYQMGIVSWGEGCDRDGKYGFYTHVFRLKKWIQKVIDQ 530
ProT_Δ146-167 FVMKSPFNNRWYQMGIVSWGEGCDRDGKYGFYTHVFRLKKWIQKVIDQ 522
              *********************************************

wt-ProT       FGE 579
ProT_Δ154-167 FGE 533
ProT_Δ146-167 FGE 525
              ***
```

Figure 2.47. Multiple sequence alignment of the wild-type human prothrombin (wt-ProT), the truncated prothrombin S525A Δ154-167 (ProT_Δ154-167), and the truncated prothrombin S525A Δ146-167 (ProT_Δ146-167). The residues of the linker 2 removed in wt-ProT sequence to generate ProT_Δ154-167 are green, while those removed to generate ProT_Δ146-167 are green and underlined. The 32 residues of the GLA domain removed from the wt-ProT sequence are blue. The wt-ProT catalytic serine that in ProT_Δ154-167 and ProT_Δ146-167 is mutated to alanine is in red.

With respect to the wild-type protein the mutant sequences were truncated by removing the flexible N-terminal region corresponding to residues 1-32 of the GLA domain (Figure 2.47). This modification was necessary to simplify the production of the prothrombin mutants in bacteria. Indeed, the fragment 1-32 contains the glutamate residues that are mutated to γ-carboxyglutamate in the wild-type protein by post-translational vitamin K-dependent processes.[176] Finally, to avoid autoactivation of the prothrombin,[148] the Ser525 of the catalytic triad was mutated to alanine (Figure 2.47).

Considering that the aptamers interact with the protease domain of the prothrombin, the crystallization of the aptamer complexes with the prethrombin-2 intermediate (see Introduction, paragraph 1.5) could provide enough structural information about the interaction. For this reason, also a prethrombin-2 variant was designed by mutating to alanine the Ser195 of the catalytic triad (PreII_S195A) (Figure 2.48).

```
wt-PreII    TATSEYQTFFNPRTFGSGEADCGLRPLFEKKSLEDKTERELLESYIDG 48
PreII_S195A TATSEYQTFFNPRTFGSGEADCGLRPLFEKKSLEDKTERELLESYIDG 48
            **************************************************

wt-PreII    RIVEGSDAEIGMSPWQVMLFRKSPQELLCGASLISDRWVLTAAHCLLY 96
PreII_S195A RIVEGSDAEIGMSPWQVMLFRKSPQELLCGASLISDRWVLTAAHCLLY 96
            **************************************************

wt-PreII    PPWDKNFTENDLLVRIGKHSRTRYERNIEKISMLEKIYIHPRYNWREN 144
PreII_S195A PPWDKNFTENDLLVRIGKHSRTRYERNIEKISMLEKIYIHPRYNWREN 144
            **************************************************

wt-PreII    LDRDIALMKLKKPVAFSDYIHPVCLPDRETAASLLQAGYKGRVTGWGN 192
PreII_S195A LDRDIALMKLKKPVAFSDYIHPVCLPDRETAASLLQAGYKGRVTGWGN 192
            **************************************************

wt-PreII    LKETWTANVGKGQPSVLQVVNLPIVERPVCKDSTRIRITDNMFCAGYK 240
PreII_S195A LKETWTANVGKGQPSVLQVVNLPIVERPVCKDSTRIRITDNMFCAGYK 240
            **************************************************

wt-PreII    PDEGKRGDACEGDSGGPFVMKSPFNNRWYQMGIVSWGEGCDRDGKYGF 288
PreII_S195A PDEGKRGDACEGDAGGPFVMKSPFNNRWYQMGIVSWGEGCDRDGKYGF 288
            ************:*************************************

wt-PreII    YTHVFRLKKWIQKVIDQFGE 308
PreII_S195A YTHVFRLKKWIQKVIDQFGE 308
            ********************
```

Figure 2.48. Sequence alignment of the wild-type human prethrombin-2 (wt-PreII) and the prethrombin-2 S195A mutant (PreII_S195A). The wt-PreII catalytic serine that in PreII_S195A is mutated to alanine is in red.

2.3.5. Recombinant production of prethrombin-2 and prothrombin mutants

The recombinant production of the prethrombin-2 and prothrombin mutants was performed at the Institute of Structural Biology of the Helmholtz Zentrum München (Munich, Germany) under the supervision of Dr. Grzegorz Popowicz.

Prethrombin-2

The gene encoding the prethrombin-2 was cloned into pETM-11 vector in order to add a 6xHis-tag to the N-terminal tail of the protein. Then, the gene sequence was mutated to encode for 6xHis-tagged PreII_S195A variant (H_6PreII_S195A), in which the catalytic serine residue was replaced with an alanine residue (Figure 2.49).

```
H6PreII_S195A MKHHHHHHPMSDYDIPTTENLYFQGAMATATSEYQTFFNPRTFGSGEA 48
H6PreII_S195A DCGLRPLFEKKSLEDKTERELLESYIDGRIVEGSDAEIGMSPWQVMLF 96
H6PreII_S195A RKSPQELLCGASLISDRWVLTAAHCLLYPPWDKNFTENDLLVRIGKHS 144
H6PreII_S195A RTRYERNIEKISMLEKIYIHPRYNWRENLDRDIALMKLKKPVAFSDYI 192
H6PreII_S195A HPVCLPDRETAASLLQAGYKGRVTGWGNLKETWTANVGKGQPSVLQVV 240
H6PreII_S195A NLPIVERPVCKDSTRIRITDNMFCAGYKPDEGKRGDACEGDAGGPFVM 288
H6PreII_S195A KSPFNNRWYQMGIVSWGEGCDRDGKYGFYTHVFRLKKWIQKVIDQFGE 336
```

Figure 2.49. Sequence of H_6PreII_S195A. Residues from pETM-11 vector carrying the 6xHis-tag are blue, while the catalytic serine mutated to alanine is red.

An expression screening (Figure 2.50) was performed varying *Escherichia coli* strain, medium, induction method, inductor (isopropil-β-D-1-tiogalattopiranoside, IPTG) concentration, and expression temperature.

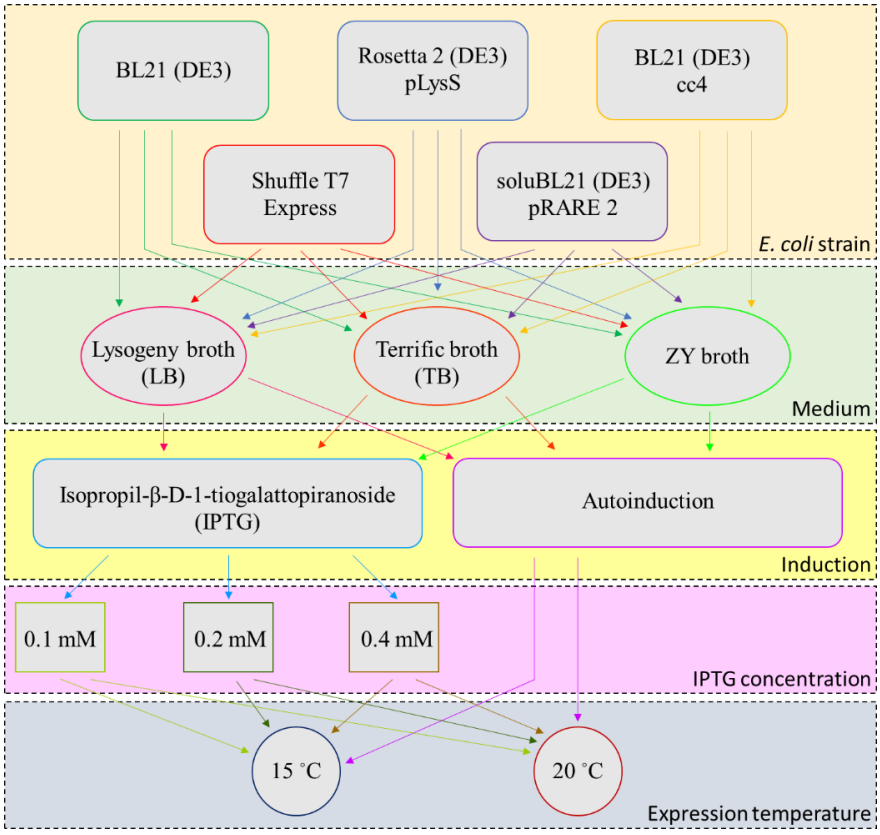

Figure 2.50. Schematic representation of the screening performed for the expression of H_6PreII_S195A.

In none of the tested combinations, there was a significant amount of soluble protein. On the contrary, in all cases the protein was found in insoluble inclusion bodies. For this reason, the expression, refolding, and purification procedures for H_6PreII_S195A, described in the Experimental Section (paragraph 3.2.5), were re-adapted by those reported in literature to produce the wild-type protein.[177] The purity of the protein was assessed by SDS-PAGE gel (Figure 2.51). 1 mg of refolded H_6PreII_S195A protein was obtained after the last purification step.

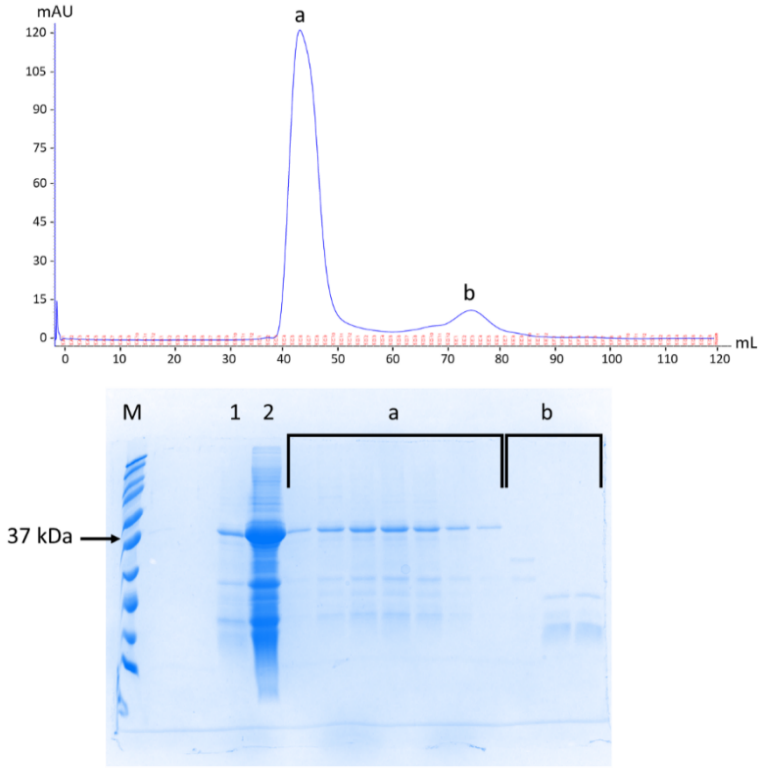

Figure 2.51. SDS-PAGE analysis of H_6PreII_S195A purified with size exclusion chromatography (S75). The corresponding purification profile is reported on the top. Lane M, protein molecular weight marker (the band corresponding to the closest molecular weight to that of H_6PreII_S195A is indicated); lane 1, protein eluted from nickel column; lane 2, protein eluted from nickel column after concentration; lanes a and b, size exclusion chromatography fractions corresponding to a and b peaks in the purification profile, respectively.

Prothrombin mutants

In order to produce the recombinant prothrombin mutants in bacteria, the gene encoding the wild-type protein was cloned into pETM-11 vector, which contains after the starting codon ATG the codon sequence for an N-terminal 6xHis-tag followed by a TEV protease site. Then, the gene sequence was mutated to encode for 6xHis-tagged ProT_Δ154-167 and ProT_Δ146-167 variants (H_6PT_Δ154-167 and H_6PT_Δ146-167) (Figure 2.52).

```
H6PT_Δ154-167 MKHHHHHHPMSDYDIPTTENLYFQGAMASSTATDVFWAKYTACETART 48
H6PT_Δ146-167 MKHHHHHHPMSDYDIPTTENLYFQGAMASSTATDVFWAKYTACETART 48
              **********************************************

H6PT_Δ154-167 PRDKLAACLEGNCAEGLGTNYRGHVNITRSGIECQLWRSRYPHKPEIN 96
H6PT_Δ146-167 PRDKLAACLEGNCAEGLGTNYRGHVNITRSGIECQLWRSRYPHKPEIN 96
              **********************************************

H6PT_Δ154-167 STTHPGADLQENFCRNPDSSTTGPWCYTTDPTVRRQECSIPVCGQDQV 144
H6PT_Δ146-167 STTHPGADLQENFCRNPDSSTTGPWCYTTDPTVRRQECSIPVCGQE-- 142
              *******************************************

H6PT_Δ154-167 TVAMTEQCVPDRGQQYQGRLAVTTHGLPCLAWASAQAKALSKHQDFNS 192
H6PT_Δ146-167 ------QCVPDRGQQYQGRLAVTTHGLPCLAWASAQAKALSKHQDFNS 184
                    ************************************

H6PT_Δ154-167 AVQLVENFCRNPDGDEEGVWCYVAGKPGDFGYCDLNYCEEAVEEETGD 240
H6PT_Δ146-167 AVQLVENFCRNPDGDEEGVWCYVAGKPGDFGYCDLNYCEEAVEEETGD 232
              **********************************************

H6PT_Δ154-167 GLDEDSDRAIEGRTATSEYQTFFNPRTFGSGEADCGLRPLFEKKSLED 288
H6PT_Δ146-167 GLDEDSDRAIEGRTATSEYQTFFNPRTFGSGEADCGLRPLFEKKSLED 280
              **********************************************

H6PT_Δ154-167 KTERELLESYIDGRIVEGSDAEIGMSPWQVMLFRKSPQELLCGASLIS 336
H6PT_Δ146-167 KTERELLESYIDGRIVEGSDAEIGMSPWQVMLFRKSPQELLCGASLIS 328
              **********************************************

H6PT_Δ154-167 DRWVLTAAHCLLYPPWDKNFTENDLLVRIGKHSRTRYERNIEKISMLE 384
H6PT_Δ146-167 DRWVLTAAHCLLYPPWDKNFTENDLLVRIGKHSRTRYERNIEKISMLE 376
              **********************************************

H6PT_Δ154-167 KIYIHPRYNWRENLDRDIALMKLKKPVAFSDYIHPVCLPDRETAASLL 432
H6PT_Δ146-167 KIYIHPRYNWRENLDRDIALMKLKKPVAFSDYIHPVCLPDRETAASLL 424
              **********************************************

H6PT_Δ154-167 QAGYKGRVTGWGNLKETWTANVGKGQPSVLQVVNLPIVERPVCKDSTR 480
H6PT_Δ146-167 QAGYKGRVTGWGNLKETWTANVGKGQPSVLQVVNLPIVERPVCKDSTR 472
              **********************************************

H6PT_Δ154-167 IRITDNMFCAGYKPDEGKRGDACEGDAGGPFVMKSPFNNRWYQMGIVS 528
H6PT_Δ146-167 IRITDNMFCAGYKPDEGKRGDACEGDAGGPFVMKSPFNNRWYQMGIVS 520
              **********************************************

H6PT_Δ154-167 WGEGCDRDGKYGFYTHVFRLKKWIQKVIDQFGE 561
H6PT_Δ146-167 WGEGCDRDGKYGFYTHVFRLKKWIQKVIDQFGE 553
              *********************************
```

Figure 2.52. Sequence alignment of H_6PT_Δ154-167 and H_6PT_Δ146-167. Residues from pETM-11 vector carrying the 6xHis-tag and the TEV protease site are blue, while the catalytic serine residues mutated to alanine are red.

The expression conditions for the two mutants were investigated by the same screening performed previously for H_6PreII_S195A (Figure 2.50), revealing that in the *Escherichia coli* strain BL21 (DE3) the amount of soluble protein, albeit low, was higher than the other strains (Figure 2.53).

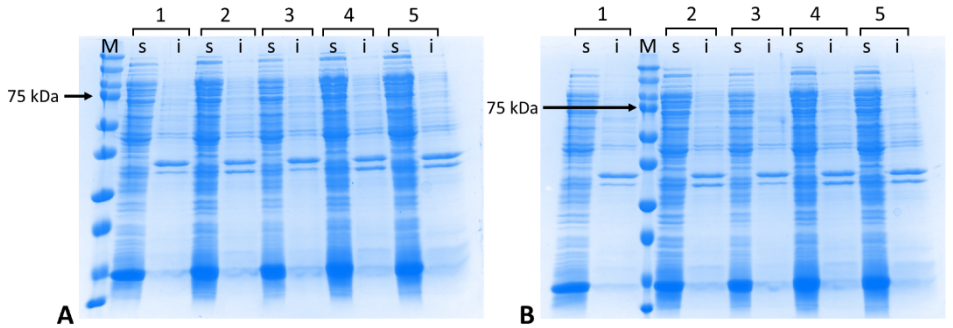

Figure 2.53. SDS-PAGE analysis of the A) H_6PT_Δ154-167 and B) H_6PT_Δ146-167 expression screening using *Escherichia coli* strain BL21 (DE3). Lane M, protein molecular weight marker (the bands corresponding to the closest molecular weight to that of the two mutants are indicated); lanes 1 and 3, soluble (s) and insoluble (i) fractions of the cells cultured in LB medium and supplemented with 0.4 mM or 0.2 mM IPTG, respectively; lanes 2 and 4, soluble (s) and insoluble (i) fractions of the cells cultured in TB medium and supplemented with 0.4 mM or 0.2 mM IPTG, respectively; lanes 5, soluble (s) and insoluble (i) fractions of the cells cultured in ZY broth medium.

It is worth noting that starting from this step the two mutants always gave the same results. Hence, the H_6PT_Δ154-167 will be referred to throughout the paragraph. The optimized expression and purification procedures, described in the Experimental Section (paragraph 3.2.5), allowed to obtain 2 mg of each prothrombin mutant. The purity of the protein was assessed by SDS-PAGE gel (Figure 2.54), after each purification step.

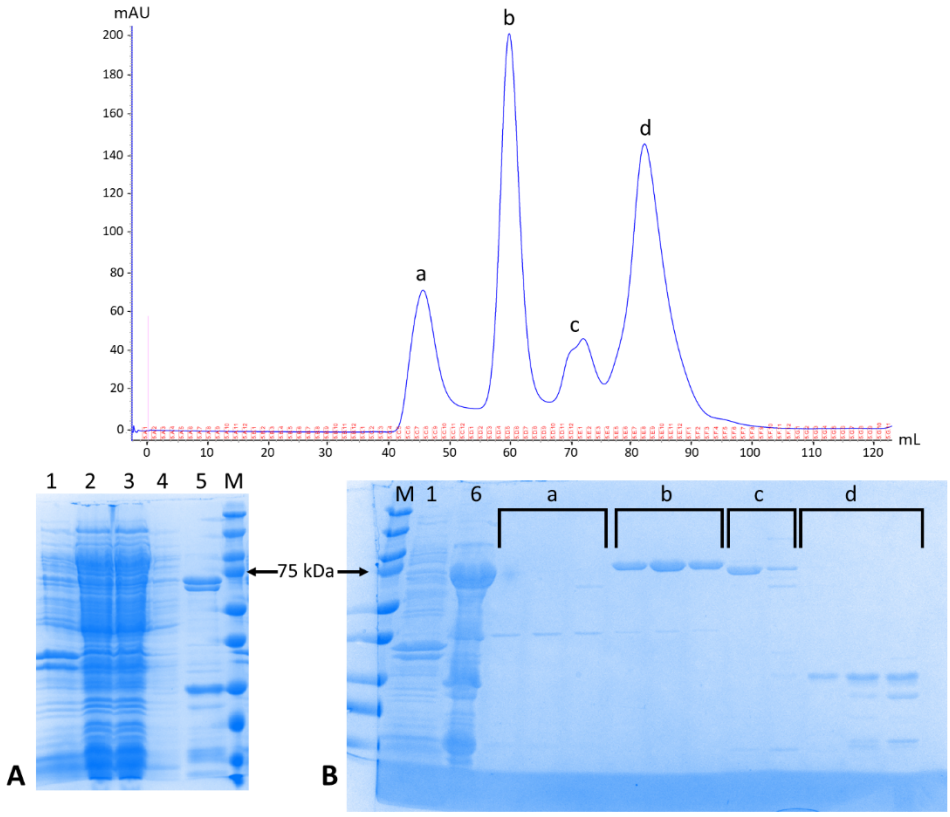

Figure 2.54. SDS-PAGE analysis of H_6PT_Δ154-167 purified with A) Ni-NTA affinity chromatography and B) size exclusion chromatography (S200). The corresponding purification profile is reported on the top. Lane M, protein molecular weight marker (the bands corresponding to the closest molecular weight to that of H_6PT_Δ154-167 are indicated); lane 1 on both gels, insoluble fraction; lane 2, soluble fraction; lanes 3, 4, and 5, flow-through, washing, and elution from nickel column, respectively; lane 6, protein eluted from nickel column after concentration; lanes a, b, c, and d, size exclusion chromatography fractions corresponding to a, b, c, and d peaks in the purification profile, respectively.

A Western blotting (Figure 2.55) was performed using the Ni-NTA-Atto 647N conjugate,[178] a dye that provide specific and highly sensitive detection of His-tagged fusion proteins. Both the 6xHis-tagged and the not tagged variants were tested. Moreover, two routinely produced protein, one containing a 6xHis-tag,

were used as control. The experiment strongly suggests that the purified proteins are the desired prothrombin mutants.

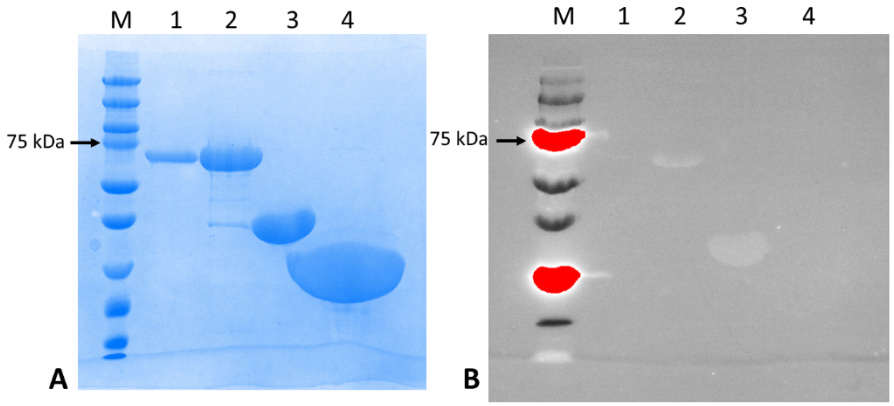

Figure 2.55. A) SDS-PAGE and B) Western blot analysis of H_6PT_Δ154-167. Lane M, protein molecular weight marker (the bands corresponding to the closest molecular weight to that of H_6PT_Δ154-167 are indicated); lane 1, prothrombin mutant after the cleavage of the 6xHis-tag; lane 2, prothrombin mutant containing the 6xHis-tag; lane 3, routinely produced protein containing a 6xHis-tag; lane 4, routinely produced protein that does not contain a 6xHis-tag.

2.3.6. Crystallization trials of the complexes between NU172 and prethrombin-2 or prothrombin mutants

The complexes between NU172 and H_6PreII_S195A, H_6PT_Δ154-167, or H_6PT_Δ146-167 were prepared in 25 mM potassium phosphate pH 7.4 and 100 mM KCl and concentrated to about 10 mg mL^{-1}, following the protocol usually used for the preparation of aptamer-thrombin complexes (see Experimental section, paragraph 3.2.1).[66,69,70,76,80] An extensive screening of the crystallization conditions was carried out by using commercial kits (NeXtal QIAGEN Classics, Classics II and Nucleix Suites; Molecular Dimensions JCSG-plus; Jena Bioscience JBScreen PACT++) and the Mosquito Crystal protein crystallization robot (SPT Labtech). Unfortunately, no good quality crystals have been obtained to date.

2.4. Concluding remarks

The study of the modulation of human α-thrombin by oligonucleotide aptamers is one of the most active research field from the development of the SELEX strategy.[68,118] Indeed, despite the excellent anticoagulant properties of TBA and NU172, the only two aptamers entered to date in clinical trials, new powerful aptamers are periodically selected.[179–181] Moreover, thrombin binding aptamers are often employed as a proof-of-concept in the analysis of new chemical modifications or biosensing strategies, leading to a continuous increase of the knowledge on this field.[182,183]

Nevertheless, at least three further aspects are still to be clarified.

- The first concerns the aptamer-guided cooperation observed between the two thrombin exosites.[93,94] Although insightful atomic-level snapshots of the recognition between thrombin and aptamers have been recently achieved through crystallographic analyses,[95] some dynamic aspects of this interaction have not been fully characterized.
- The second aspect is related to the post-SELEX modifications.[100] Indeed, despite countless functional results are presented day-by-day,[68] a comprehensive structural characterization of modified anti-thrombin aptamers both in the free and liganded state, which could facilitate a more rational use of chemical modifications, is still lacking.
- The third aspect regards the development of a dual targeting therapy i.e. the search for aptamers, able to bind both thrombin and its inactive precursor, prothrombin. In this way a single antidote-controllable anticoagulant aptamer should simultaneously limit thrombin generation and inhibit thrombin activity. For this purpose, a structural characterization of the interaction between aptamers and prothrombin is strictly required.

The research activity carried out in the frame of this PhD project has been focused on these three aspects.

In the attempt to obtain a structural evidence of the aptamer-guided inter-exosite communication in thrombin, the crystal structure of the ternary complex in which thrombin is sandwiched between two duplex/quadruplex aptamers, NU172 and HD22_27mer, was solved. The comparison of the ternary complex with the corresponding binary ones indicates a reorganization of tetrad II in the case of HD22 _27mer, which is similar to that observed for the other ternary complexes previously analysed.[95] Furthermore, the nucleobases Gua13 and Cyt14, which stack on tetrad II, adopt a novel conformation. The local structural variability of HD22_27mer highlights a higher conformational flexibility of this aptamer compared to NU172. In particular, whereas NU172 has an elongated structure with very few contacts between its two structural domains, HD22_27mer assumes a peculiar sharply kinked conformation in which the helical axis of the duplex segment and that of the G-quadruplex motif are approximately perpendicular. This bent conformation gives more space to local structural fluctuations with respect to the elongated one. Then, to achieve a dynamic view of the thrombin interaction with aptamers and to obtain an unbiased view of the inter-exosite communication, molecular dynamics simulations on TBA-thrombin-HD22_27mer and NU172-thrombin-HD22_27mer ternary complexes were performed and compared with those conducted on the free protein and on the respective binary complexes. The analysis of the dynamics of the thrombin exosites in different contexts indicates that the binding of TBA or NU172 at the exosite I makes residues at the exosite II more rigid, favouring conformations that are prone to the binding of HD22_27mer, and *vice versa*. All these observations underline that the binding of an aptamer to a thrombin exosite mainly alters the dynamics of the other exosite, although it does not undergo to a net conformational change. In particular, the reduction of the mobility of the residues of the unbound exosite is associated with the selection of the conformation that is competent for the binding of the aptamer at that site. Finally, to validate the findings emerged from the MD analyses, the

synergic action of the two duplex/quadruplex aptamers in anticoagulation experiments was evaluated. Although HD22_27mer is not able to inhibit the cleavage of the fibrinogen to fibrin, its binding to the exosite II doubles the anticoagulant activity of NU172. Such an enhancement of NU172 activity is not observed in the presence of a 30mer oligonucleotide (IGA3)[166] that does not bind the thrombin exosites. Overall, the crystallographic and dynamic analyses have provided a detailed characterization of the modulation of the inter-exosite communication by anti-thrombin aptamers that has been corroborated by experimental data. Moreover, the synergic action of the NU172 and HD22_27mer represents an important stimulus for the design of new bivalent thrombin-anchoring compounds.[79,184–186] Indeed, their tight association in the crystalline form of the ternary complex, mediated by the stacking of their duplex regions may provide clues for the rational design of monomolecular aptamers that are able to bind at once two different thrombin molecules, opening to unexplored strategies of thrombin inhibition or detection.

In the effort to obtain structural information on the effect of chemical modification on the properties of the aptamers, the crystal structures of the complexes between thrombin and three TBA variants (TBA-3L, TBA-3G, and TBA-3Leu), in which Thy3 contains functional substituents at N3 of the pyrimidine heterocycle, were solved. These studies confirmed that the arrangement of N3 substituents of Thy3 in the B-region of thrombin exosite I is governed by the strict requirement of interaction between an unmodified TT loop and the A-region. As a result, the modified pyrimidine base is positioned in proximity to thrombin Tyr76, and the visible part of the modified side chain is engaged in a hydrophobic interaction with Ile82. Moreover, a better fit on the thrombin surface and an optimization of the intermolecular contacts were observed for the three TBA variants with respect to the unmodified TBA. In particular, the modification introduced on the Thy3 causes subtle adjustments of the oligonucleotides similar to those produced by the

replacement of K^+ by Na^+ in the unmodified aptamer,[66] providing a reasonable explanation for their higher binding affinity toward thrombin with respect to that of TBA. Moreover, a preliminary analysis of the crystal structures of the complexes between thrombin and two TBA variants (cycTBA II and TBA NN/DD), carrying modifications at 5′- and 3′-ends, was performed. In particular, the structures revealed an unchanged folding of the oligonucleotide domain of both mutants that preserve the ability to recognize the protein exosite I. While the linker that connects the ends of cycTBA II does not assume a stable conformation, in TBA NN/DD the naphthalene diimides at 5′-end and dansyl groups at 3′-end firmly stack on the G-quadruplex domain, generating a compact duplex/quadruplex-like folding. Surprisingly, in two of the three crystal structures of the complex between TBA NN/DD and thrombin, the aptamer is also bound to the protein exosite II. ITC experiments will be performed in order to verify this putative unpredictable binding ability of TBA NN/DD in solution. Finally, the analysis of the physicochemical and functional properties of the first NU172 analogues, obtained by incorporation of unnatural hexitol-based nucleotides into key positions of the aptamer, was carried out. The spectroscopic data revealed that hexitol insertions at the Thy9 or Gua18 positions of NU172 leave almost unchanged both the structure and thermal stability of the aptamer. In contrast, substitutions at the Thy10, Thy14, and Thy19 positions negatively affect aptamer structural properties. In particular, based on structure–activity relationship studies, NU172-T^H9 was identified as the most interesting NU172 analogue. Indeed, its anticoagulant activity, evaluated through a fibrinogen clotting assay, was found to be comparable or slightly preferable to the unmodified oligonucleotide.

The aptitude of different anti-thrombin aptamers to recognize prothrombin pro-exosite I has been eventually studied. A complete comparative thermodynamic analysis of the binding of TBA, RE31, and NU172 aptamers to thrombin and to its zymogen prothrombin by means of ITC was performed. The results clearly

indicate the ability of the examined aptamers to interact with pro-exosite I with an affinity similar to that shown for exosite I, laying the foundations for an in-depth structural characterization. Furthermore, CD studies revealed the promotion of the aptamer folding upon prothrombin binding.

The attempts to growth crystals of the complexes between the anti-thrombin aptamers and wild-type prothrombin produced only poorly diffracting crystals. To increase the probability of having structural data, prethrombin-2 and prothrombin mutants, lacking the more flexible regions of the protein, were recombinantly produced during an internship at the Institute of Structural Biology of the Helmholtz Zentrum München (Munich, Germany). Crystallization trials using these successfully produced proteins are in progress. The crystallization trials will be extended to aptamer-protein complexes involving other thrombin/prothrombin intermediates, as prethrombin-1. Moreover, small-angle neutron scattering (SANS) experiments using wild-type prothrombin, in collaboration with Prof. Luigi Paduano of the Department of Chemical Sciences, University of Naples Federico II (Italy), are in progress.

Despite the lack of crystallographic data, the results obtained in this thesis, which represent the first detailed characterization of the binding of prothrombin with different anticoagulant aptamers, confirm the possibility to modulate two important factors of the coagulation cascade that provides a potent approach to actively and reversibly control coagulation.

SECTION 3:

Experimental section

3. EXPERIMENTAL SECTION

3.1. Materials

The human D-Phe-Pro-Arg-chloromethylketone (PPACK)-inhibited thrombin (for crystallization and ITC experiments), the active human a-thrombin (for anticoagulant activity experiments), and human prothrombin were purchased from Haematologic Technologies (USA). Fibrinogen from human plasma, TBA, NU172, and HD22_27mer were purchased from Sigma-Aldrich (United Kingdom), while RE31 aptamer (kindly gifted by Dr. Vera Spiridonova of M.V. Lomonosov Moscow State University, Moscow, Russia) from Syntol (Russia). In order to induce folding, all oligonucleotide samples were annealed by heating to 90 °C for 5 minutes and then slowly cooling down in 50-60 minutes and storing at 20 °C overnight.

All the primers used in cloning and mutagenesis experiments were purchased from Eurofins Genomics (Germany). The expression plasmids pET21a and pDEST40 encoding human wild-type prethrombin-2 and prothrombin, respectively, were kindly gifted by Prof. Enrico Di Cera of the Saint Louis University School of Medicine (Missouri, USA).

3.2. Methods

3.2.1. Crystallography

A standard protocol was followed for the preparation of the binary complexes between thrombin and modified oligonucleotides in 25 mM potassium phosphate buffer pH 7.4 and 100 mM KCl.[66,69,70,76,80] Briefly, a 2-fold molar excess of the oligonucleotide, previously annealed, was deposited onto a frozen sample of thrombin. The system was left at 4 °C overnight. The final solution was extensively washed to remove the excess of the aptamers and was finally concentrated to about 9 mg mL^{-1}. In the case of the ternary complex NU172-thrombin-HD22_27mer, prepared in 10 mM sodium phosphate buffer pH 7.0 and

100 mM NaCl, a 2-fold molar excess of HD22_27mer was deposited onto a frozen solution of thrombin and incubated at 4 °C for 7 h. Then the solution was frozen again and a 2-fold molar excess of a NU172 solution was deposited onto it. The system was kept at 4 °C overnight and then, washed and concentrated to about 8 mg mL^{-1}.

For all complexes, an initial screening of hanging drop crystallization experiments mixing 0.5 µL complex solution with 0.5 µL reservoir solution was carried out at 20 °C using precipitant solutions of a commercially available crystallization screen (Hampton Research Index) and/or reproducing the conditions reported in the literature for the crystallization of other aptamer-thrombin complexes.[66,69–71,76,80,83,95] Crystals suitable for X-ray diffraction data collection growth after a fine optimization of starting conditions (Figure 3.1).

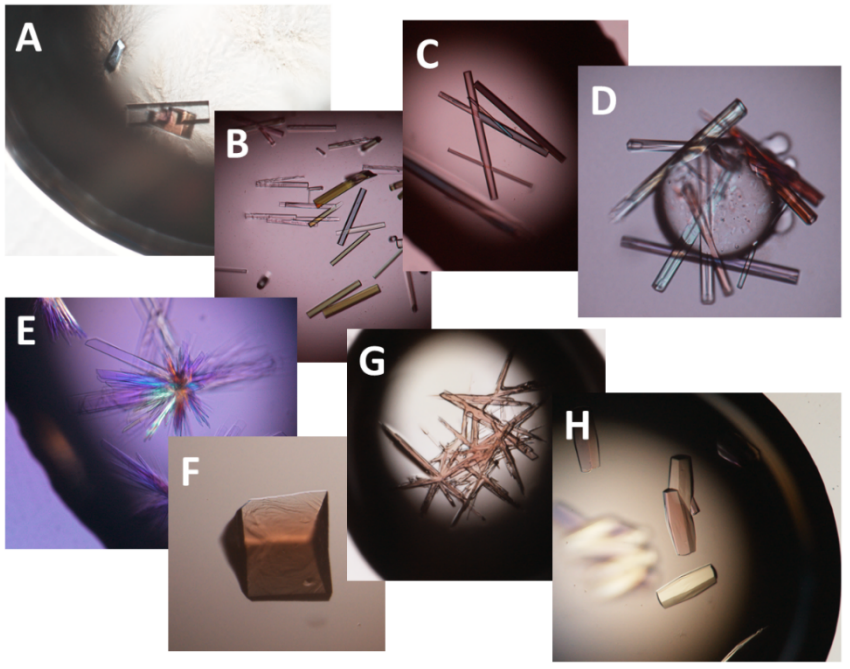

Figure 3.1. Crystals of the complexes between thrombin and A) NU172 and HD22_27mer (ternary complex), B) TBA-3L, C) TBA-3G, D) TBA-3Leu, E) cycTBA II, F) TBA NN/DD (condition A), G) TBA NN/DD (condition B), and H) TBA NN/DD (condition C).

The crystallization conditions for each complex, as well as general information about data collection, structure determination, refinement, and structural analysis are summarized in Table 3.1 and Table 3.2.

Table 3.1. Crystallization, data collection, structure determination, refinement, and structural analysis summary for NU172-thrombin-HD22_27mer, TBA-3L-thrombin, TBA-3G-thrombin, and TBA-3Leu-thrombin complexes.

	Ternary complex	**TBA-3L**	**TBA-3G**	**TBA-3Leu**
Condition	26% *w/v* PEG 3350 0.2 M ammonium acetate 0.1 M Bis-Tris pH 6.5	35% *v/v* pentaerythritol propoxylate 0.2 M KCl 50 mM HEPES pH 7.5		18% *w/v* PEG 4000 18% *v/v* 2-propanol 0.1 M tri-sodium citrate pH 5.6
Cryoprotector	25% *v/v* ethylene glycol	-		
Data collection	Institute of Biostructures and Bioimages (CNR, Naples, Italy) using a Rigaku Micromax 007 HF generator equipped with a Saturn944 CCD detector	i04 beamline of the Diamond Light Source synchrotron (Harwell Science and Innovation Campus, Oxfordshire, United Kingdom)		
Wavelength	CuKα radiation λ = 1.5418 Å	λ = 0.9795 Å		
Data processing	HKL2000[187]	autoPROC[188–192] + STARANISO[193]		
Molecular replacement	Phaser MR[194] (CCP4)[190]			
Search model	Human α-thrombin (PDB code: 1PPB)[60,61]			
Manual model building	WinCoot[195]			
Refinement	REFMAC5[196] (CCP4)[190]			
Structural analysis - RMSD	Superpose[197] (CCP4)[190]			
Structural analysis - Buried area	PISA[198] (CCP4)[190]			
Structural analysis - Interactions	DIMPLOT (LigPlot+)[199] HBOND[a]	Contact (CCP4)[190]		

[a]HBOND (http://cib.cf.ocha.ac.jp/bitool/HBOND/).

Table 3.2. Crystallization, data collection, structure determination, and refinement summary for cycTBAII-thrombin and TBANN/DD-thrombin complexes.

	CycTBA II	**TBA NN/DD A**	**TBA NN/DD B**	**TBA NN/DD C**
Condition	54% *v/v* Tacsimate™ pH 7.0 1% *v/v* acetonitrile	20% *w/v* PEG 4000 20% *v/v* 2-propanol 0.1 M tri-sodium citrate pH 5.6	25% *w/v* PEG 3350 0.2 M ammonium acetate 0.1 M Bis-Tris pH 6.5	46% *v/v* Tacsimate™ pH 7.0
Cryoprotector	20% *v/v* glycerol	-	25% *v/v* glycerol	20% *v/v* glycerol
Data collection	XRD2 beamline of the Elettra Synchrotron Trieste (Italy)			
Wavelength	λ = 1.0000 Å			
Data processing	iMOSFLM[200] + Pointless[188,201]/ Aimless[192]/ Ctruncate[202] (CCP4)[190]	autoPROC[188–192]		
Molecular replacement	Phaser MR[194] (CCP4)[190]			
Search model	Human α-thrombin (PDB code: 1PPB)[60,61]			
Manual model building	WinCoot[195]			
Refinement	REFMAC5[196] (CCP4)[190]			

Crystallographic figures were prepared using PyMOL (DeLano Scientific, Palo Alto, CA, USA).

3.2.2. Molecular dynamics: models and protocols

All-atom molecular dynamics (MD) simulations in explicit solvent were performed on the free thrombin and on its binary and ternary complexes with TBA, NU172, and HD22_27mer in the absence of the PPACK inhibitor at the active site. In detail, the crystal structure of human a-thrombin (PDB code: 1PPB)[60,61] was used as starting model in the MD of the free protein. In the simulations of aptamer-thrombin complexes, the X-ray structures of TBA-thrombin (PDB code: 4DIH)[66], NU172-thrombin (PDB code: 6GN7)[80],

HD22_27mer-thrombin (PDB code: 4I7Y)[83], TBAΔT3-thrombin-HD22_27mer (PDB code: 5EW1)[95] and NU172-thrombin-HD22_27mer (here presented) were used. Disordered regions (termini of the light chain, the C-terminal end of the heavy chain and the γ-autolysis loop) were rebuilt, where necessary, using the unbound-thrombin structure (PDB code: 1PPB)[60,61] as template. The Gua1 nucleobase of HD22_27mer aptamer was also rebuilt in TBAΔT3-thrombin-HD22_27mer ternary complex. As the TBA-like aptamer lacking the Thy3 nucleobase (TBADT3) in the ternary complex is related by a 180° rotation around the quadruplex axis to the parent TBA present in the binary complex (PDB code: 4DIH)[66], in order to compare MD results, the parent TBA structure was also replaced in the starting model of the TBAΔT3-thrombin-HD22_27mer ternary complex. The endogenous sodium ion bound to the protein was kept in the starting models. The sodium ions in the G-quadruplex motif of aptamers were also maintained in all aptamer structures. For the convenience of counting, thrombin residues were sequentially numbered from residue 1 to 36 for the light chain and from residue 37 to 295 for the heavy chain (MD notation). In Table 3.3 the correspondence between the MD and CS (crystal structures) notations is reported. Thrombin exosites are not confined to a single protein segment but comprise distant regions of the polypeptide chain. In detail, residues 45 (CS 24), 104–111 (CS 73–79), 114 (CS 82) and 150 (CS 117) belong to exosite I whereas residues 121–134 (CS 89–101), 159–166 (CS 126–130), 205–210 (CS 164–169) and 280–293 (CS 232–245) belong to exosite II.

Table 3.3. Comparison between the crystallographic (CS) and molecular dynamics (MD) notations of the thrombin light (blue) and heavy (black) chains.

Sequence	CS	MD	Sequence	CS	MD	Sequence	CS	MD
Thr	1h	1	**Ala**	22	43	**Pro**	60c	85
Phe	1g	2	**Glu**	23	44	**Trp**	60d	86
Gly	1f	3	**Ile**	24	45	**Asp**	60e	87
Ser	1e	4	**Gly**	25	46	**Lys**	60f	88
Gly	1d	5	**Met**	26	47	**Asn**	60g	89
Glu	1c	6	**Ser**	27	48	**Phe**	60h	90
Ala	1b	7	**Pro**	28	49	**Thr**	60i	91
Asp	1a	8	**Trp**	29	50	**Glu**	61	92
Cys	1	9	**Gln**	30	51	**Asn**	62	93
Gly	2	10	**Val**	31	52	**Asp**	63	94
Leu	3	11	**Met**	32	53	**Leu**	64	95
Arg	4	12	**Leu**	33	54	**Leu**	65	96
Pro	5	13	**Phe**	34	55	**Val**	66	97
Leu	6	14	**Arg**	35	56	**Arg**	67	98
Phe	7	15	**Lys**	36	57	**Ile**	68	99
Glu	8	16	**Ser**	36a	58	**Gly**	69	100
Lys	9	17	**Pro**	37	59	**Lys**	70	101
Lys	10	18	**Gln**	38	60	**His**	71	102
Ser	11	19	**Glu**	39	61	**Ser**	72	103
Leu	12	20	**Leu**	40	62	**Arg**	73	104
Glu	13	21	**Leu**	41	63	**Thr**	74	105
Asp	14	22	**Cys**	42	64	**Arg**	75	106
Lys	14a	23	**Gly**	43	65	**Tyr**	76	107
Thr	14b	24	**Ala**	44	66	**Glu**	77	108
Glu	14c	25	**Ser**	45	67	**Arg**	77a	109
Arg	14d	26	**Leu**	46	68	**Asn**	78	110
Glu	14e	27	**Ile**	47	69	**Ile**	79	111
Leu	14f	28	**Ser**	48	70	**Glu**	80	112
Leu	14g	29	**Asp**	49	71	**Lys**	81	113
Glu	14h	30	**Arg**	50	72	**Ile**	82	114
Ser	14i	31	**Trp**	51	73	**Ser**	83	115
Tyr	14j	32	**Val**	52	74	**Met**	84	116
Ile	14k	33	**Leu**	53	75	**Leu**	85	117
Asp	14l	34	**Thr**	54	76	**Glu**	86	118
Gly	14m	35	**Ala**	55	77	**Lys**	87	119
Arg	15	36	**Ala**	56	78	**Ile**	88	120
Ile	16	37	**His**	57	79	**Tyr**	89	121
Val	17	38	**Cys**	58	80	**Ile**	90	122
Glu	18	39	**Leu**	59	81	**His**	91	123
Gly	19	40	**Leu**	60	82	**Pro**	92	124
Ser	20	41	**Tyr**	60a	83	**Arg**	93	125
Asp	21	42	**Pro**	60b	84	**Tyr**	94	126

Continued on next page →

Sequence	CS	MD	Sequence	CS	MD	Sequence	CS	MD
Asn	95	127	**Lys**	135	171	**Ile**	174	215
Trp	96	128	**Gly**	136	172	**Arg**	175	216
Arg	97	129	**Arg**	137	173	**Ile**	176	217
Glu	97a	130	**Val**	138	174	**Thr**	177	218
Asn	98	131	**Thr**	139	175	**Asp**	178	219
Leu	99	132	**Gly**	140	176	**Asn**	179	220
Asp	100	133	**Trp**	141	177	**Met**	180	221
Arg	101	134	**Gly**	142	178	**Phe**	181	222
Asp	102	135	**Asn**	143	179	**Cys**	182	223
Ile	103	136	**Leu**	144	180	**Ala**	183	224
Ala	104	137	**Lys**	145	181	**Gly**	184	225
Leu	105	138	**Glu**	146	182	**Tyr**	184a	226
Met	106	139	**Thr**	147	183	**Lys**	185	227
Lys	107	140	**Trp**	148	184	**Pro**	186	228
Leu	108	141	**Thr**	149	185	**Asp**	186a	229
Lys	109	142	**Ala**	149a	186	**Glu**	186b	230
Lys	110	143	**Asn**	149b	187	**Gly**	186c	231
Pro	111	144	**Val**	149c	188	**Lys**	186d	232
Val	112	145	**Gly**	149d	189	**Arg**	187	233
Ala	113	146	**Lys**	149e	190	**Gly**	188	234
Phe	114	147	**Gly**	150	191	**Asp**	189	235
Ser	115	148	**Gln**	151	192	**Ala**	190	236
Asp	116	149	**Pro**	152	193	**Cys**	191	237
Tyr	117	150	**Ser**	153	194	**Glu**	192	238
Ile	118	151	**Val**	154	195	**Gly**	193	239
His	119	152	**Leu**	155	196	**Asp**	194	240
Pro	120	153	**Gln**	156	197	**Ser**	195	241
Val	121	154	**Val**	157	198	**Gly**	196	242
Cys	122	155	**Val**	158	199	**Gly**	197	243
Leu	123	156	**Asn**	159	200	**Pro**	198	244
Pro	124	157	**Leu**	160	201	**Phe**	199	245
Asp	125	158	**Pro**	161	202	**Val**	200	246
Arg	126	159	**Ile**	162	203	**Met**	201	247
Glu	127	160	**Val**	163	204	**Lys**	202	248
Thr	128	161	**Glu**	164	205	**Ser**	203	249
Ala	129	162	**Arg**	165	206	**Pro**	204	250
Ala	129a	163	**Pro**	166	207	**Phe**	204a	251
Ser	129b	164	**Val**	167	208	**Asn**	204b	252
Leu	129c	165	**Cys**	168	209	**Asn**	205	253
Leu	130	166	**Lys**	169	210	**Arg**	206	254
Gln	131	167	**Asp**	170	211	**Trp**	207	255
Ala	132	168	**Ser**	171	212	**Tyr**	208	256
Gly	133	169	**Thr**	172	213	**Gln**	209	257
Tyr	134	170	**Arg**	173	214	**Met**	210	258

Continued on next page →

Sequence	CS	MD	Sequence	CS	MD	Sequence	CS	MD
Gly	211	259	**Tyr**	225	273	**Gln**	239	287
Ile	212	260	**Gly**	226	274	**Lys**	240	288
Val	213	261	**Phe**	227	275	**Val**	241	289
Ser	214	262	**Tyr**	228	276	**Ile**	242	290
Trp	215	263	**Thr**	229	277	**Asp**	243	291
Gly	216	264	**His**	230	278	**Gln**	244	292
Glu	217	265	**Val**	231	279	**Phe**	245	293
Gly	219	266	**Phe**	232	280	**Gly**	246	294
Cys	220	267	**Arg**	233	281	**Glu**	247	295
Asp	221a	268	**Leu**	234	282			
Arg	221	269	**Lys**	235	283			
Asp	222	270	**Lys**	236	284			
Gly	223	271	**Trp**	237	285			
Lys	224	272	**Ile**	238	286			

MD simulations were performed using the GROMACS[203] software with Amber99sb as force field. The models were immersed in triclinic boxes filled with water molecules (TIP3P water model) and counterions to balance charges (Table 3.4).

Table 3.4. Parameters and statistics of MD simulations.

System	Box dimensions (nm^3)	Waters	Na^+ ions	Cl^- ions	RMSIP[a]
Thrombin	7.67 x 7.75 x 7.70	13486	1	4	0.70
TBA-thrombin	8.62 x 7.69 x 7.66	14882	11	0	0.63
NU172-thrombin	7.90 x 7.94 x 9.86	18724	22	0	0.68
HD22_27mer-thrombin	8.50 x 7.83 x 8.72	17361	23	0	0.68
TBA-thrombin-HD22_27mer	9.40 x 7.72 x 9.06	19639	37	0	0.66
NU172-thrombin-HD22_27mer	8.41 x 8.82 x 11.04	24570	48	0	0.54

[a]The RMSIP values were calculated by dividing the last 400 ns of each trajectory in two equivalent halves.

The simulations were run applying periodic boundary conditions. All systems were initially energy minimized using steepest descent for 50000 steps. Then, they were equilibrated at the temperature of 300 K for 500 ps and at the pressure of 1 atm for other 500 ps. The Parrinello-Rahman[204] and the Velocity Rescaling[205]

algorithms were applied for pressure and temperature control, respectively. The Particle Mesh Ewald[206] with a grid spacing of 0.16 nm was used to calculate electrostatic interactions. A cut-off of 10 Å was applied to account for Lennard–Jones interactions. Bond lengths were constrained with the LINCS[207] method. Simulations were run for 500 ns with a time step of 0.002 ps at constant temperature (300 K) and pressure (1 atm) (NpT ensemble).

The root-mean-square inner product (RMSIP)[208] values, computed on the protein C^{α} atoms between the two halves of the equilibrated trajectories (100-300 ns and 300-500 ns), indicate that the MD simulations reached an acceptable level of convergence (Table 3.4).

GROMACS[203] routines and the VMD[209] program were used to assess the quality of MD trajectories and to perform structural analyses.

3.2.3. Spectroscopic analysis

Circular Dichroism measurements

CD spectra were recorded on a Jasco J-715 spectropolarimeter equipped with a Peltier temperature control, using a 1.0 or 0.1 cm path length cell. Spectra were registered with 50 nm/min scanning speed, 2 s response time, 1 nm data pitch and 2.0 nm bandwidth. Each spectrum was obtained averaging three scans.

Thermal unfolding curves of NU172 and its variants were obtained by following the CD signal at 295 nm and by recording spectra in 2 °C steps with 5 s equilibration time between readings, in the 10–90 °C range, at a heating rate of 1.0 °C min^{-1}. The fraction of folded oligonucleotide was calculated as $F_{folded} = (I_{obs} - I_u)/(I_f - I_u)$, where I_{obs} is the CD signal at 295 nm at each temperature, I_f and I_u are the CD signals at 295 nm for the folded (at T = 10 °C) and unfolded (at T = 90 °C) oligonucleotide, respectively. The melting temperatures were obtained through analysis of the first derivative of the melting profiles. Moreover, when

possible, thermodynamic parameters of the unfolding process were derived from van't Hoff analysis[210] of melting profiles.

UV experiments

UV melting profiles of NU172 and its variants were recorded by using an Agilent Technology Cary Series 100 UV/Vis spectrophotometer equipped with a Peltier thermostatic cell holder. Thermal unfolding was monitored in the 10–90 °C range at two different wavelengths, 260 and 297 nm, using a 0.1 cm and 0.5 cm path-length quartz micro-cuvettes, respectively. The heating rate was 1 °C min^{-1}. UV melting profiles at both 260 nm and 297 nm were reported as normalized ΔA ($N\Delta A$) as a function of temperature. Normalized ΔA was calculated as $N\Delta A = (A_{obs} - A_{min})/(A_{max} - A_{min})$, where A_{obs} is the UV absorbance at 260 or 297 nm at each temperature, A_{max} and A_{min} are the highest and the lowest absorbance recorded in the melting experiment, respectively. Melting temperatures were obtained through analysis of the first derivative of the melting profiles. Van't Hoff analysis[210] was carried out when possible.

Anticoagulant activity measurements

The thrombin-induced clotting of fibrinogen was measured spectrophotometrically.[211] A 1.8 mg mL^{-1} solution of fibrinogen in Phosphate Buffered Saline (PBS) was placed in a PS cuvette to which the oligonucleotide was added and left to equilibrate in the instrument for 5 min. Then, thrombin was added up to a final concentration of 5 nm. The time required for fibrin polymerization was determined from a UV scattering curve (380 nm), recorded over time in the presence of aptamer(s). Each curve was determined in triplicate. The clotting time was derived from the maximum of the second derivative of each scattering curve. The basal clotting time was determined in the absence of oligonucleotides and subtracted to the fibrinogen clotting times of the aptamers.

3.2.4. ITC studies

Binding energies for the interactions between aptamers and thrombin or prothrombin were determined at 25 °C, using a Nano-ITC III (TA instruments, New Castle, DE, USA) with a nominal cell volume of 1 mL. Protein solutions (6.3 - 7.0 μM) were titrated with each aptamer solution (55 μM) by injecting 10 μL aliquots at 500 - 600 seconds intervals, with stirring at 250 rpm, for a total of 25 injections. Small heat changes recorded after full saturation, caused by ligand dilution and other nonspecific effects, have been subtracted from the areas of the initial peaks. Data fitting was conducted with the NanoAnalyze software package supplied by the manufacturer. The binding enthalpy change, Δ_bH, is given by the height of the sigmoidal binding curve; the stoichiometry of the process comes from the molar ratio corresponding to the inflexion point; the binding constant, K_b, is obtained by fitting experimental data to an independent binding model. The other thermodynamic parameters were estimated by the following standard relationships:

$$\Delta_b G = -RT\, ln(K_b)$$
$$\Delta_b G = \Delta_b H - T\Delta_b S$$

where Δ_bG is the binding free energy change, Δ_bS is the binding entropy change, R is the gas constant, and T is the temperature in Kelvin. ITC runs were repeated twice to evaluate the reproducibility of the results.

3.2.5. Recombinant production of prethrombin-2 and prothrombin mutants

For cloning in pETM-11 vector (the vector map can be found at HMGU-PEPF website), the inserts encoding for prethrombin-2 and prothrombin were generated by PCR using Phusion DNA polymerase and the plasmids donated by Prof. E. Di Cera (see paragraph 3.1) as templates. The vector and the inserts were digested using appropriate restriction enzymes (New England Biolabs Inc.) to generate

sticky ends. In particular, NcoI and NotI were used for prethrombin-2, while NcoI and KpnI for prothrombin. Inserts and vector were purified from agarose gel through the NucleoSpin Gel and PCR Clean-up kit (Macherey-Nagel) and their ligation was performed using T4 DNA ligase. QuikChange site-directed mutagenesis kit (Agilent Technologies) was used for mutagenesis experiments. Competent *Escherichia coli* strain DH5α and the Plasmid DNA purification kit (Macherey-Nagel) were used for transformation and plasmid purification. Sequencing of the coding sequences was performed by Eurofins Genomics (Germany) using Sanger method.

The multiple alignment of coding sequences of 6xHis-tagged prethrombin-2 and prothrombin mutants is reported in Figure 3.2.

```
H6PreII_S195A ATGAAACATCACCATCACCATCACCCCATGAGCGATTACGACATC 45
H6PT_Δ154-167 ATGAAACATCACCATCACCATCACCCCATGAGCGATTACGACATC 45
H6PT_Δ146-167 ATGAAACATCACCATCACCATCACCCCATGAGCGATTACGACATC 45
              *******************************************

H6PreII_S195A CCCACTACTGAGAATCTTTATTTTCAGGGCGCCATGGCG------ 84
H6PT_Δ154-167 CCCACTACTGAGAATCTTTATTTTCAGGGCGCCATGGCGTCCTCC 90
H6PT_Δ146-167 CCCACTACTGAGAATCTTTATTTTCAGGGCGCCATGGCGTCCTCC 90
              ************************************

H6PreII_S195A ---------------------------------------------- 84
H6PT_Δ154-167 ACGGCTACGGATGTGTTCTGGGCCAAGTACACAGCTTGTGAGACA 135
H6PT_Δ146-167 ACGGCTACGGATGTGTTCTGGGCCAAGTACACAGCTTGTGAGACA 135


H6PreII_S195A ---------------------------------------------- 84
H6PT_Δ154-167 GCGAGGACGCCTCGAGATAAGCTTGCTGCATGTCTGGAAGGTAAC 180
H6PT_Δ146-167 GCGAGGACGCCTCGAGATAAGCTTGCTGCATGTCTGGAAGGTAAC 180


H6PreII_S195A ---------------------------------------------- 84
H6PT_Δ154-167 TGTGCTGAGGGTCTGGGTACGAACTACCGAGGGCATGTGAACATC 225
H6PT_Δ146-167 TGTGCTGAGGGTCTGGGTACGAACTACCGAGGGCATGTGAACATC 225


H6PreII_S195A ---------------------------------------------- 84
H6PT_Δ154-167 ACCCGGTCAGGCATTGAGTGCCAGCTATGGAGGAGTCGCTACCCA 270
H6PT_Δ146-167 ACCCGGTCAGGCATTGAGTGCCAGCTATGGAGGAGTCGCTACCCA 270
```

Continued on next page →

```
H6PreII_S195A ---------------------------------------------- 84
H6PT_Δ154-167 CATAAGCCTGAAATCAACTCCACTACCCATCCTGGGGCCGACCTA 315
H6PT_Δ146-167 CATAAGCCTGAAATCAACTCCACTACCCATCCTGGGGCCGACCTA 315

H6PreII_S195A ---------------------------------------------- 84
H6PT_Δ154-167 CAGGAGAATTTCTGCCGCAACCCCGACAGCAGCACCACGGGACCC 360
H6PT_Δ146-167 CAGGAGAATTTCTGCCGCAACCCCGACAGCAGCACCACGGGACCC 360

H6PreII_S195A ---------------------------------------------- 84
H6PT_Δ154-167 TGGTGCTACACTACAGACCCCACCGTGAGGAGGCAGGAATGCAGC 405
H6PT_Δ146-167 TGGTGCTACACTACAGACCCCACCGTGAGGAGGCAGGAATGCAGC 405

H6PreII_S195A ---------------------------------------------- 84
H6PT_Δ154-167 ATCCCTGTCTGTGGCCAGGATCAAGTCACTGTAGCGATGACTGAG 450
H6PT_Δ146-167 ATCCCTGTCTGTGGCCAG----------------------GAG 426

H6PreII_S195A ---------------------------------------------- 84
H6PT_Δ154-167 CAGTGTGTCCCTGATCGGGGGCAGCAGTACCAGGGGCGCCTGGCG 495
H6PT_Δ146-167 CAGTGTGTCCCTGATCGGGGGCAGCAGTACCAGGGGCGCCTGGCG 471

H6PreII_S195A ---------------------------------------------- 84
H6PT_Δ154-167 GTGACCACACATGGGCTCCCCTGCCTGGCCTGGGCCAGCGCACAG 540
H6PT_Δ146-167 GTGACCACACATGGGCTCCCCTGCCTGGCCTGGGCCAGCGCACAG 516

H6PreII_S195A ---------------------------------------------- 84
H6PT_Δ154-167 GCCAAGGCCCTGAGCAAGCACCAGGACTTCAACTCAGCTGTGCAG 585
H6PT_Δ146-167 GCCAAGGCCCTGAGCAAGCACCAGGACTTCAACTCAGCTGTGCAG 561

H6PreII_S195A ---------------------------------------------- 84
H6PT_Δ154-167 CTGGTGGAGAACTTCTGCCGCAACCCAGACGGGGATGAGGAGGGC 630
H6PT_Δ146-167 CTGGTGGAGAACTTCTGCCGCAACCCAGACGGGGATGAGGAGGGC 606

H6PreII_S195A ---------------------------------------------- 84
H6PT_Δ154-167 GTGTGGTGCTATGTGGCCGGGAAGCCTGGCGACTTTGGGTACTGC 675
H6PT_Δ146-167 GTGTGGTGCTATGTGGCCGGGAAGCCTGGCGACTTTGGGTACTGC 651

H6PreII_S195A ---------------------------------------------- 84
H6PT_Δ154-167 GACCTCAACTATTGTGAGGAGGCCGTGGAGGAGGAGACAGGAGAT 720
H6PT_Δ146-167 GACCTCAACTATTGTGAGGAGGCCGTGGAGGAGGAGACAGGAGAT 696
```

Continued on next page →

```
H6PreII_S195A ------------------------------------ACCGCC 90
H6PT_Δ154-167 GGGCTGGATGAGGACTCAGACAGGGCCATCGAAGGGCGTACCGCC 765
H6PT_Δ146-167 GGGCTGGATGAGGACTCAGACAGGGCCATCGAAGGGCGTACCGCC 741
                                                  ******

H6PreII_S195A ACCAGTGAGTACCAGACTTTCTTCAATCCGAGGACCTTTGGCTCG 135
H6PT_Δ154-167 ACCAGTGAGTACCAGACTTTCTTCAATCCGAGGACCTTTGGCTCG 810
H6PT_Δ146-167 ACCAGTGAGTACCAGACTTTCTTCAATCCGAGGACCTTTGGCTCG 786
              *********************************************

H6PreII_S195A GGAGAGGCAGACTGTGGGCTGCGACCTCTGTTCGAGAAGAAGTCG 180
H6PT_Δ154-167 GGAGAGGCAGACTGTGGGCTGCGACCTCTGTTCGAGAAGAAGTCG 855
H6PT_Δ146-167 GGAGAGGCAGACTGTGGGCTGCGACCTCTGTTCGAGAAGAAGTCG 831
              *********************************************

H6PreII_S195A CTGGAGGACAAAACCGAAAGAGAGCTCCTGGAATCCTACATCGAC 225
H6PT_Δ154-167 CTGGAGGACAAAACCGAAAGAGAGCTCCTGGAATCCTACATCGAC 900
H6PT_Δ146-167 CTGGAGGACAAAACCGAAAGAGAGCTCCTGGAATCCTACATCGAC 876
              *********************************************

H6PreII_S195A GGGCGCATTGTGGAGGGCTCGGATGCAGAGATCGGCATGTCACCT 270
H6PT_Δ154-167 GGGCGCATTGTGGAGGGCTCGGATGCAGAGATCGGCATGTCACCT 945
H6PT_Δ146-167 GGGCGCATTGTGGAGGGCTCGGATGCAGAGATCGGCATGTCACCT 921
              *********************************************

H6PreII_S195A TGGCAGGTGATGCTTTTCCGGAAGAGTCCCCAGGAGCTGCTGTGT 315
H6PT_Δ154-167 TGGCAGGTGATGCTTTTCCGGAAGAGTCCCCAGGAGCTGCTGTGT 990
H6PT_Δ146-167 TGGCAGGTGATGCTTTTCCGGAAGAGTCCCCAGGAGCTGCTGTGT 966
              *********************************************

H6PreII_S195A GGGGCCAGCCTCATCAGTGACCGCTGGGTCCTCACCGCCGCCCAC 360
H6PT_Δ154-167 GGGGCCAGCCTCATCAGTGACCGCTGGGTCCTCACCGCCGCCCAC 1035
H6PT_Δ146-167 GGGGCCAGCCTCATCAGTGACCGCTGGGTCCTCACCGCCGCCCAC 1011
              *********************************************

H6PreII_S195A TGCCTCCTGTACCCGCCCTGGGACAAGAACTTCACCGAGAATGAC 405
H6PT_Δ154-167 TGCCTCCTGTACCCGCCCTGGGACAAGAACTTCACCGAGAATGAC 1080
H6PT_Δ146-167 TGCCTCCTGTACCCGCCCTGGGACAAGAACTTCACCGAGAATGAC 1056
              *********************************************

H6PreII_S195A CTTCTGGTGCGCATTGGCAAGCACTCCCGCACCAGGTACGAGCGA 450
H6PT_Δ154-167 CTTCTGGTGCGCATTGGCAAGCACTCCCGCACCAGGTACGAGCGA 1125
H6PT_Δ146-167 CTTCTGGTGCGCATTGGCAAGCACTCCCGCACCAGGTACGAGCGA 1101
              *********************************************

H6PreII_S195A AACATTGAAAAGATATCCATGTTGGAAAAGATCTACATCCACCCC 495
H6PT_Δ154-167 AACATTGAAAAGATATCCATGTTGGAAAAGATCTACATCCACCCC 1170
H6PT_Δ146-167 AACATTGAAAAGATATCCATGTTGGAAAAGATCTACATCCACCCC 1146
              *********************************************
```

Continued on next page →

```
H6PreII_S195A AGGTACAACTGGCGGGAGAACCTGGACCGGGACATTGCCCTGATG 540
H6PT_Δ154-167 AGGTACAACTGGCGGGAGAACCTGGACCGGGACATTGCCCTGATG 1215
H6PT_Δ146-167 AGGTACAACTGGCGGGAGAACCTGGACCGGGACATTGCCCTGATG 1191
              *****************************************

H6PreII_S195A AAGCTGAAGAAGCCTGTTGCCTTCAGTGACTACATTCACCCTGTG 585
H6PT_Δ154-167 AAGCTGAAGAAGCCTGTTGCCTTCAGTGACTACATTCACCCTGTG 1260
H6PT_Δ146-167 AAGCTGAAGAAGCCTGTTGCCTTCAGTGACTACATTCACCCTGTG 1236
              *****************************************

H6PreII_S195A TGTCTGCCCGACAGGGAGACGGCAGCCAGCTTGCTCCAGGCTGGA 630
H6PT_Δ154-167 TGTCTGCCCGACAGGGAGACGGCAGCCAGCTTGCTCCAGGCTGGA 1305
H6PT_Δ146-167 TGTCTGCCCGACAGGGAGACGGCAGCCAGCTTGCTCCAGGCTGGA 1281
              *****************************************

H6PreII_S195A TACAAGGGGCGGGTGACAGGCTGGGGCAACCTGAAGGAGACGTGG 675
H6PT_Δ154-167 TACAAGGGGCGGGTGACAGGCTGGGGCAACCTGAAGGAGACGTGG 1350
H6PT_Δ146-167 TACAAGGGGCGGGTGACAGGCTGGGGCAACCTGAAGGAGACGTGG 1326
              *****************************************

H6PreII_S195A ACAGCCAACGTTGGTAAGGGGCAGCCCAGTGTCCTGCAGGTGGTG 720
H6PT_Δ154-167 ACAGCCAACGTTGGTAAGGGGCAGCCCAGTGTCCTGCAGGTGGTG 1395
H6PT_Δ146-167 ACAGCCAACGTTGGTAAGGGGCAGCCCAGTGTCCTGCAGGTGGTG 1371
              *****************************************

H6PreII_S195A AACCTGCCCATTGTGGAGCGGCCGGTCTGCAAGGACTCCACCCGG 765
H6PT_Δ154-167 AACCTGCCCATTGTGGAGCGGCCGGTCTGCAAGGACTCCACCCGG 1440
H6PT_Δ146-167 AACCTGCCCATTGTGGAGCGGCCGGTCTGCAAGGACTCCACCCGG 1416
              *****************************************

H6PreII_S195A ATCCGCATCACTGACAACATGTTCTGTGCTGGTTACAAGCCTGAT 810
H6PT_Δ154-167 ATCCGCATCACTGACAACATGTTCTGTGCTGGTTACAAGCCTGAT 1485
H6PT_Δ146-167 ATCCGCATCACTGACAACATGTTCTGTGCTGGTTACAAGCCTGAT 1461
              *********************************************

H6PreII_S195A GAAGGGAAACGAGGGGATGCCTGTGAAGGTGACGCTGGGGGACCC 855
H6PT_Δ154-167 GAAGGGAAACGAGGGGATGCCTGTGAAGGTGACGCTGGGGGACCC 1530
H6PT_Δ146-167 GAAGGGAAACGAGGGGATGCCTGTGAAGGTGACGCTGGGGGACCC 1506
              *********************************************

H6PreII_S195A TTTGTCATGAAGAGCCCCTTTAACAACCGCTGGTACCAAATGGGC 900
H6PT_Δ154-167 TTTGTCATGAAGAGCCCCTTTAACAACCGCTGGTATCAAATGGGC 1575
H6PT_Δ146-167 TTTGTCATGAAGAGCCCCTTTAACAACCGCTGGTATCAAATGGGC 1551
              ********************************* *********

H6PreII_S195A ATCGTCTCATGGGGTGAAGGCTGTGACCGGGATGGGAAATATGGC 945
H6PT_Δ154-167 ATCGTCTCATGGGGTGAAGGCTGTGACCGGGATGGGAAATATGGC 1620
H6PT_Δ146-167 ATCGTCTCATGGGGTGAAGGCTGTGACCGGGATGGGAAATATGGC 1596
              *********************************************
```

Continued on next page →

```
H6PreII_S195A TTCTACACACACGTGTTCCGCCTGAAGAAGTGGATACAGAAGGTC 990
H6PT_Δ154-167 TTCTACACACATGTGTTCCGCCTGAAGAAGTGGATACAGAAGGTC 1665
H6PT_Δ146-167 TTCTACACACATGTGTTCCGCCTGAAGAAGTGGATACAGAAGGTC 1641
              *********** ********************************

H6PreII_S195A ATTGATCAGTTTGGAGAGTAG 1011
H6PT_Δ154-167 ATTGATCAGTTTGGAGAGTAA 1686
H6PT_Δ146-167 ATTGATCAGTTTGGAGAGTAA 1662
              ********************
```

Figure 3.2. Multiple coding sequence alignment of H_6PreII_S195A, H_6PT_Δ154-167, and H_6PT_Δ146-167. Additional nucleotides from pETM-11 vector carrying the 6xHis-tag and the TEV protease site are blue, while the nucleotides encoding for the alanine that replaces the catalytic serine are red. The stop codons are green.

The optimized expression, refolding, and purification procedures for H_6PreII_S195A were based as follows: the plasmid was transformed into *Escherichia coli* strain Rosetta 2 (DE3) pLysS, and the transformed cells were cultured at 37 °C and 220 rpm in 2 L of Terrific broth (TB) medium containing 30 μg mL^{-1} kanamycin. After the OD_{600} reached 1.0, the culture was cooled to 18 °C and supplemented with 0.25 mM IPTG. After overnight induction, the cells were harvested by centrifugation at 6000 rpm for 45 min at 4 °C, and the pellets were resuspended in a buffer composed of 50 mM Tris-HCl pH 8.0 and 2 mM EDTA and spun at 4000 rpm for 30 min at 4 °C. The supernatant was discarded, and the cell paste was frozen in liquid N_2 and stored at -80 °C. The cell paste was thawed at 37 °C, resuspended in lysis buffer (50 mM Tris-HCl pH 8.0, 20 mM EDTA, 500 mM NaCl, 0.1% *w/v* Triton X-100, 2 mM β-mercaptoethanol, 10 μg mL^{-1} DNase I, 10 mM $MgSO_4$, 1 mg mL^{-1} lysozyme), and sonicated at 4 °C for 3 min x 3 (~ 3 min rest) at constant duty, 50% power. The lysate was ultracentrifuged for 45 min at 4 °C and 25000 rpm. The supernatant was discarded, and the pellet was resuspended in 50 mM Tris-HCl pH 8.0, 20 mM EDTA, 2% *w/v* Triton X-100, 5 mM β-mercaptoethanol using gentle vortexing and a spatula. The homogenate was centrifuged for 30 min at 25000 rpm at 4 °C. Supernatant was discarded and the pellet was suspended in 50 mM Tris-HCl pH 8.0, 20 mM EDTA, 1 M NaCl, 5 mM β-mercaptoethanol prior to centrifugation for 30 min at

25000 rpm at 4 °C. The supernatant was discarded, and the pellet was resuspended in 50 mM Tris pH 8.0, 8 M urea, 20 mM β-mercaptoethanol for two days at 4 °C. The suspension was spun at 25000 rpm for 30 min at 4 °C. The supernatant was dialyzed against 20 mM Tris-HCl pH 8.0, 8 M urea at room temperature and then incubated with 5 mM reduced glutathione (GSH) and 2 mM oxidized glutathione (GSSG) for 3 h at room temperature. Using a peristaltic pump, the solution was added dropwise (flow rate 0.02 mL min^{-1}) at 4 °C to 2 L of stirred refolding buffer, containing 50 mM Tris-HCl pH 8.0, 10% *v/v* glycerol, and 150 mM NaCl. Pellet was removed by centrifugation for 30 min at 6000 rpm and 4 °C and the supernatant was cleared filtering through a 0.45 μm filter. Imidazole was added to the protein solution up to a concentration of 10 mM. In order to purify the refolded protein by Ni-NTA affinity chromatography, the solution was incubated at 4 °C for 4 h with 5 mL of nickel resin. Then, the resin was loaded in a column and washed with 10 times the column volume of 50 mM Tris-HCl pH 8.0, 150 mM NaCl, 10 mM imidazole. Finally, the protein was eluted with 3 column volumes of a buffer containing high imidazole concentration (50 mM Tris-HCl pH 8.0, 150 mM NaCl, 350 mM imidazole). For the final step, the protein was concentrated and applied to a size exclusion chromatography column, HiLoad Superdex 75 (S75, GE Healthcare), pre-equilibrated with the final buffer, 25 mM potassium phosphate pH 7.4 and 100 mM KCl.

The optimized expression and purification procedures for H_6PT_Δ154-167 and H_6PT_Δ146-167 prothrombin mutants were based as follows: the plasmid was transformed into *Escherichia coli* strain BL21 (DE3), and the transformed cells were cultured at 37 °C and 220 rpm in 4 L of TB medium containing 30 μg mL^{-1} kanamycin. After the OD_{600} reached 1.5, the culture was cooled to 20 °C and supplemented with 0.20 mM IPTG. After overnight induction, the cells were harvested by centrifugation at 6000 rpm for 30 min at 4 °C. The supernatant was discarded, and the cell paste was frozen in liquid N_2 and stored at -80 °C. The cell

paste was thawed at 37 °C, resuspended in lysis buffer (50 mM Tris-HCl pH 8.0, 500 mM NaCl, 0.1% *w/v* Triton X-100, 2 mM β-mercaptoethanol, 10 μg mL^{-1} DNase I, 10 mM $MgSO_4$, 1 mg mL^{-1} lysozyme), and sonicated at 4 °C for 3 min x 3 (~ 3 min rest) at constant duty, 50% power. The lysate was ultracentrifuged for 45 min at 4 °C and 25000 rpm. The protein was first purified by Ni-NTA affinity chromatography, the supernatant was applied to nickel resin and washed with 10 times the column volume of 50 mM Tris-HCl pH 8.0, 300 mM NaCl, 10 mM imidazole. The protein was eluted with 3 column volumes of a buffer containing high imidazole concentration (50 mM Tris-HCl pH 8.0, 300 mM NaCl, 350 mM imidazole). For the final step, the protein was concentrated and applied to a size exclusion chromatography column, HiLoad Superdex 200 (S200, GE Healthcare), pre-equilibrated with the final buffer, 20 mM Tris-HCl pH 8.0 and 150 mM NaCl. Alternatively, the 6xHis-tag was removed prior the last purification step by adding 1 mg of TEV protease, dialyzing the solution overnight at room temperature against 20 mM Tris-HCl pH 8.0, 150 mM NaCl, and removing TEV and uncut protein by a further Ni-NTA purification step.

For Western blot experiments, the proteins were transferred to a nitrocellulose membrane using the iBlot™ 2 Transfer Stacks and iBlot™ 2 Gel Transfer Device (Invitrogen, Thermo Fisher Scientific), blocked overnight with 5% BSA in PBS, rinsed with PBS-T (PBS containing 0.1% *w/v* Tween-20), and incubated for 1 h with Ni-NTA-Atto 647N (1:1000) in the dark. The membrane was washed with PBS-T (1 h, dark) and then imaged using a ChemiDoc XRS+ imaging system (Bio-Rad).

REFERENCES

1. Bloomfield, V. A., Crothers, D. M., Tinoco, I., Killman, P. A., Hearst, J. E., Wemmer, D. E. & Turner, D. H. *Nucleic Acids: Structure, Properties, and Functions*. (University Science Books, 2000).
2. Ni, X., Castanares, M., Mukherjee, A. & Lupold, S. E. Nucleic acid aptamers: clinical applications and promising new horizons. *Curr Med Chem* **18**, 4206–4214 (2011).
3. Ellington, A. D. & Szostak, J. W. In vitro selection of RNA molecules that bind specific ligands. *Nature* **346**, 818–822 (1990).
4. Tuerk, C. & Gold, L. Systematic evolution of ligands by exponential enrichment: RNA ligands to bacteriophage T4 DNA polymerase. *Science* **249**, 505–510 (1990).
5. Wandtke, T., Woźniak, J. & Kopiński, P. Aptamers in Diagnostics and Treatment of Viral Infections. *Viruses* **7**, 751–780 (2015).
6. Nimjee, S. M., Rusconi, C. P. & Sullenger, B. A. Aptamers: an emerging class of therapeutics. *Annu Rev Med* **56**, 555–583 (2005).
7. Prakash, J. S. & Rajamanickam, K. Aptamers and Their Significant Role in Cancer Therapy and Diagnosis. *Biomedicines* **3**, 248–269 (2015).
8. Chandola, C. & Neerathilingam, M. *Aptamers for Targeted Delivery: Current Challenges and Future Opportunities*. *Role of Novel Drug Delivery Vehicles in Nanobiomedicine* (IntechOpen, 2019). doi:10.5772/intechopen.84217.
9. Kumar Kulabhusan, P., Hussain, B. & Yüce, M. Current Perspectives on Aptamers as Diagnostic Tools and Therapeutic Agents. *Pharmaceutics* **12**, (2020).
10. McKeague, M. & DeRosa, M. C. Challenges and Opportunities for Small Molecule Aptamer Development. *Journal of Nucleic Acids* **2012**, e748913 (2012).
11. Leija-Montoya, A. G., Benítez-Hess, M. L. & Alvarez-Salas, L. M. *Application of Nucleic Acid Aptamers to Viral Detection and Inhibition*. *Nucleic Acids - From Basic Aspects to Laboratory Tools* (IntechOpen, 2016). doi:10.5772/61773.
12. Lakhin, A. V., Tarantul, V. Z. & Gening, L. V. Aptamers: Problems, Solutions and Prospects. *Acta Naturae* **5**, 34–43 (2013).
13. Sun, H., Zhu, X., Lu, P. Y., Rosato, R. R., Tan, W. & Zu, Y. Oligonucleotide Aptamers: New Tools for Targeted Cancer Therapy. *Molecular Therapy - Nucleic Acids* **3**, e182 (2014).

14. Oney, S., Lam, R. T. S., Bompiani, K. M., Blake, C. M., Quick, G., Heidel, J. D., Liu, J. Y.-C., Mack, B. C., Davis, M. E., Leong, K. W. & Sullenger, B. A. Development of universal antidotes to control aptamer activity. *Nat Med* **15**, 1224–1228 (2009).
15. Nimjee, S. M., White, R. R., Becker, R. C. & Sullenger, B. A. Aptamers as Therapeutics. *Annu Rev Pharmacol Toxicol* **57**, 61–79 (2017).
16. Ismail, S. I. & Alshaer, W. Therapeutic aptamers in discovery, preclinical and clinical stages. *Adv Drug Deliv Rev* **134**, 51–64 (2018).
17. Haßel, S. K. & Mayer, G. Aptamers as Therapeutic Agents: Has the Initial Euphoria Subsided? *Mol Diagn Ther* **23**, 301–309 (2019).
18. Zhang, N., Chen, Z., Liu, D., Jiang, H., Zhang, Z.-K., Lu, A., Zhang, B.-T., Yu, Y. & Zhang, G. Structural Biology for the Molecular Insight between Aptamers and Target Proteins. *International Journal of Molecular Sciences* **22**, 4093 (2021).
19. Bunka, D. H. J., Platonova, O. & Stockley, P. G. Development of aptamer therapeutics. *Curr Opin Pharmacol* **10**, 557–562 (2010).
20. Zhou, J. & Rossi, J. Aptamers as targeted therapeutics: current potential and challenges. *Nat Rev Drug Discov* **16**, 181–202 (2017).
21. Ospina-Villa, J. D., Cisneros-Sarabia, A., Sánchez-Jiménez, M. M. & Marchat, L. A. Current Advances in the Development of Diagnostic Tests Based on Aptamers in Parasitology: A Systematic Review. *Pharmaceutics* **12**, (2020).
22. Li, L., Xu, S., Yan, H., Li, X., Yazd, H. S., Li, X., Huang, T., Cui, C., Jiang, J. & Tan, W. Nucleic Acid Aptamers for Molecular Diagnostics and Therapeutics: Advances and Perspectives. *Angewandte Chemie International Edition* **60**, 2221–2231 (2021).
23. Mastronardi, E., Foster, A., Zhang, X. & DeRosa, M. C. Smart Materials Based on DNA Aptamers: Taking Aptasensing to the Next Level. *Sensors* **14**, 3156–3171 (2014).
24. Moreno, M. Sensors | Aptasensors. in *Encyclopedia of Analytical Science (Third Edition)* (eds. Worsfold, P., Poole, C., Townshend, A. & Miró, M.) 150–153 (Academic Press, 2019). doi:10.1016/B978-0-12-409547-2.13934-4.
25. Hori, S., Herrera, A., Rossi, J. J. & Zhou, J. Current Advances in Aptamers for Cancer Diagnosis and Therapy. *Cancers (Basel)* **10**, (2018).
26. Cerchia, L. Aptamers: Promising Tools for Cancer Diagnosis and Therapy. *Cancers (Basel)* **10**, (2018).

27. Keefe, A. D., Pai, S. & Ellington, A. Aptamers as therapeutics. *Nat Rev Drug Discov* **9**, 537–550 (2010).
28. Iliuk, A. B., Hu, L. & Tao, W. A. Aptamer in Bioanalytical Applications. *Anal Chem* **83**, 4440–4452 (2011).
29. Perret, G. & Boschetti, E. Aptamer affinity ligands in protein chromatography. *Biochimie* **145**, 98–112 (2018).
30. Chaloin, L., Lehmann, M. J., Sczakiel, G. & Restle, T. Endogenous expression of a high-affinity pseudoknot RNA aptamer suppresses replication of HIV-1. *Nucleic Acids Res* **30**, 4001–4008 (2002).
31. Platella, C., Riccardi, C., Montesarchio, D., Roviello, G. N. & Musumeci, D. G-quadruplex-based aptamers against protein targets in therapy and diagnostics. *Biochim Biophys Acta Gen Subj* **1861**, 1429–1447 (2017).
32. Roxo, C., Kotkowiak, W. & Pasternak, A. G-Quadruplex-Forming Aptamers—Characteristics, Applications, and Perspectives. *Molecules* **24**, (2019).
33. Sullivan, R., Adams, M. C., Naik, R. R. & Milam, V. T. Analyzing Secondary Structure Patterns in DNA Aptamers Identified via CompELS. *Molecules* **24**, (2019).
34. Burge, S., Parkinson, G. N., Hazel, P., Todd, A. K. & Neidle, S. Quadruplex DNA: sequence, topology and structure. *Nucleic Acids Res* **34**, 5402–5415 (2006).
35. Parkinson, G. N. Fundamentals of quadruplex structures. in *Quadruplex nucleic acids* 1–30 (2006).
36. Wei, D., Parkinson, G. N., Reszka, A. P. & Neidle, S. Crystal structure of a c-kit promoter quadruplex reveals the structural role of metal ions and water molecules in maintaining loop conformation. *Nucleic Acids Res* **40**, 4691–4700 (2012).
37. Dai, J., Punchihewa, C., Ambrus, A., Chen, D., Jones, R. A. & Yang, D. Structure of the intramolecular human telomeric G-quadruplex in potassium solution: a novel adenine triple formation. *Nucleic Acids Res* **35**, 2440–2450 (2007).
38. Campbell, N. H., Parkinson, G. N., Reszka, A. P. & Neidle, S. Structural basis of DNA quadruplex recognition by an acridine drug. *J Am Chem Soc* **130**, 6722–6724 (2008).
39. Parkinson, G. N., Lee, M. P. H. & Neidle, S. Crystal structure of parallel quadruplexes from human telomeric DNA. *Nature* **417**, 876–880 (2002).

40. Geng, Y., Liu, C., Zhou, B., Cai, Q., Miao, H., Shi, X., Xu, N., You, Y., Fung, C. P., Din, R. U. & Zhu, G. The crystal structure of an antiparallel chair-type G-quadruplex formed by Bromo-substituted human telomeric DNA. *Nucleic Acids Res* **47**, 5395–5404 (2019).
41. Dai, J., Carver, M., Punchihewa, C., Jones, R. A. & Yang, D. Structure of the Hybrid-2 type intramolecular human telomeric G-quadruplex in K+ solution: insights into structure polymorphism of the human telomeric sequence. *Nucleic Acids Res* **35**, 4927–4940 (2007).
42. Rhodes, D. & Lipps, H. J. G-quadruplexes and their regulatory roles in biology. *Nucleic Acids Research* **43**, 8627–8637 (2015).
43. Marchand, A. & Gabelica, V. Folding and misfolding pathways of G-quadruplex DNA. *Nucleic Acids Res* **44**, 10999–11012 (2016).
44. Cang, X., Šponer, J. & Cheatham, T. E. Explaining the varied glycosidic conformational, G-tract length and sequence preferences for anti-parallel G-quadruplexes. *Nucleic Acids Res* **39**, 4499–4512 (2011).
45. Lane, A. N., Chaires, J. B., Gray, R. D. & Trent, J. O. Stability and kinetics of G-quadruplex structures. *Nucleic Acids Res* **36**, 5482–5515 (2008).
46. Bhattacharyya, D., Mirihana Arachchilage, G. & Basu, S. Metal Cations in G-Quadruplex Folding and Stability. *Front Chem* **4**, (2016).
47. Largy, E., Mergny, J.-L. & Gabelica, V. Role of Alkali Metal Ions in G-Quadruplex Nucleic Acid Structure and Stability. *Met Ions Life Sci* **16**, 203–258 (2016).
48. Chen, Y. & Yang, D. Sequence, Stability, Structure of G-Quadruplexes and Their Drug Interactions. *Curr Protoc Nucleic Acid Chem* **CHAPTER**, Unit17.5 (2012).
49. Palta, S., Saroa, R. & Palta, A. Overview of the coagulation system. *Indian J Anaesth* **58**, 515–523 (2014).
50. Periayah, M. H., Halim, A. S. & Mat Saad, A. Z. Mechanism Action of Platelets and Crucial Blood Coagulation Pathways in Hemostasis. *Int J Hematol Oncol Stem Cell Res* **11**, 319–327 (2017).
51. Di Cera, E. Thrombin as procoagulant and anticoagulant. *J Thromb Haemost* **5 Suppl 1**, 196–202 (2007).
52. Di Cera, E. Thrombin. *Mol. Aspects Med.* **29**, 203–254 (2008).
53. Di Cera, E. Thrombin as an anticoagulant. *Prog Mol Biol Transl Sci* **99**, 145–184 (2011).
54. Tanaka, K. A., Key, N. S. & Levy, J. H. Blood coagulation: hemostasis and thrombin regulation. *Anesth Analg* **108**, 1433–1446 (2009).

55. Bock, P. E., P. Panizzi, & I.M.A. Verhamme. Exosites in the substrate specificity of blood coagulation reactions. *J Thromb Haemost* **5**, 81–94 (2007).
56. Verhamme, I. M., Olson, S. T., Tollefsen, D. M. & Bock, P. E. Binding of exosite ligands to human thrombin. Re-evaluation of allosteric linkage between thrombin exosites I and II. *J. Biol. Chem.* **277**, 6788–6798 (2002).
57. Huntington, J. A. Molecular recognition mechanisms of thrombin. *J Thromb Haemost* **3**, 1861–1872 (2005).
58. Blajchman, M. A. An overview of the mechanism of action of antithrombin and its inherited deficiency states. *Blood Coagul Fibrinolysis* **5 Suppl 1**, S5-11; discussion S59-64 (1994).
59. Li, W., Johnson, D. J. D., Esmon, C. T. & Huntington, J. A. Structure of the antithrombin-thrombin-heparin ternary complex reveals the antithrombotic mechanism of heparin. *Nat Struct Mol Biol* **11**, 857–862 (2004).
60. Bode, W., Mayr, I., Baumann, U., Huber, R., Stone, S. R. & Hofsteenge, J. The refined 1.9 A crystal structure of human alpha-thrombin: interaction with D-Phe-Pro-Arg chloromethylketone and significance of the Tyr-Pro-Pro-Trp insertion segment. *EMBO J* **8**, 3467–3475 (1989).
61. Bode, W., Turk, D. & Karshikov, A. The refined 1.9-A X-ray crystal structure of D-Phe-Pro-Arg chloromethylketone-inhibited human alpha-thrombin: structure analysis, overall structure, electrostatic properties, detailed active-site geometry, and structure-function relationships. *Protein Sci.* **1**, 426–471 (1992).
62. Woodruff, R. S. & Sullenger, B. A. Modulation of the coagulation cascade using aptamers. *Arterioscler Thromb Vasc Biol* **35**, 2083–2091 (2015).
63. Liu, M., Zaman, K. & Fortenberry, Y. M. Overview of the Therapeutic Potential of Aptamers Targeting Coagulation Factors. *International Journal of Molecular Sciences* **22**, 3897 (2021).
64. Bock, L. C., Griffin, L. C., Latham, J. A., Vermaas, E. H. & Toole, J. J. Selection of single-stranded DNA molecules that bind and inhibit human thrombin. *Nature* **355**, 564–566 (1992).
65. Derszniak, K., Przyborowski, K., Matyjaszczyk, K., Moorlag, M., de Laat, B., Nowakowska, M. & Chlopicki, S. Comparison of Effects of Anti-thrombin Aptamers HD1 and HD22 on Aggregation of Human Platelets, Thrombin Generation, Fibrin Formation, and Thrombus Formation Under Flow Conditions. *Front Pharmacol* **10**, (2019).

66. Russo Krauss, I., Merlino, A., Randazzo, A., Novellino, E., Mazzarella, L. & Sica, F. High-resolution structures of two complexes between thrombin and thrombin-binding aptamer shed light on the role of cations in the aptamer inhibitory activity. *Nucleic Acids Res.* **40**, 8119–8128 (2012).
67. Russo Krauss, I., Napolitano, V., Petraccone, L., Troisi, R., Spiridonova, V., Mattia, C. A. & Sica, F. Duplex/quadruplex oligonucleotides: Role of the duplex domain in the stabilization of a new generation of highly effective anti-thrombin aptamers. *Int. J. Biol. Macromol.* **107**, 1697–1705 (2018).
68. Riccardi, C., Napolitano, E., Platella, C., Musumeci, D. & Montesarchio, D. G-quadruplex-based aptamers targeting human thrombin: Discovery, chemical modifications and antithrombotic effects. *Pharmacology & Therapeutics* **217**, 107649 (2021).
69. Russo Krauss, I., Merlino, A., Giancola, C., Randazzo, A., Mazzarella, L. & Sica, F. Thrombin-aptamer recognition: a revealed ambiguity. *Nucleic Acids Res.* **39**, 7858–7867 (2011).
70. Pica, A., Russo Krauss, I., Merlino, A., Nagatoishi, S., Sugimoto, N. & Sica, F. Dissecting the contribution of thrombin exosite I in the recognition of thrombin binding aptamer. *FEBS J.* **280**, 6581–6588 (2013).
71. Dolot, R., Lam, C. H., Sierant, M., Zhao, Q., Liu, F.-W., Nawrot, B., Egli, M. & Yang, X. Crystal structures of thrombin in complex with chemically modified thrombin DNA aptamers reveal the origins of enhanced affinity. *Nucleic Acids Res* **46**, 4819–4830 (2018).
72. Spiridonova, V. A., Barinova, K. V., Glinkina, K. A., Melnichuk, A. V., Gainutdynov, A. A., Safenkova, I. V. & Dzantiev, B. B. A family of DNA aptamers with varied duplex region length that forms complexes with thrombin and prothrombin. *FEBS Lett.* **589**, 2043–2049 (2015).
73. Mazurov, A. V., Titaeva, E. V., Khaspekova, S. G., Storojilova, A. N., Spiridonova, V. A., Kopylov, A. M. & Dobrovolsky, A. B. Characteristics of a new DNA aptamer, direct inhibitor of thrombin. *Bull Exp Biol Med* **150**, 422–425 (2011).
74. Spiridonova, V. A., Novikova, T. M., Sizov, V. A., Shashkovskaya, V. S., Titaeva, E. V., Dobrovolsky, A. B., Zharikova, E. B. & Mazurov, A. V. DNA Aptamers to Thrombin Exosite I. Structure-Function Relationships and Antithrombotic Effects. *Biochemistry (Mosc)* **84**, 1521–1528 (2019).
75. Spiridonova, V. A., Ka, G., Aa, G. & Am, A. Production of Thrombin Complexes with DNA Aptamers Containing G-Quadruplex and Different Duplexes. *Journal of Nephrology & Therapeutics* **4**, 1–6 (2014).

76. Russo Krauss, I., Spiridonova, V., Pica, A., Napolitano, V. & Sica, F. Different duplex/quadruplex junctions determine the properties of anti-thrombin aptamers with mixed folding. *Nucleic Acids Res.* **44**, 983–991 (2016).
77. ARCA Biopharma, Inc. *Phase 2 Study of NU172 Anticoagulation in Patients Undergoing Coronary Artery Bypass Graft Surgery OFF-Pump*. https://clinicaltrials.gov/ct2/show/NCT00808964 (2011).
78. Zavyalova, E., Ustinov, N., Golovin, A., Pavlova, G. & Kopylov, A. G-Quadruplex Aptamers to Human Thrombin Versus Other Direct Thrombin Inhibitors: The Focus on Mechanism of Action and Drug Efficiency as Anticoagulants. *Curr Med Chem* **23**, 2230–2244 (2016).
79. Rangnekar, A., Nash, J. A., Goodfred, B., Yingling, Y. G. & LaBean, T. H. Design of Potent and Controllable Anticoagulants Using DNA Aptamers and Nanostructures. *Molecules* **21**, (2016).
80. Troisi, R., Napolitano, V., Spiridonova, V., Russo Krauss, I. & Sica, F. Several structural motifs cooperate in determining the highly effective anti-thrombin activity of NU172 aptamer. *Nucleic Acids Res.* **46**, 12177–12185 (2018).
81. Tasset, D. M., Kubik, M. F. & Steiner, W. Oligonucleotide inhibitors of human thrombin that bind distinct epitopes. *J. Mol. Biol.* **272**, 688–698 (1997).
82. Macaya, R. F., Waldron, J. A., Beutel, B. A., Gao, H., Joesten, M. E., Yang, M., Patel, R., Bertelsen, A. H. & Cook, A. F. Structural and functional characterization of potent antithrombotic oligonucleotides possessing both quadruplex and duplex motifs. *Biochemistry* **34**, 4478–4492 (1995).
83. Russo Krauss, I., Pica, A., Merlino, A., Mazzarella, L. & Sica, F. Duplex-quadruplex motifs in a peculiar structural organization cooperatively contribute to thrombin binding of a DNA aptamer. *Acta Crystallogr D Biol Crystallogr* **69**, 2403–2411 (2013).
84. Stone, S. R. & Hofsteenge, J. Effect of heparin on the interaction between thrombin and hirudin. *Eur. J. Biochem.* **169**, 373–376 (1987).
85. Gandhi, P. S., Chen, Z., Mathews, F. S. & Di Cera, E. Structural identification of the pathway of long-range communication in an allosteric enzyme. *Proc. Natl. Acad. Sci. U.S.A.* **105**, 1832–1837 (2008).
86. Chen, K., Stafford, A. R., Wu, C., Yeh, C. H., Kim, P. Y., Fredenburgh, J. C. & Weitz, J. I. Exosite 2-Directed Ligands Attenuate Protein C Activation by

the Thrombin-Thrombomodulin Complex. *Biochemistry* **56**, 3119–3128 (2017).
87. Fredenburgh, J. C., Stafford, A. R. & Weitz, J. I. Evidence for allosteric linkage between exosites 1 and 2 of thrombin. *J. Biol. Chem.* **272**, 25493–25499 (1997).
88. Koeppe, J. R., Seitova, A., Mather, T. & Komives, E. A. Thrombomodulin tightens the thrombin active site loops to promote protein C activation. *Biochemistry* **44**, 14784–14791 (2005).
89. Sabo, T. M., Farrell, D. H. & Maurer, M. C. Conformational analysis of gamma′ peptide (410-427) interactions with thrombin anion binding exosite II. *Biochemistry* **45**, 7434–7445 (2006).
90. Petrera, N. S., Stafford, A. R., Leslie, B. A., Kretz, C. A., Fredenburgh, J. C. & Weitz, J. I. Long range communication between exosites 1 and 2 modulates thrombin function. *J. Biol. Chem.* **284**, 25620–25629 (2009).
91. Malovichko, M. V., Sabo, T. M. & Maurer, M. C. Ligand binding to anion-binding exosites regulates conformational properties of thrombin. *J. Biol. Chem.* **288**, 8667–8678 (2013).
92. Billur, R., Sabo, T. M. & Maurer, M. C. Thrombin Exosite Maturation and Ligand Binding at ABE II Help Stabilize PAR-Binding Competent Conformation at ABE I. *Biochemistry* **58**, 1048–1060 (2019).
93. Olmsted, I. R., Xiao, Y., Cho, M., Csordas, A. T., Sheehan, J. H., Meiler, J., Soh, H. T. & Bornhop, D. J. Measurement of aptamer-protein interactions with back-scattering interferometry. *Anal. Chem.* **83**, 8867–8870 (2011).
94. Feng, X., Yu, C., Feng, F., Lu, P., Chai, Y., Li, Q., Zhang, D., Wang, X. & Yao, L. Direct Measurement of Through-Bond Effects in Molecular Multivalent Interactions. *Chemistry* **25**, 2978–2982 (2019).
95. Pica, A., Russo Krauss, I., Parente, V., Tateishi-Karimata, H., Nagatoishi, S., Tsumoto, K., Sugimoto, N. & Sica, F. Through-bond effects in the ternary complexes of thrombin sandwiched by two DNA aptamers. *Nucleic Acids Res.* **45**, 461–469 (2017).
96. Koeppe, J. R. & Komives, E. A. Amide H/2H exchange reveals a mechanism of thrombin activation. *Biochemistry* **45**, 7724–7732 (2006).
97. Handley, L. D., Fuglestad, B., Stearns, K., Tonelli, M., Fenwick, R. B., Markwick, P. R. L. & Komives, E. A. NMR reveals a dynamic allosteric pathway in thrombin. *Sci Rep* **7**, (2017).
98. Lee, W. A., Fishback, J. A., Shaw, J.-P., Bock, L. C., Griffin, L. C. & Cundy, K. C. A Novel Oligodeoxynucleotide Inhibitor of Thrombin. II.

Pharmacokinetics in the Cynomolgus Monkey. *Pharm Res* **12**, 1943–1947 (1995).

99. De Caterina, R., Husted, S., Wallentin, L., Andreotti, F., Arnesen, H., Bachmann, F., Baigent, C., Huber, K., Jespersen, J., Kristensen, S. D., Lip, G. Y. H., Morais, J., Rasmussen, L. H., Siegbahn, A., Verheugt, F. W. A., Weitz, J. I., & European Society of Cardiology Working Group on Thrombosis Task Force on Anticoagulants in Heart Disease. Parenteral anticoagulants in heart disease: current status and perspectives (Section II). Position paper of the ESC Working Group on Thrombosis-Task Force on Anticoagulants in Heart Disease. *Thromb Haemost* **109**, 769–786 (2013).
100. Gao, S., Zheng, X., Jiao, B. & Wang, L. Post-SELEX optimization of aptamers. *Anal Bioanal Chem* **408**, 4567–4573 (2016).
101. Wang, R. E., Wu, H., Niu, Y. & Cai, J. Improving the stability of aptamers by chemical modification. *Curr Med Chem* **18**, 4126–4138 (2011).
102. Saneyoshi, H., Mazzini, S., Aviñó, A., Portella, G., González, C., Orozco, M., Marquez, V. E. & Eritja, R. Conformationally rigid nucleoside probes help understand the role of sugar pucker and nucleobase orientation in the thrombin-binding aptamer. *Nucleic Acids Res* **37**, 5589–5601 (2009).
103. Pasternak, A., Hernandez, F. J., Rasmussen, L. M., Vester, B. & Wengel, J. Improved thrombin binding aptamer by incorporation of a single unlocked nucleic acid monomer. *Nucleic Acids Res* **39**, 1155–1164 (2011).
104. Aviñó, A., Mazzini, S., Ferreira, R., Gargallo, R., Marquez, V. E. & Eritja, R. The effect on quadruplex stability of North-nucleoside derivatives in the loops of the thrombin-binding aptamer. *Bioorg Med Chem* **20**, 4186–4193 (2012).
105. Kotkowiak, W., Lisowiec-Wachnicka, J., Grynda, J., Kierzek, R., Wengel, J. & Pasternak, A. Thermodynamic, Anticoagulant, and Antiproliferative Properties of Thrombin Binding Aptamer Containing Novel UNA Derivative. *Mol Ther Nucleic Acids* **10**, 304–316 (2018).
106. Ying, G., Lu, X., Mei, J., Zhang, Y., Chen, J., Wang, X., Ou, Z. & Yi, Y. A structure-activity relationship of a thrombin-binding aptamer containing LNA in novel sites. *Bioorg Med Chem* **27**, 3201–3207 (2019).
107. Kotkowiak, W., Wengel, J., Scotton, C. J. & Pasternak, A. Improved RE31 Analogues Containing Modified Nucleic Acid Monomers: Thermodynamic, Structural, and Biological Effects. *J Med Chem* **62**, 2499–2507 (2019).
108. Virgilio, A., Esposito, V., Pecoraro, A., Russo, A., Vellecco, V., Pepe, A., Bucci, M., Russo, G. & Galeone, A. Structural properties and

anticoagulant/cytotoxic activities of heterochiral enantiomeric thrombin binding aptamer (TBA) derivatives. *Nucleic Acids Res* **48**, 12556–12565 (2020).
109. Martino, L., Virno, A., Randazzo, A., Virgilio, A., Esposito, V., Giancola, C., Bucci, M., Cirino, G. & Mayol, L. A new modified thrombin binding aptamer containing a 5′-5′ inversion of polarity site. *Nucleic Acids Res* **34**, 6653–6662 (2006).
110. Esposito, V., Galeone, A., Mayol, L., Randazzo, A., Virgilio, A. & Virno, A. A mini-library of TBA analogues containing 3′-3′ and 5′-5′ inversion of polarity sites. *Nucleosides Nucleotides Nucleic Acids* **26**, 1145–1149 (2007).
111. Varizhuk, A. M., Tsvetkov, V. B., Tatarinova, O. N., Kaluzhny, D. N., Florentiev, V. L., Timofeev, E. N., Shchyolkina, A. K., Borisova, O. F., Smirnov, I. P., Grokhovsky, S. L., Aseychev, A. V. & Pozmogova, G. E. Synthesis, characterization and in vitro activity of thrombin-binding DNA aptamers with triazole internucleotide linkages. *Eur J Med Chem* **67**, 90–97 (2013).
112. Borbone, N., Bucci, M., Oliviero, G., Morelli, E., Amato, J., D'Atri, V., D'Errico, S., Vellecco, V., Cirino, G., Piccialli, G., Fattorusso, C., Varra, M., Mayol, L., Persico, M. & Scuotto, M. Investigating the role of T7 and T12 residues on the biological properties of thrombin-binding aptamer: enhancement of anticoagulant activity by a single nucleobase modification. *J Med Chem* **55**, 10716–10728 (2012).
113. Kolganova, N. A., Tsvetkov, V. B., Smirnov, I. P. & Timofeev, E. N. Probing the Nitroindole-Modified Central Loop of Thrombin Aptamer HD1 as a Recognition Site. *Nucleic Acid Ther* **29**, 208–217 (2019).
114. Varada, M., Aher, M., Erande, N., Kumar, V. A. & Fernandes, M. Methoxymethyl Threofuranosyl Thymidine (4′-MOM-TNA-T) at the T7 Position of the Thrombin-Binding Aptamer Boosts Anticoagulation Activity, Thermal Stability, and Nuclease Resistance. *ACS Omega* **5**, 498–506 (2020).
115. Kovačič, M., Podbevšek, P., Tateishi-Karimata, H., Takahashi, S., Sugimoto, N. & Plavec, J. Thrombin binding aptamer G-quadruplex stabilized by pyrene-modified nucleotides. *Nucleic Acids Res* **48**, 3975–3986 (2020).
116. Yum, J. H., Ishizuka, T., Fukumoto, K., Hori, D., Bao, H.-L., Xu, Y., Sugiyama, H. & Park, S. Systematic Approach to DNA Aptamer Design Using Amino Acid–Nucleic Acid Hybrids (ANHs) Targeting Thrombin. *ACS Biomater. Sci. Eng.* **7**, 1338–1343 (2021).

117. Bao, H.-L., Ishizuka, T., Yamashita, A., Furukoji, E., Asada, Y. & Xu, Y. Improving Thermodynamic Stability and Anticoagulant Activity of a Thrombin Binding Aptamer by Incorporation of 8-trifluoromethyl-2′-deoxyguanosine. *J. Med. Chem.* **64**, 711–718 (2021).
118. Avino, A., Fabrega, C., Tintore, M. & Eritja, R. Thrombin binding aptamer, more than a simple aptamer: chemically modified derivatives and biomedical applications. *Curr Pharm Des* **18**, 2036–2047 (2012).
119. Kolganova, N. A., Varizhuk, A. M., Novikov, R. A., Florentiev, V. L., Pozmogova, G. E., Borisova, O. F., Shchyolkina, A. K., Smirnov, I. P., Kaluzhny, D. N. & Timofeev, E. N. Anomeric DNA quadruplexes. *Artif DNA PNA XNA* **5**, e28422 (2014).
120. Van Riesen, A. J., Fadock, K. L., Deore, P. S., Desoky, A., Manderville, R. A., Sowlati-Hashjin, S. & Wetmore, S. D. Manipulation of a DNA aptamer-protein binding site through arylation of internal guanine residues. *Org Biomol Chem* **16**, 3831–3840 (2018).
121. Kotkowiak, W., Czapik, T. & Pasternak, A. Novel isoguanine derivative of unlocked nucleic acid-Investigations of thermodynamics and biological potential of modified thrombin binding aptamer. *PLoS One* **13**, e0197835 (2018).
122. Scuotto, M., Persico, M., Bucci, M., Vellecco, V., Borbone, N., Morelli, E., Oliviero, G., Novellino, E., Piccialli, G., Cirino, G., Varra, M., Fattorusso, C. & Mayol, L. Outstanding effects on antithrombin activity of modified TBA diastereomers containing an optically pure acyclic nucleotide analogue. *Org. Biomol. Chem.* **12**, 5235–5242 (2014).
123. Cai, B., Yang, X., Sun, L., Fan, X., Li, L., Jin, H., Wu, Y., Guan, Z., Zhang, L., Zhang, L. & Yang, Z. Stability and bioactivity of thrombin binding aptamers modified with D-/L-isothymidine in the loop regions. *Org Biomol Chem* **12**, 8866–8876 (2014).
124. Tsvetkov, V. B., Varizhuk, A. M., Pozmogova, G. E., Smirnov, I. P., Kolganova, N. A. & Timofeev, E. N. A Universal Base in a Specific Role: Tuning up a Thrombin Aptamer with 5-Nitroindole. *Sci Rep* **5**, (2015).
125. Nagatoishi, S., Isono, N., Tsumoto, K. & Sugimoto, N. Loop residues of thrombin-binding DNA aptamer impact G-quadruplex stability and thrombin binding. *Biochimie* **93**, 1231–1238 (2011).
126. Chai, Z., Guo, L., Jin, H., Li, Y., Du, S., Shi, Y., Wang, C., Shi, W. & He, J. TBA loop mapping with 3′-inverted-deoxythymidine for fine-tuning of the binding affinity for α-thrombin. *Org. Biomol. Chem.* **17**, 2403–2412 (2019).

127. Peng, C. G. & Damha, M. J. G-quadruplex induced stabilization by 2′-deoxy-2′-fluoro-D-arabinonucleic acids (2′F-ANA). *Nucleic Acids Res* **35**, 4977–4988 (2007).
128. Virgilio, A., Petraccone, L., Scuotto, M., Vellecco, V., Bucci, M., Mayol, L., Varra, M., Esposito, V. & Galeone, A. 5-Hydroxymethyl-2′-deoxyuridine residues in the thrombin binding aptamer: investigating anticoagulant activity by making a tiny chemical modification. *Chembiochem* **15**, 2427–2434 (2014).
129. Smirnov, I., Kolganova, N., Troisi, R., Sica, F. & Timofeev, E. Expanding the recognition interface of the thrombin-binding aptamer HD1 through modification of residues T3 and T12. *Mol Ther Nucleic Acids* **23**, 863–871 (2021).
130. Riccardi, C., Meyer, A., Vasseur, J.-J., Russo Krauss, I., Paduano, L., Oliva, R., Petraccone, L., Morvan, F. & Montesarchio, D. Stability Is Not Everything: The Case of the Cyclisation of a Thrombin-Binding Aptamer. *ChemBioChem* **20**, 1789–1794 (2019).
131. Riccardi, C., Meyer, A., Vasseur, J.-J., Russo Krauss, I., Paduano, L., Morvan, F. & Montesarchio, D. Fine-tuning the properties of the thrombin binding aptamer through cyclization: Effect of the 5′-3′ connecting linker on the aptamer stability and anticoagulant activity. *Bioorg Chem* **94**, 103379 (2020).
132. Riccardi, C., Meyer, A., Vasseur, J.-J., Cavasso, D., Russo Krauss, I., Paduano, L., Morvan, F. & Montesarchio, D. Design, Synthesis and Characterization of Cyclic NU172 Analogues: A Biophysical and Biological Insight. *Int J Mol Sci* **21**, (2020).
133. De Fenza, M., Eremeeva, E., Troisi, R., Yang, H., Esposito, A., Sica, F., Herdewijn, P., D'Alonzo, D. & Guaragna, A. Structure-Activity Relationship Study of a Potent α-Thrombin Binding Aptamer Incorporating Hexitol Nucleotides. *Chemistry* **26**, 9589–9597 (2020).
134. Herdewijn, P. Nucleic acids with a six-membered 'carbohydrate' mimic in the backbone. *Chem Biodivers* **7**, 1–59 (2010).
135. Hendrix, C., Rosemeyer, H., Verheggen, I., Aerschot, A. V., Seela, F. & Herdewijn, P. 1′, 5′ -Anhydrohexitol Oligonucleotides: Synthesis, Base Pairing and Recognition by Regular Oligodeoxyribonucleotides and Oligoribonucleotides. *Chemistry – A European Journal* **3**, 110–120 (1997).
136. Zhou, J., Abramov, M., Liu, F., Amrane, S., Bourdoncle, A., Herdewijn, P. & Mergny, J.-L. Effects of six-membered carbohydrate rings on structure,

stability, and kinetics of G-quadruplexes. *Chemistry* **19**, 14719–14725 (2013).
137. Kang, H., Fisher, M. H., Xu, D., Miyamoto, Y. J., Marchand, A., Van Aerschot, A., Herdewijn, P. & Juliano, R. L. Inhibition of MDR1 gene expression by chimeric HNA antisense oligonucleotides. *Nucleic Acids Res* **32**, 4411–4419 (2004).
138. Zhou, Z., Zhu, J., Zhang, L., Du, Y., Dong, S. & Wang, E. G-quadruplex-based fluorescent assay of S1 nuclease activity and K+. *Anal Chem* **85**, 2431–2435 (2013).
139. Krishnaswamy, S. The Transition of Prothrombin to Thrombin. *J Thromb Haemost* **11**, 265–276 (2013).
140. Mann, K. G., Elion, J., Butkowski, R. J., Downing, M. & Nesheim, M. E. Prothrombin. *Methods Enzymol* **80 Pt C**, 286–302 (1981).
141. Pozzi, N., Chen, Z., Pelc, L. A., Shropshire, D. B. & Di Cera, E. The linker connecting the two kringles plays a key role in prothrombin activation. *Proc Natl Acad Sci U S A* **111**, 7630–7635 (2014).
142. Adams, T. E. & Huntington, J. A. Structural transitions during prothrombin activation: On the importance of fragment 2. *Biochimie* **122**, 235–242 (2016).
143. Haynes, L. M., Bouchard, B. A., Tracy, P. B. & Mann, K. G. Prothrombin activation by platelet-associated prothrombinase proceeds through the prethrombin-2 pathway via a concerted mechanism. *J Biol Chem* **287**, 38647–38655 (2012).
144. Whelihan, M. F., Zachary, V., Orfeo, T. & Mann, K. G. Prothrombin activation in blood coagulation: the erythrocyte contribution to thrombin generation. *Blood* **120**, 3837–3845 (2012).
145. Bradford, H. N., Orcutt, S. J. & Krishnaswamy, S. Membrane binding by prothrombin mediates its constrained presentation to prothrombinase for cleavage. *J Biol Chem* **288**, 27789–27800 (2013).
146. Pozzi, N., Chen, Z. & Di Cera, E. How the Linker Connecting the Two Kringles Influences Activation and Conformational Plasticity of Prothrombin. *J Biol Chem* **291**, 6071–6082 (2016).
147. Chinnaraj, M., Chen, Z., Pelc, L. A., Grese, Z., Bystranowska, D., Di Cera, E. & Pozzi, N. Structure of prothrombin in the closed form reveals new details on the mechanism of activation. *Sci Rep* **8**, 2945 (2018).
148. Pozzi, N., Chen, Z., Zapata, F., Niu, W., Barranco-Medina, S., Pelc, L. A. & Di Cera, E. Autoactivation of thrombin precursors. *J Biol Chem* **288**, 11601–11610 (2013).

149. Papaconstantinou, M. E., Gandhi, P. S., Chen, Z., Bah, A. & Di Cera, E. Na+ binding to meizothrombin desF1. *Cell Mol Life Sci* **65**, 3688–3697 (2008).
150. Pozzi, N., Bystranowska, D., Zuo, X. & Di Cera, E. Structural Architecture of Prothrombin in Solution Revealed by Single Molecule Spectroscopy. *J Biol Chem* **291**, 18107–18116 (2016).
151. Krishnaswamy, S. Prothrombinase complex assembly. Contributions of protein-protein and protein-membrane interactions toward complex formation. *J Biol Chem* **265**, 3708–3718 (1990).
152. Rosing, J., Tans, G., Govers-Riemslag, J. W., Zwaal, R. F. & Hemker, H. C. The role of phospholipids and factor Va in the prothrombinase complex. *J Biol Chem* **255**, 274–283 (1980).
153. Betz, A. & Krishnaswamy, S. Regions remote from the site of cleavage determine macromolecular substrate recognition by the prothrombinase complex. *J Biol Chem* **273**, 10709–10718 (1998).
154. Hsu, H.-J., Tsai, K.-C., Sun, Y.-K., Chang, H.-J., Huang, Y.-J., Yu, H.-M., Lin, C.-H., Mao, S.-S. & Yang, A.-S. Factor Xa active site substrate specificity with substrate phage display and computational molecular modeling. *J Biol Chem* **283**, 12343–12353 (2008).
155. Weitz, J. I. Anticoagulation therapy in 2015: where we are and where we are going. *J Thromb Thrombolysis* **39**, 264–272 (2015).
156. Anderson, P. J., Nesset, A., Dharmawardana, K. R. & Bock, P. E. Role of proexosite I in factor Va-dependent substrate interactions of prothrombin activation. *J Biol Chem* **275**, 16435–16442 (2000).
157. Kretz, C. A., Stafford, A. R., Fredenburgh, J. C. & Weitz, J. I. HD1, a thrombin-directed aptamer, binds exosite 1 on prothrombin with high affinity and inhibits its activation by prothrombinase. *J Biol Chem* **281**, 37477–37485 (2006).
158. Kretz, C. A., Cuddy, K. K., Stafford, A. R., Fredenburgh, J. C., Roberts, R. & Weitz, J. I. HD1, a thrombin- and prothrombin-binding DNA aptamer, inhibits thrombin generation by attenuating prothrombin activation and thrombin feedback reactions. *Thromb Haemost* **103**, 83–93 (2010).
159. Bompiani, K. M., Monroe, D. M., Church, F. C. & Sullenger, B. A. A high affinity, antidote-controllable prothrombin and thrombin-binding RNA aptamer inhibits thrombin generation and thrombin activity. *J Thromb Haemost* **10**, 870–880 (2012).

160. Zavyalova, E. G., Ustinov, N. B. & Kopylov, A. M. Exploring the efficiency of thrombin inhibitors with a quantitative model of the coagulation cascade. *FEBS Lett* **594**, 995–1004 (2020).
161. Pozzi, N., Chen, Z., Gohara, D. W., Niu, W., Heyduk, T. & Di Cera, E. Crystal structure of prothrombin reveals conformational flexibility and mechanism of activation. *J Biol Chem* **288**, 22734–22744 (2013).
162. Nimjee, S. M., Oney, S., Volovyk, Z., Bompiani, K. M., Long, S. B., Hoffman, M. & Sullenger, B. A. Synergistic effect of aptamers that inhibit exosites 1 and 2 on thrombin. *RNA* **15**, 2105–2111 (2009).
163. Troisi, R., Balasco, N., Vitagliano, L. & Sica, F. Molecular dynamics simulations of human α-thrombin in different structural contexts: evidence for an aptamer-guided cooperation between the two exosites. *J Biomol Struct Dyn* **39**, 2199–2209 (2021).
164. Troisi, R., Balasco, N., Santamaria, A., Vitagliano, L. & Sica, F. Structural and functional analysis of the simultaneous binding of two duplex/quadruplex aptamers to human α-thrombin. *Int J Biol Macromol* **181**, 858–867 (2021).
165. Müller, J., Freitag, D., Mayer, G. & Pötzsch, B. Anticoagulant characteristics of HD1-22, a bivalent aptamer that specifically inhibits thrombin and prothrombinase. *J Thromb Haemost* **6**, 2105–2112 (2008).
166. Yoshida, W., Mochizuki, E., Takase, M., Hasegawa, H., Morita, Y., Yamazaki, H., Sode, K. & Ikebukuro, K. Selection of DNA aptamers against insulin and construction of an aptameric enzyme subunit for insulin sensing. *Biosens Bioelectron* **24**, 1116–1120 (2009).
167. Ni, S., Yao, H., Wang, L., Lu, J., Jiang, F., Lu, A. & Zhang, G. Chemical Modifications of Nucleic Acid Aptamers for Therapeutic Purposes. *Int J Mol Sci* **18**, (2017).
168. Odeh, F., Nsairat, H., Alshaer, W., Ismail, M. A., Esawi, E., Qaqish, B., Bawab, A. A. & Ismail, S. I. Aptamers Chemistry: Chemical Modifications and Conjugation Strategies. *Molecules* **25**, (2019).
169. Ni, S., Zhuo, Z., Pan, Y., Yu, Y., Li, F., Liu, J., Wang, L., Wu, X., Li, D., Wan, Y., Zhang, L., Yang, Z., Zhang, B.-T., Lu, A. & Zhang, G. Recent Progress in Aptamer Discoveries and Modifications for Therapeutic Applications. *ACS Appl. Mater. Interfaces* **13**, 9500–9519 (2021).
170. Dolinnaya, N. G., Yuminova, A. V., Spiridonova, V. A., Arutyunyan, A. M. & Kopylov, A. M. Coexistence of G-quadruplex and duplex domains within the secondary structure of 31-mer DNA thrombin-binding aptamer. *J Biomol Struct Dyn* **30**, 524–531 (2012).

171. Mergny, J. L., Phan, A. T. & Lacroix, L. Following G-quartet formation by UV-spectroscopy. *FEBS Lett* **435**, 74–78 (1998).
172. Kopylov, M., Jackson, T. M. & Stroupe, M. E. Bulged and Canonical G-Quadruplex Conformations Determine NDPK Binding Specificity. *Molecules* **24**, (2019).
173. Baldrich, E. & O'Sullivan, C. K. Ability of thrombin to act as molecular chaperone, inducing formation of quadruplex structure of thrombin-binding aptamer. *Anal Biochem* **341**, 194–197 (2005).
174. Beals, J. M. & Castellino, F. J. Circular dichroism analysis of the secondary structures of bovine blood coagulation factor IX, factor X, and prothrombin. *J Protein Chem* **7**, 593–612 (1988).
175. Chen, Z., Pelc, L. A. & Di Cera, E. Crystal structure of prethrombin-1. *Proc Natl Acad Sci U S A* **107**, 19278–19283 (2010).
176. Girardot, J.-M., Delaney, R. & Connor Johnson, B. Carboxylation, the completion step in prothrombin biosynthesis. *Biochemical and Biophysical Research Communications* **59**, 1197–1203 (1974).
177. Marino, F., Pelc, L. A., Vogt, A., Gandhi, P. S. & Di Cera, E. Engineering thrombin for selective specificity toward protein C and PAR1. *J Biol Chem* **285**, 19145–19152 (2010).
178. Hovius, R., Guignet, E., Segura, J.-M., Piguet, J., Vogel, H. & Bäumle, M. Single Molecule Detection with Atto 647N NTA. *BioFiles: Sigma Aldrich* (2006).
179. Wakui, K., Yoshitomi, T., Yamaguchi, A., Tsuchida, M., Saito, S., Shibukawa, M., Furusho, H. & Yoshimoto, K. Rapidly Neutralizable and Highly Anticoagulant Thrombin-Binding DNA Aptamer Discovered by MACE SELEX. *Mol Ther Nucleic Acids* **16**, 348–359 (2019).
180. Zhou, Y., Qi, X., Liu, Y., Zhang, F. & Yan, H. DNA-Nanoscaffold-Assisted Selection of Femtomolar Bivalent Human α-Thrombin Aptamers with Potent Anticoagulant Activity. *Chembiochem* **20**, 2494–2503 (2019).
181. Kong, D., Movahedi, M., Mahdavi-Amiri, Y., Yeung, W., Tiburcio, T., Chen, D. & Hili, R. Evolutionary Outcomes of Diversely Functionalized Aptamers Isolated from in Vitro Evolution. *ACS Synth Biol* **9**, 43–52 (2020).
182. Deng, B., Lin, Y., Wang, C., Li, F., Wang, Z., Zhang, H., Li, X.-F. & Le, X. C. Aptamer binding assays for proteins: The thrombin example—A review. *Analytica Chimica Acta* **837**, 1–15 (2014).
183. Zhou, W., Huang, P.-J. J., Ding, J. & Liu, J. Aptamer-based biosensors for biomedical diagnostics. *Analyst* **139**, 2627–2640 (2014).

184. Müller, J., Wulffen, B., Pötzsch, B. & Mayer, G. Multidomain targeting generates a high-affinity thrombin-inhibiting bivalent aptamer. *Chembiochem* **8**, 2223–2226 (2007).
185. Hasegawa, H., Savory, N., Abe, K. & Ikebukuro, K. Methods for Improving Aptamer Binding Affinity. *Molecules* **21**, 421 (2016).
186. Riccardi, C., Napolitano, E., Musumeci, D. & Montesarchio, D. Dimeric and Multimeric DNA Aptamers for Highly Effective Protein Recognition. *Molecules* **25**, (2020).
187. Otwinowski, Z. & Minor, W. Processing of X-ray diffraction data collected in oscillation mode. *Methods Enzymol* **276**, 307–326 (1997).
188. Evans, P. Scaling and assessment of data quality. *Acta Crystallogr D Biol Crystallogr* **62**, 72–82 (2006).
189. Kabsch, W. XDS. *Acta Crystallogr D Biol Crystallogr* **66**, 125–132 (2010).
190. Winn, M. D., Ballard, C. C., Cowtan, K. D., Dodson, E. J., Emsley, P., Evans, P. R., Keegan, R. M., Krissinel, E. B., Leslie, A. G. W., McCoy, A., McNicholas, S. J., Murshudov, G. N., Pannu, N. S., Potterton, E. A., Powell, H. R., Read, R. J., Vagin, A. & Wilson, K. S. Overview of the CCP4 suite and current developments. *Acta Cryst D* **67**, 235–242 (2011).
191. Vonrhein, C., Flensburg, C., Keller, P., Sharff, A., Smart, O., Paciorek, W., Womack, T. & Bricogne, G. Data processing and analysis with the autoPROC toolbox. *Acta Crystallogr D Biol Crystallogr* **67**, 293–302 (2011).
192. Evans, P. R. & Murshudov, G. N. How good are my data and what is the resolution? *Acta Crystallogr D Biol Crystallogr* **69**, 1204–1214 (2013).
193. Tickle, I. J., Flensburg, C., Keller, P., Paciorek, W., Sharff, A., Vonrhein, C. & Bricogne, G. STARANISO. *Global Phasing Ltd., Cambridge, United Kingdom.* (2019).
194. McCoy, A. J., Grosse-Kunstleve, R. W., Adams, P. D., Winn, M. D., Storoni, L. C. & Read, R. J. Phaser crystallographic software. *J Appl Cryst* **40**, 658–674 (2007).
195. Emsley, P., Lohkamp, B., Scott, W. G. & Cowtan, K. Features and development of Coot. *Acta Cryst D* **66**, 486–501 (2010).
196. Murshudov, G. N., Skubák, P., Lebedev, A. A., Pannu, N. S., Steiner, R. A., Nicholls, R. A., Winn, M. D., Long, F. & Vagin, A. A. REFMAC5 for the refinement of macromolecular crystal structures. *Acta Cryst D* **67**, 355–367 (2011).

197. Krissinel, E. & Henrick, K. Secondary-structure matching (SSM), a new tool for fast protein structure alignment in three dimensions. *Acta Cryst D* **60**, 2256–2268 (2004).
198. Krissinel, E. & Henrick, K. Inference of Macromolecular Assemblies from Crystalline State. *Journal of Molecular Biology* **372**, 774–797 (2007).
199. Laskowski, R. A. & Swindells, M. B. LigPlot+: multiple ligand-protein interaction diagrams for drug discovery. *J Chem Inf Model* **51**, 2778–2786 (2011).
200. Battye, T. G. G., Kontogiannis, L., Johnson, O., Powell, H. R. & Leslie, A. G. W. iMOSFLM: a new graphical interface for diffraction-image processing with MOSFLM. *Acta Crystallogr D Biol Crystallogr* **67**, 271–281 (2011).
201. Evans, P. R. An introduction to data reduction: space-group determination, scaling and intensity statistics. *Acta Crystallogr D Biol Crystallogr* **67**, 282–292 (2011).
202. French, S. & Wilson, K. On the treatment of negative intensity observations. *Acta Cryst A* **34**, 517–525 (1978).
203. Spoel, D. V. D., Lindahl, E., Hess, B., Groenhof, G., Mark, A. E. & Berendsen, H. J. C. GROMACS: Fast, flexible, and free. *Journal of Computational Chemistry* **26**, 1701–1718 (2005).
204. Parrinello, M. & Rahman, A. Polymorphic transitions in single crystals: A new molecular dynamics method. *J. Appl. Phys.* **52**, 7182–7190 (1981).
205. Bussi, G., Donadio, D. & Parrinello, M. Canonical sampling through velocity rescaling. *J. Chem. Phys.* **126**, 014101 (2007).
206. Darden, T., York, D. & Pedersen, L. Particle mesh Ewald: An N·log(N) method for Ewald sums in large systems. *J. Chem. Phys.* **98**, 10089–10092 (1993).
207. Hess, B., Bekker, H., Berendsen, H. J. C. & Fraaije, J. G. E. M. LINCS: A linear constraint solver for molecular simulations. *J. Comput. Chem* **18**, 1463–1472 (1997).
208. Amadei, A., Ceruso, M. A. & Nola, A. D. On the convergence of the conformational coordinates basis set obtained by the essential dynamics analysis of proteins' molecular dynamics simulations. *Proteins: Structure, Function, and Bioinformatics* **36**, 419–424 (1999).
209. Humphrey, W., Dalke, A. & Schulten, K. VMD: visual molecular dynamics. *J Mol Graph* **14**, 33–38, 27–28 (1996).

210. Marky, L. A. & Breslauer, K. J. Calculating thermodynamic data for transitions of any molecularity from equilibrium melting curves. *Biopolymers* **26**, 1601–1620 (1987).
211. De Cristofaro, R. & Di Cera, E. Phenomenological analysis of the clotting curve. *J Protein Chem* **10**, 455–468 (1991).